# PERFORMANCE MAPPING AND LIFE-CYCLE COST MODELING FOR HEAT EXCHANGER GEOMETRY OPTIMIZATION IN VAPOR COMPRESSION CHILLERS

A Thesis

by

DEOKGEUN PARK

Submitted to the Office of Graduate and Professional Studies of
Texas A&M University
in partial fulfillment of the requirements for the degree of

MASTER OF SCIENCE

| | |
|---|---|
| Chair of Committee, | Bryan P. Rasmussen |
| Committee Members, | Michael Pate |
| | Xingyong Song |
| Head of Department, | Andreas Polycarpou |

May 2021

Major Subject: Mechanical Engineering

# ABSTRACT

With the significance of chillers in end energy use and the environment, chiller manufacturers face different regulations around the globe and changes in consumer demands. In the product development phase, components are put together to meet the cooling capacity and efficiency. However, many configurations are possible to meet such system requirements. An optimization study of heat exchanger geometries within a given chiller configuration is proposed to enable the economic comparison between different configurations. The heat exchangers will be optimized to meet the system requirements while minimizing the life cycle cost of the chiller. The resulting refrigerant cost and heat exchanger raw material cost can be used to compare different chiller configurations to one another. Several topics in chiller modeling will be addressed to conduct heat exchanger optimization within a chiller configuration. A universal method to empirically map heat exchangers will be developed to relieve the computational time associated with nested iterations. Using the mapping method, the iterative finite control volume heat exchanger model will be mapped to a non-iterative empirical map of the heat exchanger. A shell and tube heat exchanger model will be used to demonstrate the universal heat exchanger mapping method. An optimization framework is then formulated and demonstrated with a set of case studies. Lastly, modeling the chiller system and the chiller optimizer will be developed into an easy-to-use software that can carry out heat exchanger optimization study in a chiller configuration and inter-configuration cost comparison of chillers.

## DEDICATION

To my parents, my brother, Owly, Potato, Nacho, and friends.

ACKNOWLEDGEMENTS

I would like to thank my committee chair, Prof. Bryan Rasmussen, for his generosity and excellence in guidance. I learned so much about life and research at the Thermo-Fluids Control Laboratory because of Prof. Rasmussen. I would also like to thank the members of my committee, Dr. Michael Pate and Dr. Xingyong Song, for their support throughout this research.

Thanks to my friends at Thermo-Fluids Control Laboratory and my family for the help and support.

## CONTRIBUTORS AND FUNDING SOURCES

### Contributors

This work was supervised by a thesis committee consisting of Dr. Bryan Rasmussen and Dr. Michael Pate of the Department of Mechanical Engineering and Dr. Xingyong Song of the Department of Engineering Technology and Industrial Distribution.

Dr. Mostafa Ghoreyshi worked on the centrifugal compressor model as described in the Appendix. The software implementation of heat transfer correlations in Chapter III was conducted in part by Fangzhou Guo of the Department of Mechanical Engineering. Joe Wynn of Emerson Commercial and Residential Solutions provided general oversight and guidance. The student author completed all other work conducted for the thesis.


### Funding Sources

The graduate study was supported by Professor Bryan Rasmussen and Emerson Commercial and Residential Solutions.


### Disclaimer

The opinions made in this thesis are that of the author only and do not reflect the views of Emerson Commercial and Residential Solutions. Material on heat exchanger mapping method was submitted to Purdue 2020 Conferences in Compressor Engineering, Refrigeration and Air Conditioning, and High Performance Buildings hosted by the Ray W. Herrick Laboratories.

TABLE OF CONTENTS

LIST OF FIGURES

LIST OF TABLES

Page

# CHAPTER I

# INTRODUCTION*

Widely used in buildings and industrial processes, chillers are large machines that consume significant portions of the building and process energy. In the United States, building cooling alone used 3.84 Quads of primary energy in 2014 (The U.S. Department of Energy, 2015). A report by (Westphalen & Koszalinski, 2001) noted that central chillers cooled around 32 % of the total cooled floor space in the United States. The portion of the energy consumed by the chillers varies from building to building. However, (North Carolina Energy Office, 2010) states that the chillers use more than 50% of electrical energy in buildings during seasonal periods in parts of the United States.

Chillers are also an essential part of the industry. For example, in semiconductor manufacturing, air-conditioning in the cleanroom takes about five to ten times the electric energy than a common building (Chang & Tu, 2002). Large energy use is needed to control temperature and humidity in the cleanroom because it is vital for the end product quality (Chang, 2004). Chillers alone consume about 27% of total electric energy in a semiconductor manufacturing facility (Hu & Chuah, 2003).

---

* Parts of this chapter are reprinted from Park, D., Guo, F., & Rasmussen, B. P. (2021). A Method of Mapping Heat Exchanger as Simple Polynomials. *International Refrigeration and Air Conditioning Conference*. (In Press).

High global warming potential (GWP) refrigerants used in the chillers also poses environmental concerns. GWP is a measure of kg $CO_2$ equivalent in a 100-year timeline of 1 kg of refrigerant used in the vapor compression cycle (US EPA, 2016). Among the various government entities to mandate phasing out of high GWP refrigerants, the United States Environmental Protection Agency (EPA) plans to end high GWP refrigerants usage in the United States. High GWP refrigerants such as R134a cannot be used on new chiller equipment as of January 1$^{st}$, 2024 (US EPA, 2017). Only small exceptions will be made for military applications and human-rated spacecraft and its support equipment (US EPA, 2017).

With the high impact on end energy use and the environment, both the regulatory agencies and customers demand higher efficiency chillers and phasing out of high GWP refrigerants used in the chillers. Standards such as ASHRAE 90.1 detail minimum full load and integrated part-load value (IPLV) efficiencies for chillers used in buildings (ASHRAE, 2019). Full load efficiencies are defined with coefficient of performance (COP) and energy efficiency ratio (EER). As shown in Equation 1, COP is defined as a ratio of the cooling capacity ($Q_e$) to the compressor power input ($W_i$). Both the cooling capacity and compressor power input are usually measured in Watts. As shown in Equation 2, EER is similarly defined as COP. However, the units for the cooling capacity ($Q_e$) is in Btu/hr and the compressor power input ($W_i$) is measured in Watts. COP can be converted to EER using Equation 3.

$$COP = \frac{Q_e}{W_i} \tag{1}$$

$$EER = \frac{Q_e}{W_i} \tag{2}$$

$$EER = 3.412\ COP \tag{3}$$

Definition of IPLV and chiller testing procedures are outlined in Air-conditioning, Heating, & Refrigeration Institute (AHRI) standard 550/590. The performance of chillers and heat pumps using the vapor compression cycle is rated with this standard. IPLV, as defined in Equation 4, is a weighted full and part-load COPs at 100% capacity ($COP_{100}$), 75% capacity ($COP_{75}$), 50% capacity ($COP_{50}$) and 25% capacity ($COP_{25}$). IPLV rating aims to represent an efficiency for a typical building, operating in average weather in the United States (AHRI, 2016). There is no single way of measuring chillers' performance, and each country has different agencies setting the standards and policies. A review of nine standards worldwide shows that air-cooled chillers have minimum full load COP ranges from 2.40 to 3.06 for and water-cooled chillers have minimum full load COP ranges from 3.80 to 6.39 (Yu *et al.*, 2014).

$$IPLV = 0.01 \cdot COP_{100} + 0.42 \cdot COP_{75} + 0.45 \cdot COP_{50} + 0.12 \cdot COP_{25} \tag{4}$$

Chiller manufacturers face the emergence of new and different regulations around the globe and changes in customer demands. Product development cycles of chillers involve retrofitting existing products and developing new products to comply with such regulations and meet the customer needs. Components are put together to meet the system level requirements such as cooling capacity and system efficiency. However, many chiller configurations are possible in meeting such requirements. The difficulty lies in deciding which configuration is better than others. For example, different types of compressors can be used in a chiller. In order to evaluate the advantages and disadvantages of using a particular compressor instead of another, there needs to be a way to compare different system configurations.

One way to evaluate the cost-effectiveness of a chiller configuration is to let the design of the evaporator and condenser be iteratively solved to meet the system requirements while minimizing the product life cycle costs. A chiller configuration can then be compared to other configurations based on the resulting raw material cost or the life cycle cost. The optimization of chiller configuration enables economic comparison and cost reduction through the heat exchanger geometries.

## Needed Areas of Research

Several chiller modeling areas need to be addressed to conduct the optimization of heat exchangers in chiller configurations. First, the iterative heat exchanger models nested in the iterative system model pose considerable computational time for model convergence. Therefore, a universal and non-iterative map for the heat exchangers is developed to decrease the computational time. Secondly, a framework for optimizing the heat exchange design that will satisfy system requirements and minimize product life cycle cost is needed. Thirdly, an easy-to-use graphic user interface (GUI) is needed to promote wide usage of the research conducted in the chiller product development process. Lastly, a sample set of case studies is necessary to demonstrate the economic comparison and optimization capabilities of the models and the software developed. Details about these needed areas of research are going to be covered in the following subsections.

*Heat Exchanger Modeling*

The flowchart in Figure 1 shows an example of an algorithm used to solve a chiller model. The component models for the evaporator and the condenser, just like the system model, require iterations to converge to a solution. The consequence of this is "nested iterations" for the system level convergence.

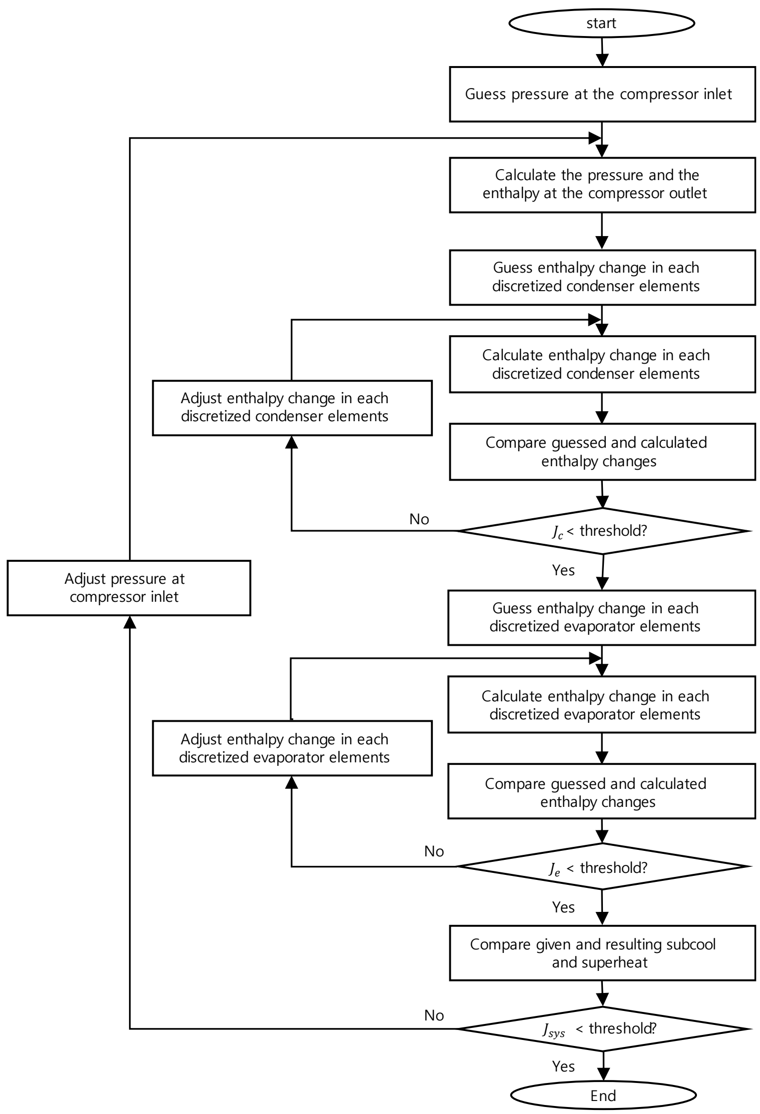


**Figure 1. Flowchart of Chiller Solving Algorithm with Nested Iterations – Reprinted from (Park *et al.*, 2021).**

The nested iterations necessary for the system-level convergence cause an increase in computational time. However, with the implementation of non-iterative component models, the system-level convergence process gets simplified, as shown in Figure 2.

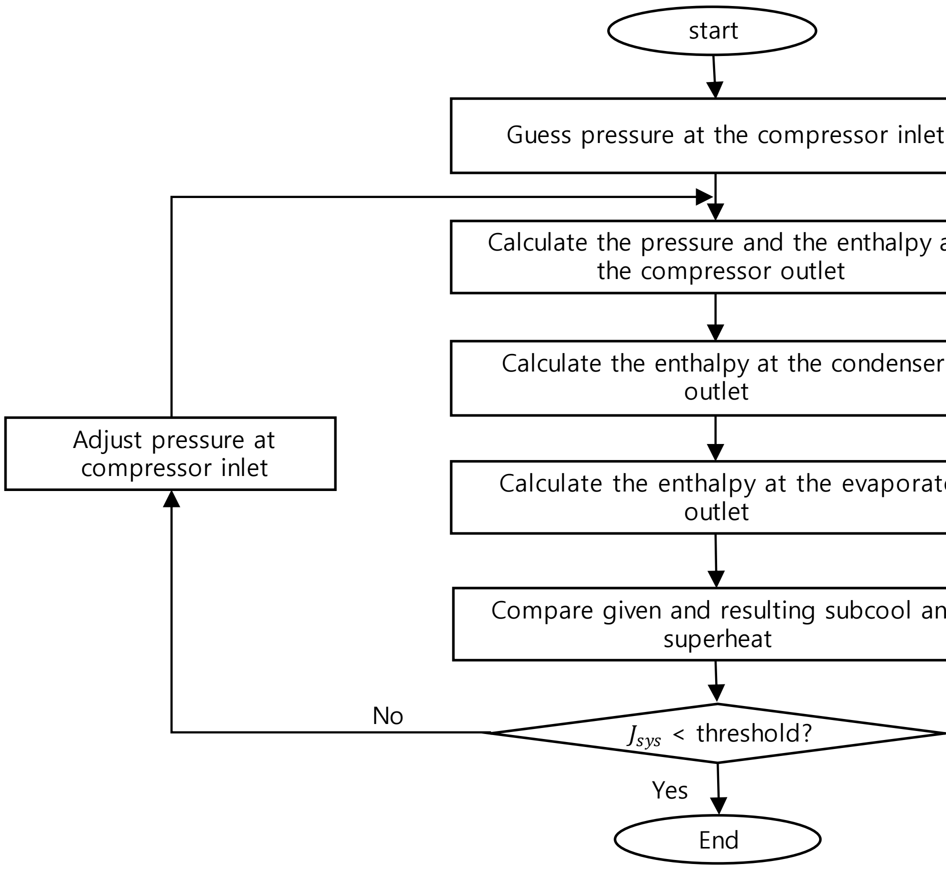


**Figure 2. Flowchart of Chiller Solving Algorithm with Non-iterative Heat Exchanger Models – Reprinted from (Park *et al.*, 2021).**

For heat exchangers, artificial neural network (ANN) models can be used as non-iterative empirical models to eliminate the nested iterations. Various types of condensers, liquid line suction heat exchangers and evaporators, run-around heat exchangers, compact heat exchangers, plate type heat exchangers, fin and tube heat exchangers, solar energy collectors, shell and tube heat exchangers, direct contact type heat exchanger, earth to air heat exchangers, heat exchangers used in power plants and special-purpose heat exchangers are modeled using ANN in the literature (Mohanraj *et al*., 2015). ANN mimics the way the biological system processes information. Figure 3 shows an example structure of an ANN. Hidden layers are placed in between the input and output layers, which are provided. Neurons are set inside the hidden layers, and the weights between the neurons are solved to fit the given data. Then, an ANN model can be used to make predictions. In the case of the shell and tube heat exchanger, ANN models are used by Mandavgane and Pandharipande (2006), Pandharipande *et al.* (2004), and Jasim (2013) to predict cold and hot outlet temperatures. Studies by Xie *et al.* (2007) and Wang *et al.* (2006) modeled heat transfer rate, and El-Said *et al.* (2021) modeled pressure drop in the heat exchanger, along with outlet temperature predictions. Hojjat (2020) modeled Nusselt number and pressure drop, and Iyengar (2015) modeled the overall heat transfer and pressure drop. Ahilan *et al*. (2011b) predicted overall heat transfer using ANN. The fouling coefficient of the heat exchangers was modeled by Kashani *et al*. (2012) and Ahilan *et al.* (2011a).

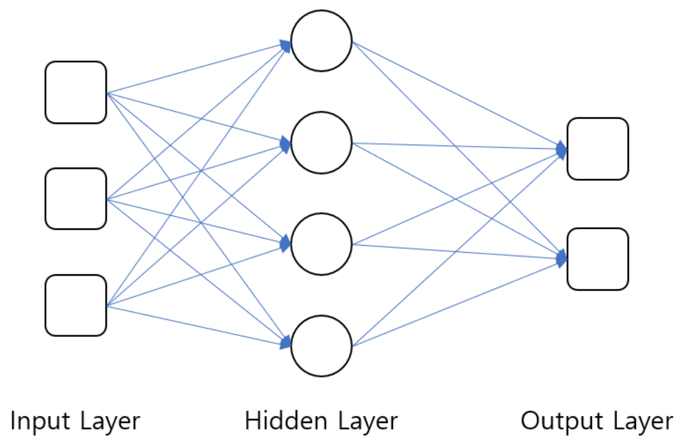


**Figure 3. Artificial Neural Network**

However, there are issues with modeling heat exchangers with ANN. Some of the shortcomings of ANN include overfitting and the need to optimize the network parameters. Overfitting can occur when there is over-training with too many iterations (Yin *et al.*, 2003). To prevent over-training of ANN, error backpropagation and Levenberg-Marquardt algorithms for overtraining resilience (EBaLM-OTR) technique are proposed (Wijayasekara *et al.*, 2011). In addition, learning rate, number of hidden layers, and number of neurons in the hidden layers are a few examples of the network parameters that need to be optimized. Choosing the number of neurons in the hidden layer is a trial and error process (Gang & Wang, 2013). There is no formula for the optimal number of neurons in the hidden layers, and this problem is still an active area of research. Equation 5 is an example of the suggested number of neurons in the hidden layer (Kalogirou & Bojic, 2000). $n_{hn}$ is the number of hidden neurons and $n_i$ and $n_o$ are the number of inputs and outputs, respectively. $n_{td}$ represents the number of training data. Others provide an upper limit for the number of neurons in the hidden layers to be one more than twice the inputs. (Islamoglu *et al.*, 2005). However, such a rule for an upper bound cannot guarantee network generalization (Rafiq *et al.*, 2001).

$$n_{hn} = \frac{n_i + n_o}{2} + \sqrt{n_{td}} \tag{5}$$

An alternative non-iterative empirical mapping method, universal for all heat exchangers, is proposed to relieve the need for optimization associated with ANN models. Non-iterative maps representing the heat exchanger effectiveness, pressure loss, refrigerant charge, and mass as a function of inlet conditions and heat exchanger design variables are developed in Chapter III. A method of empirically mapping heat exchangers will enable solving of steady-state conditions for different chiller configurations with shorter computational times. Evaluation of economic viability and comparison between different chiller configurations over a wide range of test conditions will also be enabled by the mapping of heat exchangers.

*An Optimization Framework for Chillers*

Studies on chiller optimization are mainly divided into two branches of research: optimization of components such as the heat exchangers and optimization of system-level control parameters such as condensing set points, speeds of the compressors, and heat exchanger fans. In component optimization, most of the heat exchanger geometry optimization study focuses on various optimization algorithms to minimize capital and operational costs. A study on plate-fin heat exchanger design optimization conducted by (Xie *et al*., 2008) considers volume and pressure drop minimization in its objective function. (Sanaye & Hajabdollahi, 2010) incorporated heat exchanger effectiveness in addition to the operational and capital costs in the optimization. The researchers also utilized artificial neural network analysis to decide the optimal system design. A study (Rao & Patel, 2010) compared particle swarm and genetic algorithm optimization techniques for a plate-fin heat exchanger with space restrictions and the objective function to minimize entropy generation, total volume, and annual cost. While these studies focused on plate-fin heat exchangers, others have focused on the shell and tube heat exchangers. (Azad & Amidpour, 2011) optimized shell and tube heat exchanger for its operational and capital costs using Generic algorithm (GA) and constructed theory. (Guo *et al*., 2009) also used GA and field synergy number in the objective function. Cost reduction and improved heat exchanger performance were reported in these studies.

While the heat exchanger geometry optimization is limited to a component-level solution, others have investigated system-level optimization. An adaptive control strategy that can identify the control parameters was used on an indirect seawater-cooled chilling system with multiple pumps (Wang & Burnett, 2001). A control strategy for charging and discharging cool storage with real-time electricity pricing was explored by (Braun, 2007), which requires little plant information and low-cost measurements. Optimal control by (Yu *et al*., 2008) found the optimum set point of condensing temperature by optimizing the condenser fan and compressor speeds.

For this study, heat exchanger design optimization framework for chillers needs to be developed to meet the system level requirements while minimizing life cycle costs through the component level optimization of heat exchanger geometries. Using the developed optimization framework, following optimization cases will be developed in Chapter VI:

- Baseline case (without heat exchanger geometry optimization)
- Optimization case for refrigerant and raw heat exchanger material cost
- Optimization case for chiller life cycle cost

*Easy-to-use GUI*

There are software tools for vapor compression system design that exist in the market today. The U.S. Department of Energy and Oak Ridge National Laboratory's Heat Pump Design Model (HPDM) program is an excellent example of an easy-to-use simulation tool. It allows the users to conduct a steady-state analysis of heat pumps and air conditioners (ORNL, n.d). However, HPDM's modeling scope is limited to air-to-air systems. The heat pump simulator from ETU Software has an integrated CAD function and can calculate heat pump systems' performance with hourly building thermal behavior models (ETU Software GmbH, n.d.).

Similarly, an easy-to-use software tool is needed to promote a wide implementation in the product development process. The software will allow engineers easy access to chiller configuration optimization and economic comparison studies. Before moving on to Chapter II with the compressor modeling, the vapor compression cycle basics will be covered next.

## Vapor Compression Cycle

There are four main components in an ideal vapor compression cycle: compressor, condenser, expansion valve, and evaporator. The compressor is a device that turns low pressure working fluid vapor into high pressure vapor. There are two main types of compressors: positive displacement and centrifugal. Positive displacement compressors have a fixed volume, where the fluid is drawn into the compression chamber, and the compression process occurs. Centrifugal compressors have a continuous compression process where the fluid is drawn into an eyelet, and the impeller accelerates the fluid. A diffuser and volute at the outlet of the compressor are used to increase the pressure of the working fluid.

After the fluid leaves the compressor, high-pressure fluid is then cooled through the condenser, a heat exchanger that moves heat from the working fluid to the secondary fluid. In an ideal vapor compression system, the heat exchanger pressure drop is considered negligible. Inside the condenser, the working fluid changes its phase from superheated vapor at the inlet to a two-phase fluid inside the heat exchanger. As the fluid moves towards the outlet of the condenser, the fluid is further cooled to a subcooled liquid. Subcool is defined in Equation 6 as a function of degree subcool ($T_{sc}$), saturation temperature in the condenser ($T_{sat}$) and temperature at the condenser outlet ($T_{co}$).

$$T_{sc} = T_{sat} - T_{co} \tag{6}$$

The subcooled liquid out of the condenser then flows towards an expansion valve. The high pressure fluid is expanded through an orifice in the expansion valve, resulting in a reduction in pressure. The expansion process is an isenthalpic process, where the enthalpy remains constant throughout the process. The lower pressure fluid then goes into the evaporator, where the working fluid is boiled away as it absorbs the heat from the secondary fluid. At the outlet of the evaporator, fluid is in a superheated vapor state. Degree superheat ($T_{sh}$) is defined in Equation 7 as a function of temperature of the working fluid at the evaporator outlet ($T_{eo}$) and saturation temperature in the evaporator ($T_{sat}$). With basics of vapor-compression cycle covered, Chapter II and Chapter III will detail the component-level modeling of compressors and different types of heat exchangers.

$$T_{sh} = T_{eo} - T_{sat} \tag{7}$$

# CHAPTER II

# COMPRESSOR MODEL

Although there can be many variations in chiller configurations, a chiller can be classified by the type of compressor used to power the system: centrifugal and positive displacement types. Centrifugal compressor works by the rotation of the impeller blades, circulating and increasing the working fluid's pressure. A positive displacement type compressor, on the other hand, works by compressing the working fluid with either a piston, scroll, or a screw. Generally, positive displacement chillers operate in lower capacity ranges compared to centrifugal chillers. According to the EPA, positive displacement chillers typically have a capacity range of 10 - 7,000 kW, while the capacity range for centrifugal chillers usually falls between 200 to 21,000 kW (US EPA, 2015).

Modeling of chiller components can be categorized into physics-based models and empirical map-based models. Physics-based modeling predicts the outlet conditions by simulating the physical mechanisms inside of the component. Detailed information about the component’s geometry and physical properties is needed to create a physics-based model. In contrast, the map-based approach bypasses the component's detailed physics and seeks to generate a mapping function that directly relates the inlet conditions to the outlet conditions. Non-iterative map-based modeling of the compressor was chosen to bypass the need for model calibration and its computational speed. However, a physics-based modeling approach was explored by Dr. Mostafa Ghoreyshi in parallel, and the details are attached in the Appendix section.

**Compressor Mapping**

A map-based model of the screw compressor is referenced from Section 5.2 of Air-Conditioning, Heating and Refrigeration Institute (AHRI) Standard 540. Equation 8 shows the polynomial map used to represent the power input ($W_i$), refrigerant mass flow rate ($\dot{m}_r$) and refrigerating capacity ($Q_e$) of a compressor. $a_n$ are the coefficients and $T_e$ and $T_c$ are saturated suction and saturated discharge temperature, respectively.

$$\{W_i, \dot{m}_r, \dot{Q}_e\} = a_1 + a_2 T_e + a_3 T_c + a_4 {T_e}^2 + a_5 T_e T_c + a_6 {T_c}^2 + a_7 {T_e}^3 + a_8 T_c {T_e}^2 + a_9 T_e {T_c}^2 + a_{10} {T_c}^3 \tag{8}$$

A publicly available performance table of 100RT equivalent screw compressor was retrieved from a commercial compressor manufacture's website with R134a as the refrigerant.[1] Using the polynomial fit outlined in AHRI Standard 540, map-based prediction of the outlet conditions was compared with the data used to generate the mapping function in Figure 4 and Figure 5. Both the compressor power and refrigerant mass flow rate show good predictions.

---

[1] Bitzer's 60 Hz compact screw compressor, CSVH26-200Y, was retrieved from Bitzer's official website (*BITZER Software v6.16.0 Rev2522*, n.d.).

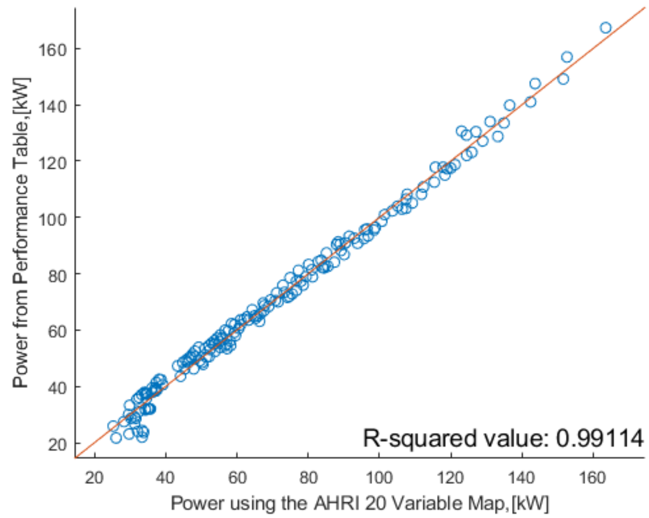


**Figure 4. AHRI Map and Performance Table Comparison for Power**

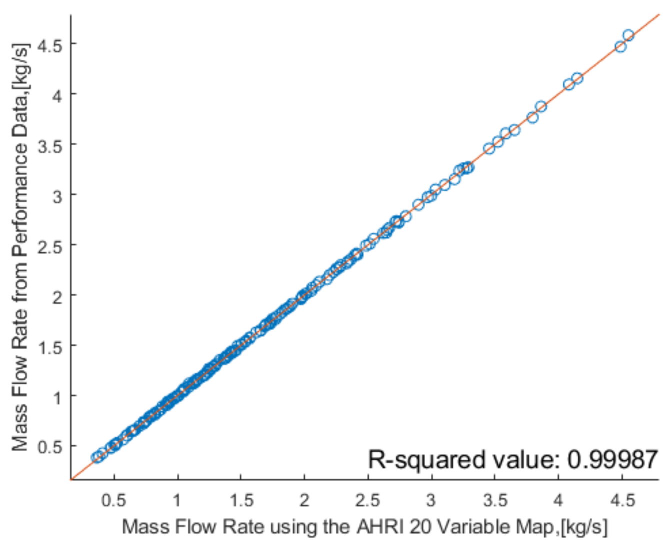


**Figure 5. AHRI Map and Performance Table Comparison for Mass Flow Rate**

A mapping method by (Arpagaus *et al*., 2017) was used to model the centrifugal compressor. In Equation 9, non-dimensional mass flow rate ($X$) is defined as a function of mass flow rate ($\dot{m}$), density ($\rho$) and speed of sound ($a$) at compressor inlet. In

Equation 10, non-dimensional rotational speed ($Y$) is defined. $n$ is the compressor speed and $D$ is the impeller tip diameter.

$$X = \frac{\dot{m}}{\rho a D^2} \tag{9}$$

$$Y = \frac{nD}{a} \tag{10}$$

As shown in Equations 11 and 12, the pressure ratio ($\Pi$) and the isentropic efficiency ($\eta$) of the centrifugal compressor are mapped using the non-dimensional mass flow rate and non-dimensional rotational speed. A performance table of an equivalent tonnage centrifugal compressor, based on computational fluid dynamics (CFD), was provided by a research partner[2]. Due to the proprietary nature of the data, the performance map and the polynomial coefficients for the centrifugal compressor were not included in this paper.

$$\eta = b_1 + b_2X + b_3Y + b_4X^2 + b_5Y^2 + b_6XY + b_7X^2Y + b_8XY^2 + b_9Y^3 \tag{11}$$

$$\Pi = c_1Y + c_2Y^2 + c_3XY + c_4X^2Y + c_5XY^2 + c_6Y^3 \tag{12}$$

Figure 6 shows a good prediction of compressor isentropic efficiency. However, one can notice the deviation from prediction increases as the isentropic efficiency decreases, which corresponds to the data from lower rpm lines. As later discussed in Chapter VI, the system is always assumed to cycle from the 50% load point to achieve a 25% load point. Therefore, the compressor is mostly operating in the higher rpm lines and higher isentropic efficiency region. Deviation of predicted isentropic efficiency is minimal

[2] Emerson Commercial and Residential Solutions

in the operational region of the plot. Figure 7 shows a good prediction of the pressure ratio compared to the performance data. With both the positive displacement and centrifugal compressor modeling covered in this chapter, heat exchanger modeling will be covered in the next chapter.

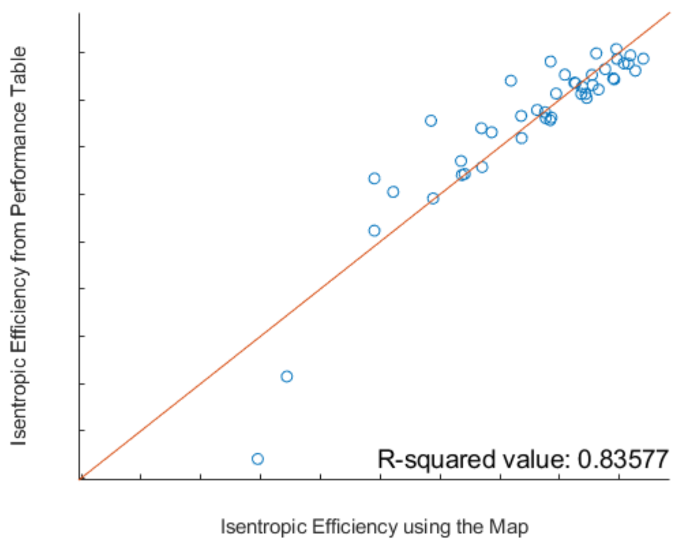


**Figure 6. Map and Performance Table Comparison for Centrifugal Compressor Isentropic Efficiency**

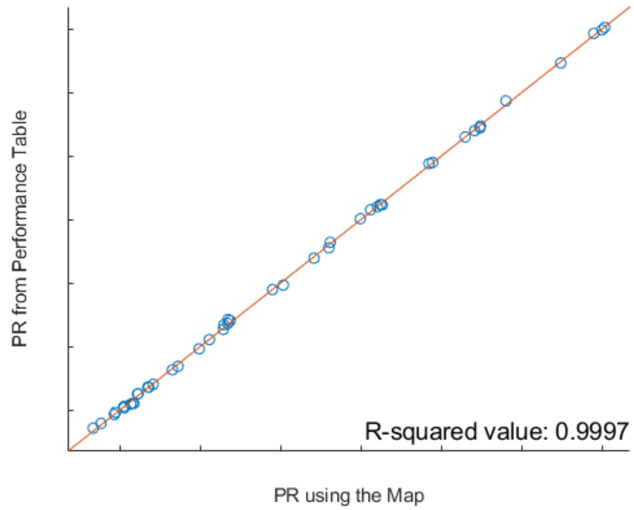


**Figure 7. Map and Performance Table Comparison for Centrifugal Compressor Pressure Ratio (PR)**

# CHAPTER III

# HEAT EXCHANGER MODEL*

Various types of heat exchangers are used as condensers and evaporators in chillers. Regardless of the type, heat exchangers are discretized into elements based on fluid phase or fixed volume to model the detailed heat transfer inside and outside the heat exchanger. As described later in this chapter, the two ways to discretize heat exchangers are the moving boundary method and the finite control volume method. Both approaches, however, require iterations to match the interelement boundary conditions. Presented in Chapter I, iteration necessary for the heat exchanger models nested inside of the iterative system model poses a considerable computational time for model solving. The method of turning finite control volume heat exchanger models into non-iterative empirical maps will be developed in this chapter to address the issue of significant computational time associated with nested iterations. First, the finite control volume method and the heat transfer correlations used for each heat exchanger type will be discussed in detail. Then, the universal and non-iterative heat exchanger mapping method using Monte Carlo sampling will be presented. Lastly, the thermal effect of compressor lubricating oil, mixed into the refrigerant, will be modeled.

---

* Parts of this chapter are reprinted from Park, D., Guo, F., & Rasmussen, B. P. (2021). A Method of Mapping Heat Exchanger as Simple Polynomials. *International Refrigeration and Air Conditioning Conference*. (In Press).

## Heat Exchanger Discretization Method

There are two approaches to discretizing the heat exchanger into elements. The moving boundary method divides the heat exchanger based on the phase of the working fluid. As shown in Figure 8, two-phase fluid is lumped into an element, and the boundary is drawn between the two-phase and single-phase interface. The element boundary is moved along with the location of the interface.

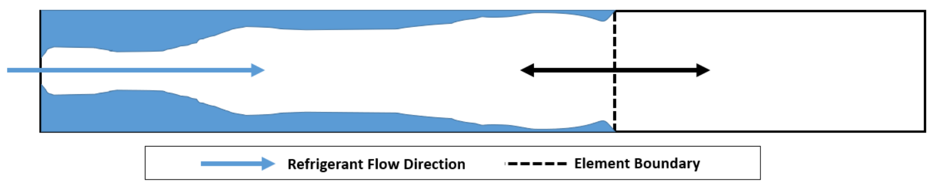


**Figure 8. Discretization Using Moving Boundary Method**

In contrast to the moving boundary method, the finite control volume method discretizes the heat exchanger based on a set volume. The location and volume of each element are fixed in space, and an element can have fluid of multiple phases. Such elements are called transition elements. Figure 9 shows a heat exchanger with finite control volumes. For this study, the finite control volume method was used in modeling the heat exchangers.

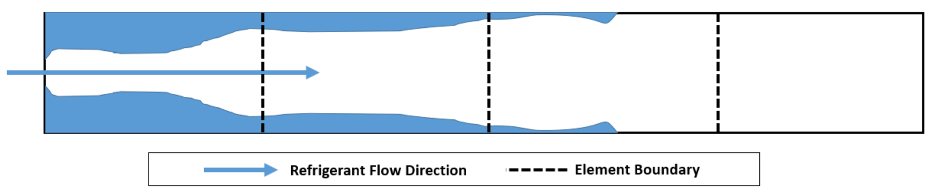


**Figure 9. Discretization Using Finite Control Volume Method**

A discretized heat exchanger element is shown in Figure 10. For each element, refrigerant enthalpy, pressure, and mass flow rate at the inlet are given. Secondary fluid inlet temperature and mass flow rate are given as well. Assuming steady-state conditions, the heat exchanger wall temperature will remain constant, and Equation 13 shows the heat transfer rate from the refrigerant to the heat exchanger wall ($\dot{Q}_i$) equaling the heat transfer rate from the heat exchanger wall to the secondary fluid ($\dot{Q}_o$) and heat transfer rate in the refrigerant ($\dot{Q}_r$). Inside ($\alpha_i$) and outside heat transfer coefficient ($\alpha_o$) for the heat exchanger is referenced from the literature. Given refrigerant ($T_r$) and secondary fluid temperatures at the inlet ($T_o$) and the inside ($A_i$) and outside heat transfer area ($A_o$), the heat exchanger wall temperature ($T_w$) can be solved using Equation 14 and Equation 15. Then, the heat transfer rate from the refrigerant to the heat exchanger wall can be back-calculated. The enthalpy of the refrigerant at the outlet ($h_{out}$) can be calculated using the refrigerant mass flow rate ($\dot{m}_r$) and the refrigerant inlet enthalpy ($h_{in}$), shown in Equation 16. With basic finite control volume modeling of heat exchangers covered, heat exchanger solving method, heat transfer correlations for various heat exchangers, and the heat exchanger mapping method will be presented in the following subsections.

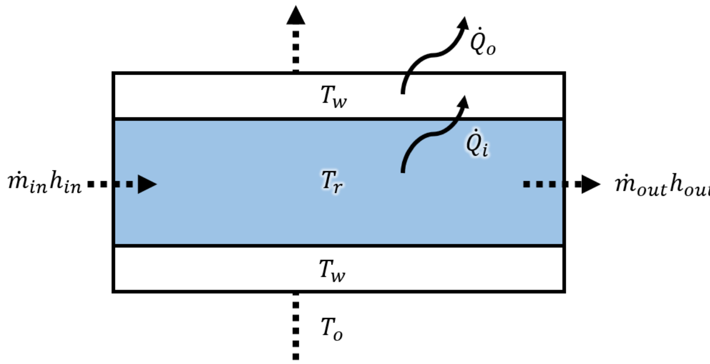


**Figure 10. A Discretized Heat Exchanger Element – Reprinted from (Park *et al.*, 2021).**

$$\dot{Q}_i = \dot{Q}_o = \dot{Q}_r \tag{13}$$

$$\dot{Q}_i = \alpha_i A_i (T_r - T_w) \tag{14}$$

$$\dot{Q}_o = \alpha_o A_o (T_w - T_o) \tag{15}$$

$$\dot{Q}_r = \dot{m}_r (h_{out} - h_{in}) \tag{16}$$

### Heat Exchanger Solving Method

Individual heat exchanger types were modeled with appropriate heat transfer coefficients from the literature. However, all heat exchangers share a common iterative and systematic method of solving their discretized elements. An optimizer is used to iteratively solve the heat exchanger elemental convergence. $u_{ext}$ and $u_{ini}$ are inputs to the optimizer. As shown in Equation 17, $u_{ext}$ is a vector of external conditions such as enthalpy of the refrigerant at the inlet ($h_{ri}$) and temperature of secondary fluid at the inlet ($T_{si}$). Elemental enthalpy change ($u_{ini}$) is defined in Equation 18. A vector of enthalpy change in each heat exchanger elements ($\overline{\Delta h}_r$) is guessed by the optimizer to minimize the value of the cost function ($J$), which will be defined later in this section

$$u_{ext} = \begin{bmatrix} h_{ri} \\ T_{si} \end{bmatrix} \tag{17}$$

$$u_{ini} = \begin{bmatrix} \overline{\Delta h}_r \end{bmatrix} \tag{18}$$

Equation 19-21 defines transformation matrix $R$ that maps working fluid elemental enthalpy change ($u_{ini}$) to a vector of elemental working fluid enthalpy changes ($\overline{\Delta h}_r$) and secondary fluid temperature change ($\overline{\Delta T}_s$). $r$ is defined as the refrigerant mass flow rate ($\dot{m}_r$) divided by external fluid mass flow rate ($\dot{m}_{ext}$) and heat capacity ($C_{ext}$).

$$\begin{bmatrix} \overline{\Delta h}_r \\ \overline{\Delta T}_s \end{bmatrix} = R u_{ini} \tag{19}$$

$$R = \begin{bmatrix} 1 & 0 & 0 \\ 0 & \ddots & 0 \\ 0 & 0 & 1 \\ \hline r & 0 & 0 \\ 0 & \ddots & 0 \\ 0 & 0 & r \end{bmatrix} \tag{20}$$

$$r = -\frac{\dot{m}_r}{\dot{m}_{ext} C_{ext}} \tag{21}$$

$R u_{ini}$ added to $u_{ext}$ yields a vector of outlet enthalpies of the refrigerant and the secondary fluid out of the elements, as shown in Equation 22. $N$ and $M$ are transformation matrices that depend on the geometric nature of each heat exchanger type. $N$ and $M$ transform the guessing inputs, $u_{ini}$ and $u_{ext}$, into the enthalpy and temperature inputs to the element-wise solver, respectively.

$$\begin{bmatrix} \bar{h}_{ro} \\ \bar{T}_{so} \end{bmatrix} = \begin{bmatrix} \overline{\Delta h}_r \\ \overline{\Delta T}_s \end{bmatrix} + \begin{bmatrix} \bar{h}_{ri} \\ \bar{T}_{si} \end{bmatrix} \tag{22}$$

$$\begin{bmatrix} \bar{h}_{ri} \\ \bar{T}_{si} \end{bmatrix} = \left( \begin{bmatrix} N_1 & 0 \\ 0 & M_1 \end{bmatrix} \begin{bmatrix} \bar{h}_{ro} \\ \bar{T}_{so} \end{bmatrix} + \begin{bmatrix} N_2 & 0 \\ 0 & M_2 \end{bmatrix} u_{ext} \right) \tag{23}$$

From $u_{ini}$, input vector to the element-wise solver ($u_{eli}$) is determined. With $u_{eli}$, the element-wise solver computes the enthalpy and temperature at the outlet. Equation 24-26 shows this process. For simplicity, parts of Equation 25 are redefined with expressions from Equation 27-29

$$u_{eli} = \begin{bmatrix} \bar{h}_{ri} \\ \bar{T}_{si} \end{bmatrix} \tag{24}$$

$$u_{eli} = \left( \begin{bmatrix} I - N_1 & 0 \\ 0 & I - M_1 \end{bmatrix}^{-1} \right) * \left( \begin{bmatrix} N_1 & 0 \\ 0 & M_1 \end{bmatrix} R u_{ini} + \begin{bmatrix} N_2 & 0 \\ 0 & M_2 \end{bmatrix} u_{ext} \right) \tag{25}$$

$$u_{elo} = \begin{bmatrix} \bar{h}_{ro} \\ \bar{T}_{so} \end{bmatrix} \tag{26}$$

$$K = \begin{bmatrix} I - N_1 & 0 \\ 0 & I - M_1 \end{bmatrix}^{-1} \tag{27}$$

$$NM_1 = \begin{bmatrix} N_1 & 0 \\ 0 & M_1 \end{bmatrix} \tag{28}$$

$$NM_2 = \begin{bmatrix} N_2 & 0 \\ 0 & M_2 \end{bmatrix} \tag{29}$$

As shown in Equation 30, $u_{opt}$ is the elemental solver residual is the difference between the output vector from the elemental solver ($u_{elo}$) and input vector to the element-wise solver ($u_{eli}$). Objective function ($J$) is shown in Equation 31. An optimized is used to iteratively solve until the objective function is sufficiently small and satisfies the stopping criterion. As the iteration halts, the resulting refrigerant charge and heat exchanger mass information are stored together, along with the capacity of the heat exchanger

$$u_{opt} = u_{elo} - u_{eli} \tag{30}$$

$$J = \left\| \frac{u_{opt} - u_{ini}}{u_{opt}} \right\|_2 \tag{31}$$

A simple heat exchanger in Figure 11 will be used to construct a sample set of matrices. The heat exchanger has two rows of tubes with secondary fluid flowing inside of the tubes. Refrigerant is in a crossflow configuration, flowing from the bottom to the top. Each tube is discretized into two elements and numbered from the top left to the bottom right element. Example matrices $R$ , $K$, $NM_1$ and $NM_2$ are presented below in Equation 32-35. With the heat exchanger solving process defined, heat transfer correlation for each type of heat exchanger will be covered in the following subsections.

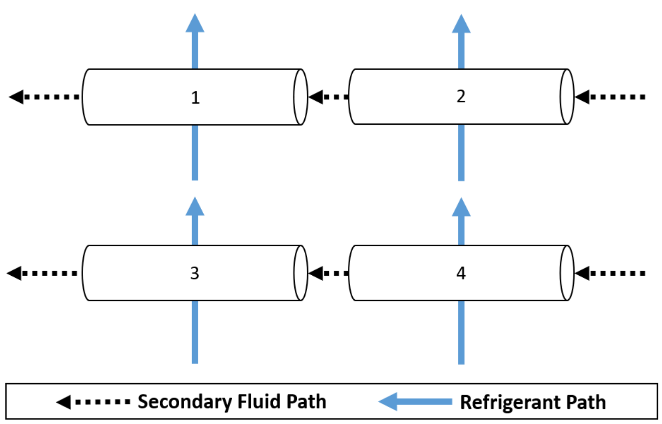


**Figure 11. Discretized Heat Exchanger Elements**

$$R = \begin{bmatrix} 1 & 0 & 0 & 0 \\ 0 & 1 & 0 & 0 \\ 0 & 0 & 1 & 0 \\ 0 & 0 & 0 & 1 \\ r & 0 & 0 & 0 \\ 0 & r & 0 & 0 \\ 0 & 0 & r & 0 \\ 0 & 0 & 0 & r \end{bmatrix} \tag{32}$$

$$K = \begin{bmatrix} 1 & 0 & 1 & 0 & 0 & 0 & 0 & 0 \\ 0 & 1 & 0 & 1 & 0 & 0 & 0 & 0 \\ 0 & 0 & 1 & 0 & 0 & 0 & 0 & 0 \\ 0 & 0 & 0 & 1 & 0 & 0 & 0 & 0 \\ 0 & 0 & 0 & 0 & 1 & 1 & 0 & 0 \\ 0 & 0 & 0 & 0 & 0 & 1 & 0 & 0 \\ 0 & 0 & 0 & 0 & 0 & 0 & 1 & 1 \\ 0 & 0 & 0 & 0 & 0 & 0 & 0 & 1 \end{bmatrix} \tag{33}$$

$$NM_1 = \begin{bmatrix} 0 & 0 & 1 & 0 & 0 & 0 & 0 & 0 \\ 0 & 0 & 0 & 1 & 0 & 0 & 0 & 0 \\ 0 & 0 & 0 & 0 & 0 & 0 & 0 & 0 \\ 0 & 0 & 0 & 0 & 0 & 0 & 0 & 0 \\ 0 & 0 & 0 & 0 & 0 & 1 & 0 & 0 \\ 0 & 0 & 0 & 0 & 0 & 0 & 0 & 0 \\ 0 & 0 & 0 & 0 & 0 & 0 & 0 & 1 \\ 0 & 0 & 0 & 0 & 0 & 0 & 0 & 0 \end{bmatrix} \tag{34}$$

$$NM_2 = \begin{bmatrix} 0 & 0 \\ 0 & 0 \\ 1 & 0 \\ 1 & 0 \\ 0 & 0 \\ 0 & 1 \\ 0 & 0 \\ 0 & 1 \end{bmatrix} \tag{35}$$

## Fin and Tube Heat Exchanger (FTHX)

Widely used in HVAC systems, FTHX consists of tubes that channel the working fluid inside and fins located on the secondary fluid side. FTHXs are most often used with air as the secondary fluid. In such applications, air thermal resistance takes up around 90% of total thermal resistance (Wang *et al.*, 2002). To increase the performance of the heat exchangers, fins are placed on the secondary fluid side to increase the surface area, shown in Figure 12.

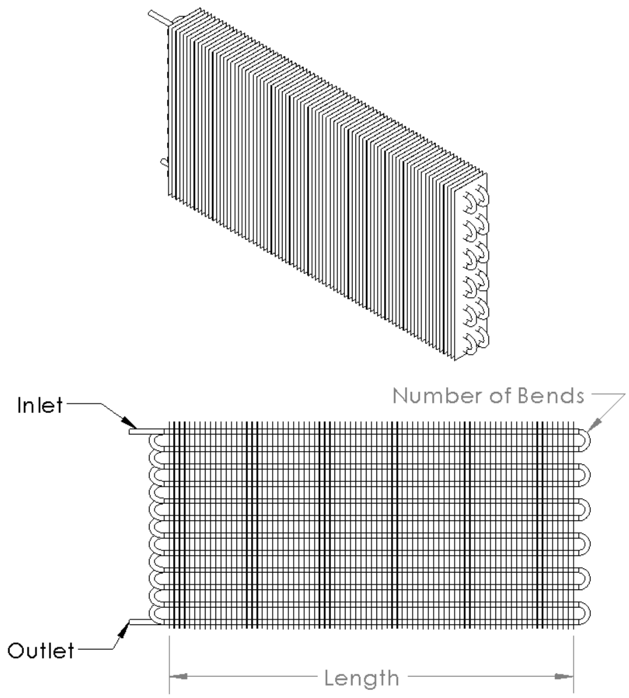


**Figure 12. Fin and Tube Heat Exchanger**

Fin and tube condenser is modeled with Gnielinski correlation for the single-phase heat transfer coefficient inside the circular tubes. As shown in Equation 36, Nusselt number ($Nu$) is defined as a function of friction factor ($f$), Reynold's number ($Re$) and Prandtl number ($Pr$).

$$Nu = \frac{\frac{f}{8}(Re - 1000)Pr}{1 + 12.7\sqrt{\frac{f}{8}}\left(Pr^{\frac{2}{3}} - 1\right)} \tag{36}$$

$$for\ 0.5 \leq Pr \leq 2000$$

$$2300 \leq Re \leq 10\text{^}6$$

For the condensing of two-phase fluid inside the circular tubes, heat transfer correlation by Dobson and Chato (1998) is used. For Soliman's modified Froude number ($Fr_{so}$) larger than 20, Nusselt number defined in Equation 37 as a function of superficial liquid Reynolds number ($Re_l$), liquid Prandtl number ($Pr_l$) and turbulent-turbulent Lockhart Martinelli parameter ($X_{tt}$).

$$Nu = 0.023\, {Re_l}^{0.8} {Pr_l}^{0.4} \left[1 + \frac{2.22}{{X_{tt}}^{0.89}}\right] \tag{37}$$

$$for\ Fr_{so} > 20$$

For Soliman's modified Froude number less than 20, Nusselt number is separated into film condensation and forced-convective heat transfer in Equation 38. Nusselt number is defined as a function of vapor-only Reynolds number ($Re_{vo}$), Galileo number ($Ga$), liquid Jakob number ($Ja_l$), subtended angle from the top of the tube to the liquid level ($\theta_l$) and forced-convective Nusselt number ($Nu_{forced}$). In Equation 39-41, forced-convective Nusselt number is defined empirically, depending on the Froude number ($Fr_l$).

$$Nu = \frac{0.23\, {Re_{vo}}^{0.12}}{1 + 1.11{X_{tt}}^{0.58}} \left[\frac{Ga\, \mathrm{Pr}_l}{Ja_l}\right]^{0.25} + \left(1 - \frac{\theta_l}{\pi}\right) Nu_{forced} \tag{38}$$

$$for\ Fr_{so} < 20$$

$$Nu_{forced} = 0.0195\, {Re_l}^{0.8} {Pr_l}^{0.4} \left[1.376 + \frac{c_1}{{X_{tt}}^{c_2}}\right] \tag{39}$$

$$\begin{cases} c_1 = 4.172 + 5.48\, Fr_l - 1.564\, Fr_l^2 \\ c_2 = 1.773 - 0.169\, Fr_l \end{cases} \quad for\ 0 < Fr_l \leq 0.7 \tag{40}$$

$$\begin{cases} c_1 = 7.242 \\ c_2 = 1.655 \end{cases} \quad (41)$$
$$for\ \ 0.7 < Fr_l$$

For the evaporating two-phase fluid inside the circular tubes, heat transfer correlation by Wattelet *et al.* (1994) is used. Two-phase heat transfer coefficient ($\alpha_{tp}$) is defined as a function of nucleate boiling heat transfer coefficient ($\alpha_{nb}$) and convective boiling heat transfer coefficient ($\alpha_{cb}$).

$$\alpha_{tp} = (\alpha_{nb}^{2.5} + \alpha_{cb}^{2.5})^{1/2.5} \quad (42)$$

Colburn J factor analogy is used for the outside heat transfer coefficient ($\alpha_o$) defined in Equation 43. Mass flux ($G$) and Prandtl number ($Pr$) are calculated whereas the specific heat ($C_p$) and the J-factor ($J_H$) are defined as a function of temperature and Reynold's number, respectively.

$$\alpha_o = \frac{J_H \cdot G \cdot C_p}{Pr^{\frac{2}{3}}} \quad (43)$$

**Shell and Tube Direct Expansion Heat Exchanger (STDX)**

STDX consists of inner tubes with the working fluid flowing inside and a shell that houses both the inner tube bundles and a pool of secondary fluid. CAD drawings of STDX are shown in Figure 13 and Figure 14. The simple yet robust design of the STDX allows application in wide pressure ranges and easy maintenance. A cross-section view of STDX in Figure 14 shows some of the design variables used in heat exchanger optimization and the location of refrigerant and the secondary fluid.

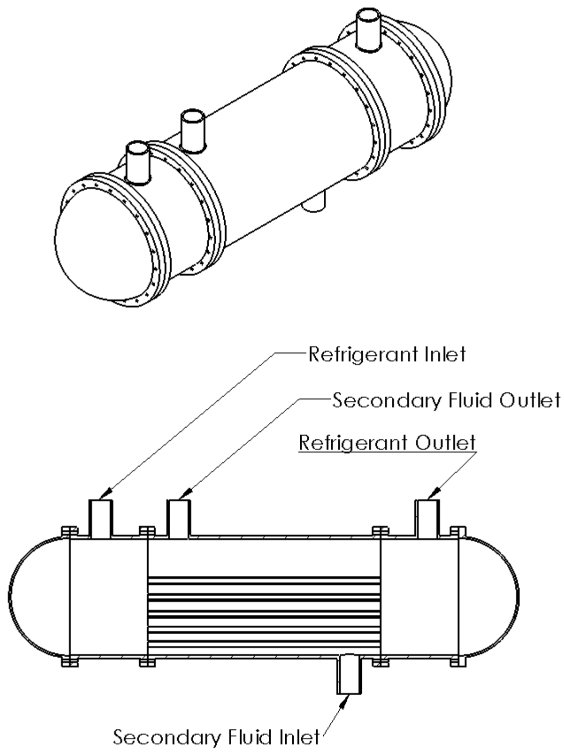


**Figure 13. Single Pass Direct Expansion Shell and Tube Type Heat Exchanger**

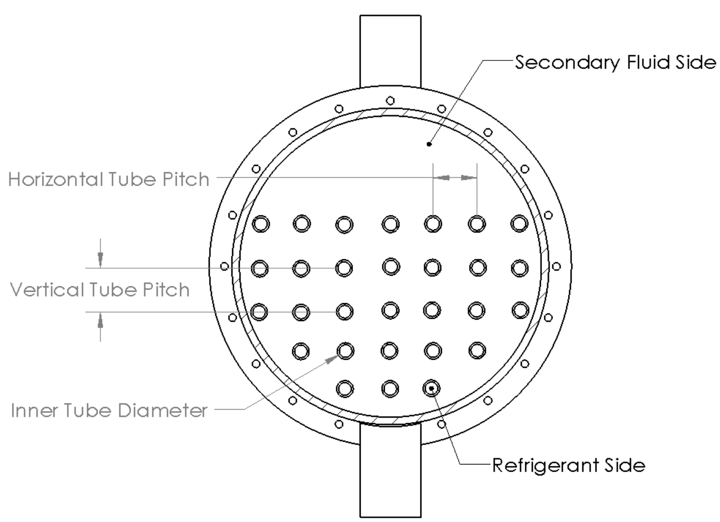


**Figure 14. Single Pass Direct Expansion Shell and Tube Type Heat Exchanger Cross-section**

The heat transfer coefficients for STDX were referenced from the thesis work of (Hellborg, 2017). The Delaware method was chosen as the shell side heat transfer coefficient. For simplicity, all baffled sections of the heat exchanger were assumed to have the same length, and therefore, the inlet and outlet section adjustment factors were negligible. Shown in Equation 44, shell side heat transfer coefficient ($\alpha_s$) is defined as the product of ideal heat transfer coefficient ($\alpha_{ideal}$) and the correction factors $J_C$, $J_B$, $J_L$ and $J_R$. The ideal heat transfer coefficient is defined in Equation 45 as a function of Colburn j-factor ($j$), specific heat capacity ($C_p$), mass flow rate ($\dot{m}$), Prandtl number ($Pr$) and cross-flow area ($S_m$), defined in Equation 46. Variables for the cross-flow area is tabularized in Table 1.

$$\alpha_s = \alpha_{ideal} J_C J_B J_L J_R \tag{44}$$

$$\alpha_{ideal} = \frac{j C_p \dot{m}}{S_m Pr^{\frac{2}{3}}} \tag{45}$$

$$S_m = B\left(D_s - D_{otl} + \frac{D_{otl} - D_o}{P_T}(P_T - D_o)\right) \tag{46}$$

**Table 1. Variable List for Cross-flow Area**

| Variable | Definition |
|---|---|
| $B$ | Baffle distance |
| $D_o$ | Outer tube diameter |
| $D_{otl}$ | Outer tube limit diameter |
| $D_s$ | Shell diameter |
| $P_T$ | Transverse tube pitch |

Colburn j-factor ($j$) is defined in Equation 47. Delaware heat transfer method coefficients ($a, a_{1-4}$) are defined in Equation 48-52. Depending on the Reynold's number and tube arrangement, $a_1$ through $a_4$ are defined.

$$j = a_1 \left( \frac{1.33}{\frac{P_T}{D_o}} \right)^a Re^{a_2} \tag{47}$$

$$a = \frac{a_3}{1 + 0.14 Re^{a_4}} \tag{48}$$

$$a_1 = \begin{cases} In - lined: \begin{cases} 0.970, & if\ Re < 10 \\ 0.900, & if\ 10 < Re < 100 \\ 0.408, & if\ 100 < Re < 1000 \\ 0.107, & if\ 1000 < Re < 10000 \\ 0.370, & if\ 10000 < Re \end{cases} \\ Staggered: \begin{cases} 1.40, & if\ Re < 10 \\ 1.36, & if\ 10 < Re < 100 \\ 0.593, & if\ 100 < Re < 1000 \\ 0.321, & if\ 1000 < Re < 10000 \\ 0.321, & if\ 10000 < Re \end{cases} \end{cases} \tag{49}$$

$$a_2 = \begin{cases} In - lined: \begin{cases} -0.667, & if\ Re < 10 \\ -0.631, & if\ 10 < Re < 100 \\ -0.46, & if\ 100 < Re < 1000 \\ -0.266, & if\ 1000 < Re < 10000 \\ -0.395, & if\ 10000 < Re \end{cases} \\ Staggered: \begin{cases} -0.667, & if\ Re < 10 \\ -0.657, & if\ 10 < Re < 100 \\ -0.477, & if\ 100 < Re < 1000 \\ -0.388, & if\ 1000 < Re < 10000 \\ -0.388, & if\ 10000 < Re \end{cases} \end{cases} \tag{50}$$

$$a_3 = \begin{cases} 1.187, & if\ in - lined \\ 1.45, & if\ staggered \end{cases} \tag{51}$$

$$a_4 = \begin{cases} 0.37, & if\ in - lined \\ 0.519, & if\ staggered \end{cases} \tag{52}$$

$J_C$ is the correction factor for the window section of the heat exchanger. It depends on $F_C$, which is a fractional factor of the tube in the cross-section. A well-designed shell and tube direct expansion heat exchangers have $J_C$ close to 1.

$$J_C = 0.55 + 0.72F_C \tag{53}$$

$J_L$ is the correction factor for the baffle leakage, defined in Equations 54. The effect of fluid bypassing the baffle through the gaps between the wall and the baffles as well as baffle and the tube array is captured by $J_L$. Area factors $r_s$ and $r_l$ are a function of the cross-sectional geometries.

$$J_L = 0.44(1 - r_s) + \left(1 - 0.44(1 - r_s)\right)e^{-2.2r_l} \tag{54}$$

As shown in Equation 55, $J_B$ is the tube bundle bypass correction factor, accounting for the number of tubes and tube arrangement in the cross-section. $r_{ss}$ is defined as sealing strip ratio and $C_j$ is a calibration factor. $S_b$ and $S_m$ are tube bundle bypass area and cross-flow area, respectively.

$$J_B = \begin{cases} 1, \quad if\ r_{ss} \geq 0.5 \\ e^{-\frac{C_j S_b}{S_m\left(1-(2r_{ss})^{\frac{1}{3}}\right)}}, \quad if\ r_{ss} < 0.5 \end{cases} \tag{55}$$

$J_R$ is the laminar flow correction factor, shown in Equation 56, that depends on the Reynolds number and total number of tubes crossed, $N_{ct}$. For intermediate regime where $20 \leq Re < 100$, laminar flow correction factor is interlay interpolated.

$$J_R = \begin{cases} 1, \quad if\ Re \geq 100 \\ \left(\frac{10}{N_{ct}}\right)^{0.18}, \quad if\ Re < 20 \\ linearly\ interpolate, else \end{cases} \tag{56}$$

The heat transfer coefficient inside of the inner tube bundles is equivalent to the correlations used in FTHX. Further details on STDX modeling can be referenced in (Hellborg, 2017). Next, modeling of flooded type shell and tube heat exchanger will be presented.

### Shell and Tube Flooded Heat Exchanger (STFL)

As shown in Figure 15 and Figure 16, STFL shares similar geometries as STDX. Instead of the refrigerant flow inside of the inner tubes, STFL has a pool of refrigerant surrounding the inner tube bundle and the secondary fluid flow inside the inner tubes.

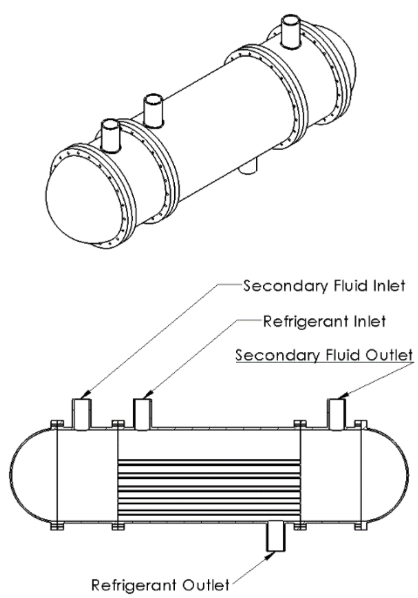


**Figure 15. Single Pass Flooded Shell and Tube Type Heat Exchanger**

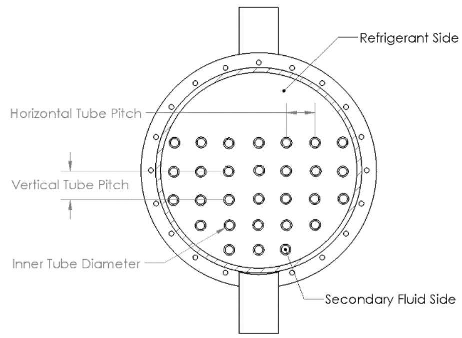


**Figure 16. Single Pass Flooded Shell and Tube Type Heat Exchanger Cross-section – Reprinted from (Park *et al.*, 2021).**

The STFL heat transfer coefficients for two-phase boiling were referenced from Hwang and Yao (1986). The average Nusselt number is defined in Equation 57, and the forced convective boiling through tube bundles are defined by the outer heat transfer coefficient ($\alpha_o$) in Equation 58 as a function of suppression factor ($S$), pool boiling heat transfer coefficient ($\bar{\alpha}_{nb}$), two-phase Reynolds number factor ($F$) and liquid-only forced convective heat transfer coefficient ($\alpha_l$).

$$\overline{Nu}_d = 0.366Re^{0.6}Pr^{\frac{1}{3}} \tag{57}$$

$$\alpha_o = S\bar{\alpha}_{nb} + F\alpha_l \tag{58}$$

Single-phase heat transfer coefficients for the STFL were modeled using the Churchill and Bernstein (1977) method. For the intermediate regime, where Re<10000, the correlation for the average Nusselt number in Equation 59 is used. For 10000<Re<40000, the following average Nusselt number in Equation 60 is used. For 40000<Re<400000, the average Nusselt number is shown below in Equation 61.

$$\overline{Nu} = 0.3 + \frac{0.62Re^{\frac{1}{2}}Pr^{\frac{1}{3}}}{\left[1 + (0.4/Pr)^{\frac{2}{3}}\right]^{\frac{1}{4}}} \tag{59}$$

$$\overline{Nu} = 0.3 + \frac{0.62Re^{\frac{1}{2}}Pr^{\frac{1}{3}}}{\left[1 + (0.4/Pr)^{\frac{2}{3}}\right]^{\frac{1}{4}}}\left[1 + \left(\frac{Re}{282000}\right)^{\frac{5}{8}}\right]^{\frac{4}{5}} \tag{60}$$

$$\overline{Nu} = 0.3 + \frac{0.62Re^{\frac{1}{2}}Pr^{\frac{1}{3}}}{\left[1 + (0.4/Pr)^{\frac{2}{3}}\right]^{\frac{1}{4}}}\left[1 + \left(\frac{Re}{282000}\right)^{\frac{1}{2}}\right] \tag{61}$$

For the condensing two-phase fluids, heat transfer coefficients from Briggs and Rose (1994) were used. The outer heat transfer coefficient ($\alpha_o$) is defined in Equation 62. Smooth tubes heat transfer coefficient is multiplied by the enhancement ratio ($\varepsilon_{\Delta T}$) that captures the heat transfer coefficient enhancement from the fins. Equation 63 defines the smooth heat transfer coefficient as a function of viscosity ($\mu_f$), thermal conductivity ($k_f$), density ($\rho_f$) of the condensate. $\tilde{\rho}$ is the difference in density of the vapor from the condensate, and $g$ is specific gravity. $h_{fg}$ is the latent heat of vaporization. $\Delta T$ is the vapor-side temperature difference and $d_{fin}$ is the diameter of the finned tube. Secondary fluid-side heat transfer coefficient is equivalent to the refrigerant-side correlation used for the FTHX. Next, the brazed plate heat exchanger is modeled.

$$\alpha_o = \varepsilon_{\Delta T}\alpha_s \tag{62}$$

$$\alpha_s = 0.728\left(\frac{k_f^3\rho_f\tilde{\rho}gh_{fg}\Delta T^3}{\mu_f d_{fin}}\right)^{0.25} \tag{63}$$

## Brazed Plate Heat Exchanger (BPHX)

BPHX is a compact heat exchanger that is comprised of channel plates sandwiched between the cover plates. The compact size of the BPHX makes it ideal for applications where the space is limited. Figure 17 shows a sample CAD model of a BPHX. Chevron-shaped ripples are stamped on the channel plate, designed to increase the heat transfer rate between the two fluids by increasing the turbulent flow presence inside the channels.

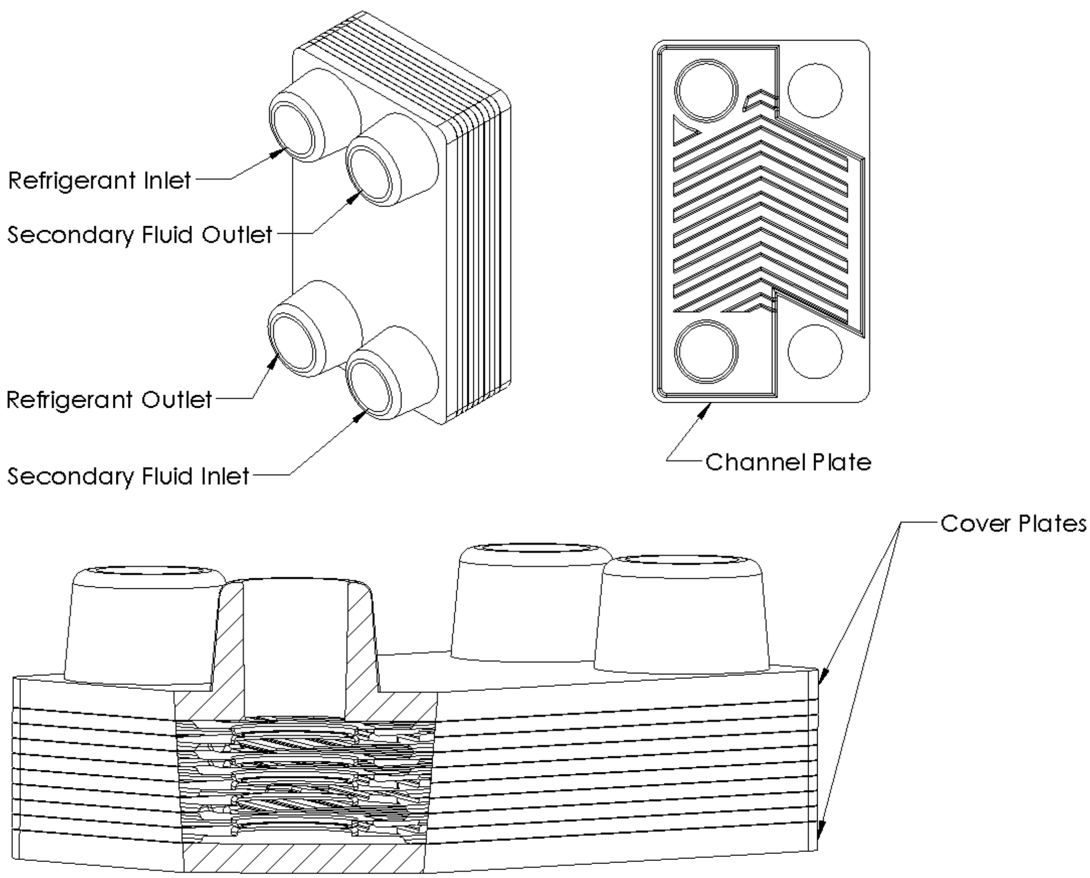


**Figure 17. A Sample CAD Model of Brazed Plate Heat Exchanger**

The heat transfer coefficients for the two-phase boiling process were referenced from Han *et al*. (2003). Nusselt number, $Nu$, is written as a function of non-dimensional geometric parameters ($Ge_1$ and $Ge_2$), equivalent Reynolds number ($Re_{eq}$) and boiling number ($Bo_{eq}$) and Prandtl number, ($Pr$).

$$Nu = Ge_1 Re_{eq}^{Ge_2} Bo_{eq}^{0.3} Pr^{0.4} \tag{64}$$

The two-phase condensing process was modeled with references from Hsieh and Lin (2002). Heat transfer coefficient ($\alpha_f$) is defined as a function of liquid thermal conductivity ($\lambda_f$), hydraulic diameter ($\mathrm{D}_h$), Reynolds number ($Re$), Prandtl number ($Pr$), average two-phase and wall viscosity ($\eta_{fm}$ and $\eta_{fw}$).

$$\alpha_f = 0.2092\left(\frac{\lambda_f}{\mathrm{D}_h}\right) Re^{0.78}\, Pr^{\frac{1}{3}}\left(\frac{\eta_{fm}}{\eta_{fw}}\right)^{0.14} \tag{65}$$

Single-phase Nusselt number correlations were modeled with correlation from Bogaert and Bölcs (1995). Nusselt number is defined as a function of Reynolds number ($Re$), Prandtl number ($Pr$), fluid dynamic viscosity ($\eta$), wall viscosity ($\eta_w$) and two constants ($B_1$ and $B_2$).

$$Nu = B_1 Re^{B_2}\, Pr^{\frac{1}{3}e^{\left(\frac{6.4}{Pr+30}\right)}}\left(\frac{\eta}{\eta_w}\right)^{\frac{0.3}{(Re+6)^{0.125}}} \tag{66}$$

$$\begin{cases} B_1 = 0.4621, B_2 = 0.4370, & if\ 0 \le Re < 20 \\ B_1 = 1.730, B_2 = 0, & if\ Re = 20 \\ B_1 = 0.0875, B_2 = 1, & if\ 20 < Re < 50 \\ B_1 = 4.4, B_2 = 0, & if\ Re = 50 \\ B_1 = 0.4223, B_2 = 0.6012, & if\ 50 < Re < 80 \\ B_1 = 5.95, B_2 = 0, & if\ Re = 80 \\ B_1 = 0.26347, B_2 = 0.7152, & if\ 80 < Re \end{cases} \tag{67}$$

## Microchannel Heat Exchanger (MCHX)

Similar to the FTHX, the microchannel heat exchanger is often used with air as the secondary fluid. Unlike FTHX, however, the MCHX achieves a more compact profile using microchannel arrays instead of more conventional cylindrical tubing for the refrigerant flow. MCHX is comprised of an inlet port (header), fins, and tubes for refrigerant flow. Fins are placed between the microchannel slabs for the secondary fluid flow across the heat exchanger. Figure 18 shows a sample CAD model of a MCHX.

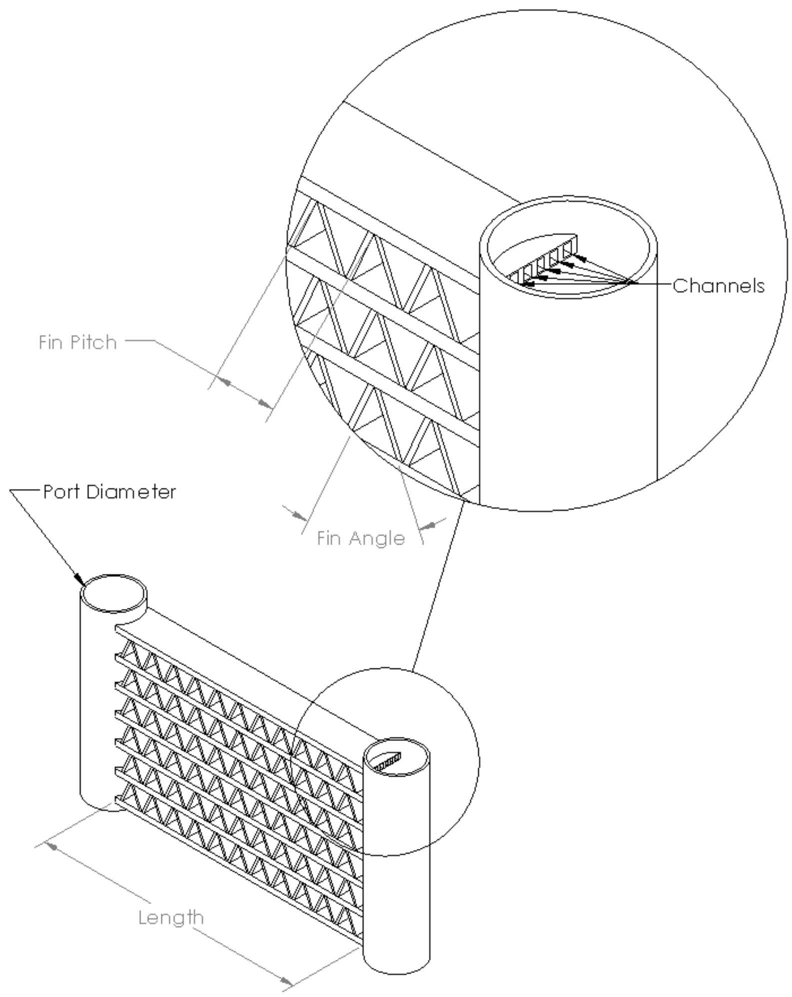


**Figure 18. A Sample CAD Model of Microchannel Heat Exchanger**

The secondary fluid-side heat transfer coefficients for the microchannel heat exchanger was modeled with Archaichia and Cowell (1988) in Equation 68 and 69. Secondary fluid-side heat transfer coefficient ($\alpha$) is defined in terms of heat capacity ($C_p$), Stanton number ($St$), and mass flux ($G_m$) Correlation for Stanton number is defined in Equation 69 in terms of louver angle ($\theta$), louver pitch-based Reynolds number ($Re_{lp}$), louver pitch ($L$), fin pitch ($F$) and tube transverse pitch ($T$). Heat transfer coefficient inside of the channels are equivalent to that of FTHX.

$$\alpha = C_p St G_m \tag{68}$$

$$St = \frac{1.544}{\theta}\left(0.936 - \frac{243}{Re_{lp}} - \frac{1.76F}{L} + 0.995\theta\right) Re_{lp}^{-0.59} \left(\frac{T}{L}\right)^{-0.09} \left(\frac{F}{L}\right)^{-0.04} \tag{69}$$

### Tube in Tube Heat Exchanger (TTHX)

A sample CAD model of tube in tube heat exchanger is shown in Figure 19. A smaller diameter tube is encased in a larger diameter tube in a TTHX, often spiraled to achieve a compact profile and induce heat transfer enhancement inside of the concentric tubes.

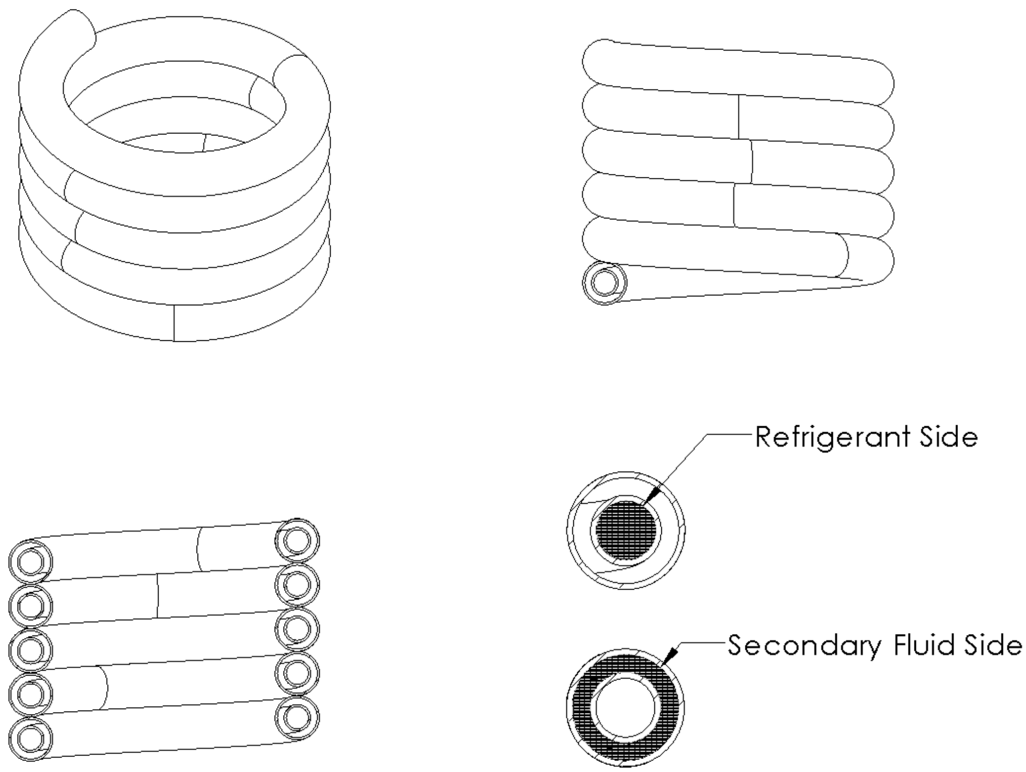


**Figure 19. A Sample CAD Model of Tube in Tube Heat Exchanger**

Single-phase heat transfer correlations for the tube in tube heat exchanger are referenced from Kumar *et al*. (2008). Single-phase Nusselt number is defined as follows in Equation 70-74. For the first two cases, the Nusselt number is defined as a function of Reynolds number ($Re$), Prandtl number ($Pr$), radius of helical pipe ($a$), and radius of coil ($R$). For all other single-phase cases, Nusselt number is referenced from Mori and Nakayama (1967) and shown in Equation 72. $K$ is Dean number and $\zeta$ is the thickness ratio, shown in Equation 73 and 74.

$$Nu = \frac{Pr}{26.2\left(Pr^{\frac{2}{3}} - 0.074\right)} Re^{0.8} \left(\frac{a}{R}\right)^{0.1} \left[1 + \frac{0.098}{\left[Re\left(\frac{a}{R}\right)^{2}\right]^{0.2}}\right] \tag{70}$$

$$for\ Pr \approx 1\ and\ Re\left(\frac{a}{R}\right)^{2} > 0.1$$

$$Nu = \frac{Pr^{0.4}}{41} Re^{\frac{5}{6}} \left(\frac{a}{R}\right)^{\frac{1}{12}} \left[1 + \frac{0.061}{\left[Re\left(\frac{a}{R}\right)^{2.5}\right]^{\frac{1}{6}}}\right] \tag{71}$$

$$for\ Pr > 1\ and\ Re\left(\frac{a}{R}\right)^{2.5} > 0.4$$

$$Nu = \frac{0.864}{\zeta} K^{0.5}(1 + 2.35K^{0.5}) \tag{72}$$

$$\zeta = \frac{2}{11}\left[1 + \sqrt{1 + \frac{77}{4}\frac{1}{Pr^{2}}}\right] \tag{73}$$

$$for\ Pr > 1$$

$$\zeta = \frac{1}{5}\left[2 + \sqrt{\frac{10}{Pr^{2}} - 1}\right] \tag{74}$$

$$for\ all\ else$$

For condensing two-phase fluids, correlation from Wongwises and Polsongkram (2006b) is used and shown in Equation 75-77. Nusselt number for two-phase condensing fluid is described as a function of equivalent Dean number ($De_{Eq}$), liquid-only Prandtl number ($Pr_l$), Boiling number ($Bo$), Martinelli parameter ($X_{tt}$), and reduced pressure ($P_r$). equivalent Dean number ($De_{Eq}$) is described as a function of liquid side and vapor side properties denoted with subscripts $l$ and $v$, respectively. $\mu$ is dynamic viscosity and $\rho$ is the density of the fluid. $d_i$ represents the inner tube inner diameter and $D_c$ is the spiral coil diameter of the TTHX. reduced pressure ($P_r$) is defined in Equation 77 as a function of saturation pressure ($P_{sat}$) and critical pressure ($P_{critical}$). Nusselt number in two-phase evaporation process is modeled with Wongwises and Polsongkram (2006a) in Equation 78. With heat transfer coefficients from the literature, the FCV model for heat exchangers is completed. To convert the FCV models into non-iterative empirical maps, the Monte Carlo sampling technique is used to characterize the heat exchangers in their operational and design spaces.

$$Nu_{tp} = 0.1352 De_{Eq}^{0.7654} Pr_l^{0.8144} (Bo \cdot 10^4)^{0.112} X_{tt}^{0.0432} P_r^{-0.3356} \tag{75}$$

$$De_{Eq} = \left[ Re_l + Re_v \left(\frac{\mu_v}{\mu_l}\right)\left(\frac{\rho_f}{\rho_g}\right)^{0.5} \right] \left(\frac{d_i}{D_C}\right)^{0.5} \tag{76}$$

$$P_r = \frac{P_{sat}}{P_{critical}} \tag{77}$$

$$Nu_{tp} = 6895.98 De_{Eq}^{0.432} Pr_l^{-5.055} (Bo \cdot 10^4)^{0.132} X_{tt}^{-0.0238} \tag{78}$$

## Monte Carlo Sampling

Monte Carlo simulation utilizes randomness in its sampling method to survey potential outcomes of its decision space. For a heat exchanger, a given range of mass flow rates, pressures, inlet quality, and heat exchanger design variables are explored with the Monte Carlo sampling method. After the points had been sampled within the operation and design space, the convergence of each sample point is checked, and poor convergence points are filtered out. The values used for the filtering parameters, final objective function value, optimality, and step size, are set by the user. Figure 20 shows the heat exchanger effectiveness of the sampled points as a function of refrigerant quality and pressures at the heat exchanger inlet. From the sampled data, a least-squares fitting is performed. Figure 21 shows a resulting surface. Not all points are located on the fitted surface. This is due to effectiveness being a function of not only the inlet quality and pressure but also of mass flow rate, which could not be plotted altogether. In the next subsection, details on this mapping process will be discussed.

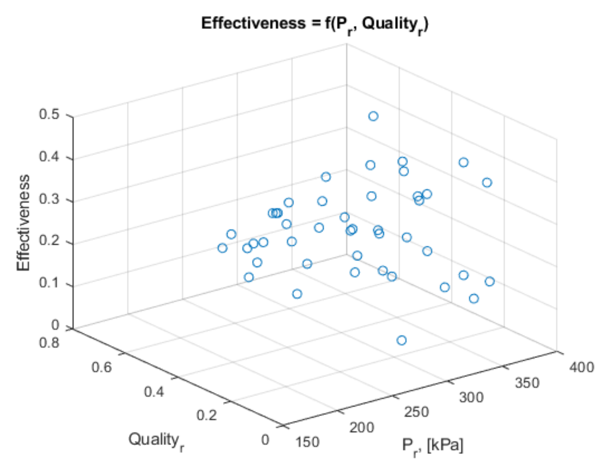


**Figure 20. Monte Carlo Sampling of Heat Exchanger Over Operational Space**

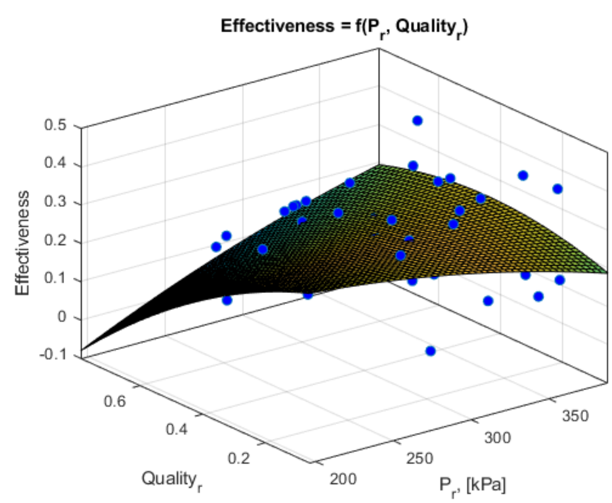


**Figure 21. Least Squares Fit of Sampled Heat Exchanger Over Its Operational Space**

## Heat Exchanger Mapping Method

Monte Carlo sampling of heat exchangers was previously performed within a given range of mass flow rates, pressures, inlet quality, and length for a shell and tube flooded type heat exchanger (STFL). After the points have been sampled within the operation and design space, the convergence of each sample point is checked, and ones with poor convergence metrics were filtered out. With filtered samples, the effectiveness of a heat exchanger (ε) is represented with Equation 79, as a function of heat exchanger capacity ($Q_{hx}$), constant pressure specific heat capacity of the secondary fluid ($C_s$), mass flow rate of the refrigerant ($\dot{m}_r$), refrigerant temperature at the inlet ($T_r$) and secondary fluid inlet temperature ($T_s$).

$$\varepsilon = \frac{Q_{hx}}{C_s \cdot \dot{m}_r \cdot (T_r - T_s)} \tag{79}$$

In Equation 80, heat exchanger effectiveness, the refrigerant charge ($m_{ch}$), pressure drop ($\Delta P_{hx}$) and mass ($m_{hx}$) are mapped as a function of pressure ($P_i$), refrigerant mass flow rate ($\dot{m}_r$), inlet quality ($x_i$), secondary fluid inlet temperature ($T_{ext}$) and design variable ($L$). Shown in Figure 22 through Figure 24 are the comparison of heat exchanger effectiveness, heat exchanger mass, and refrigerant mass from the map versus the raw data used to generate the map.

$$\begin{aligned}\{\varepsilon, m_{ch}, \Delta P_{hx}, m_{hx}\} = {} & d_1 + d_2 L + d_3 T_{ext} + d_4 P_i + d_5 \dot{m}_r + d_6 x_i + d_7 L^2 + \\ & d_8 L T_{ext} + d_9 L P_i + d_{10} L \dot{m}_r + d_{11} L x_i + d_{12} {T_{ext}}^2 + d_{13} T_{ext} P_i + d_{14} T_{ext} \dot{m}_r + \\ & d_{15} T_{ext} x_i + d_{16} {P_i}^2 + d_{17} P_i \dot{m}_r + d_{18} P_i x_i + d_{19} {\dot{m}_r}^2 + d_{20} \dot{m}_r x_i + d_{21} {x_i}^2\end{aligned} \tag{80}$$

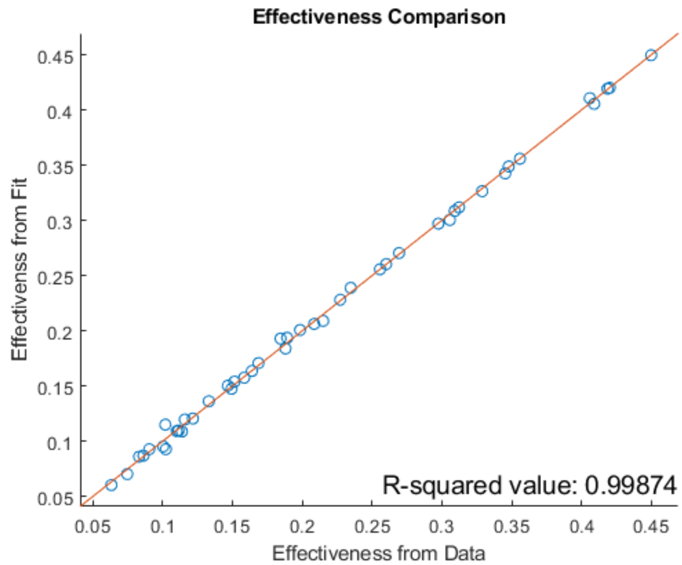


**Figure 22. Comparison of Predictions of Heat Exchanger Effectiveness with Data from Monte Carlo Sampling – Reprinted from (Park *et al.*, 2021).**

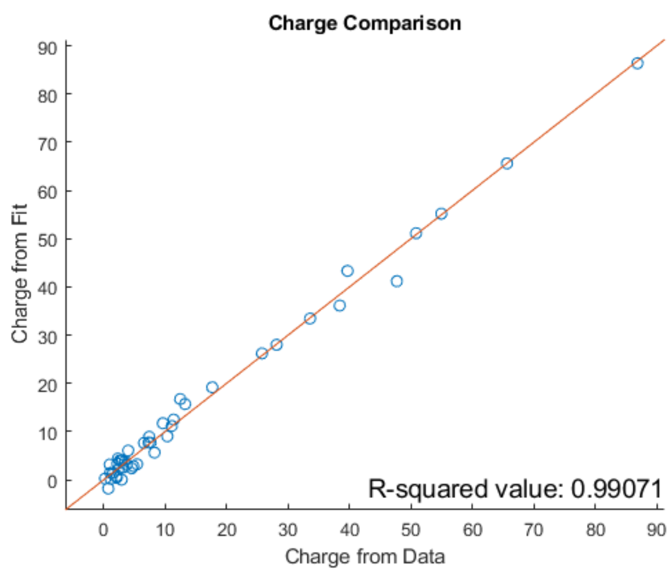


**Figure 23. Heat Exchanger Refrigerant Charge Level Comparison – Reprinted from (Park *et al.*, 2021).**

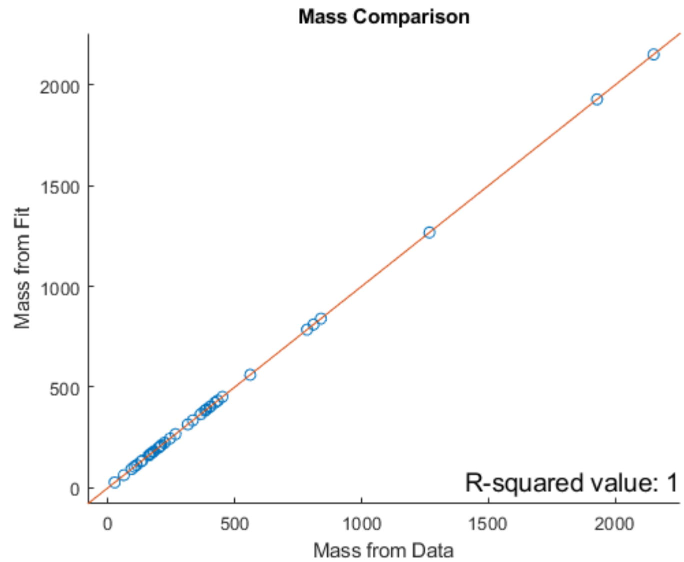


**Figure 24. Heat Exchanger Mass Comparison – Reprinted from (Park *et al.*, 2021).**

The mapping approach shows good predictions for the heat exchanger. The heat exchanger pressure loss map is not generated since the STFL is assumed to have negligible pressure loss. However, the same method can be used to map pressure losses in other types of heat exchangers. Microchannel, fin and tube, brazed plate, tube in tube, shell and tube flood type, and shell and tube direct expansion type heat exchangers were mapped using the presented method. With the heat exchanger mapping approach defined, the oil effect inside of the heat exchangers will be discussed next.

**Oil Effect**

Oil is mixed into the refrigerant to adequately lubricate the compressor in its operation. The presence of oil, however, also acts as a thermal barrier inside the heat exchangers. This is called the oil effect. A simple model is embedded into the heat exchanger solver to capture the effect of oil on heat transfer degradation. As shown in

Figure 25 and Equation 81, a simple linear relationship of percent oil in the working fluid to the heat transfer degradation is assumed. $DF$ is the degradation factor (a value between 0 and 1) and $a$ is slope on the percent oil versus degradation factor plot. $x_{oil}$ is the percent oil in the refrigerant. The user has the freedom to input $a$ in order to define the heat transfer degradation factor characteristics. In the next subsection, a method to represent heat exchangers as simple polynomials will be discussed.

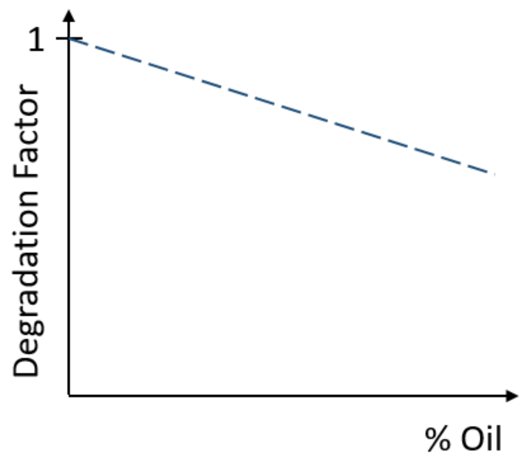


**Figure 25. Heat Transfer Degradation Factor as a Function of Percent Oil**

$$DF = ax_{oil} + 1 \tag{81}$$

# CHAPTER IV

# SYSTEM MODEL

With compressor and heat exchanger modeling discussed in Chapter II and Chapter III, system modeling is needed to complete the chiller model. Next, inter-component modeling of motor cooling and vapor injection will be covered. The cooling of the compressor motor using the refrigerant in the system will be covered in the next subsection. Afterward, vapor injection, which increases cooling capacity and system efficiency, will be covered.

## Motor Cooling

The motor used to drive the compressor needs to be adequately cooled to prevent overheating and motor failure. A small portion of refrigerant is sometimes channeled after the expansion valve to cool the compressor motor in chillers. This motor cooling circuit, using the working fluid, is modeled in Equation 82-84. Given the target motor surface temp, the refrigerant mass flow rate required to sufficiently cool the motor is searched by the optimizer. In the motor cooling model, the outlet of the motor cooling circuit is always assumed to be superheated vapor. Since the mass flow rate of the motor cooling circuit is usually ~1% and certainly no more than 3%, the combined pressure of the motor cooling line outlet pressure and evaporator outlet pressure is assumed to be equal to the evaporator outlet pressure. $\beta_{MC}$ is a calibration factor placed to match experimental data. Table 2 shows the list of variables for the motor cooling circuit.

$$\dot{Q}_m = \dot{Q}_s + \dot{Q}_{MC} \tag{82}$$

$$\dot{Q}_s = \alpha_m A_m (T_m - T_s) \tag{83}$$

$$\dot{Q}_{MC} = \beta_{MC} \dot{m} C_p (T_m - T_r) \tag{84}$$

**Table 2. Motor Cooling Circuit Inputs and Outputs**

| Type | Variable | Description |
|---|---|---|
| Program Input | $\dot{Q}_m$ | Heat transfer rate of motor heat (motor inefficiency is all converted to heat) |
| | $\alpha_m$ | Convection heat transfer coefficient of motor surface to the surroundings |
| | $A_m$ | Outer surface area of the motor assembly |
| | $T_s$ | Temperature of the surrounding |
| | $T_m$ | Target motor surface temperature |
| | $\beta_{MC}$ | Tuning factor for the motor cooling circuit |
| | $T_r$ | Saturation temperature of the refrigerant at motor cooling circuit inlet |
| Calculated Variables | $\dot{Q}_s$ | Heat transfer rate of motor to the surroundings |
| | $\dot{Q}_{MC}$ | Heat transfer rate of motor to the motor cooling circuit |
| | $\dot{m}$ | Mass flow rate of the refrigerant in the motor cooling circuit |

## Vapor Injection

Vapor injection (VI) is sometimes used to increase the cooling capacity and the system COP. In the case of VI using a subcooler, a portion of the working fluid is expanded to lower pressure and channeled into the subcooler to further subcool the working fluid in the mainline. The evaporated working fluid out of the subcooler is then injected into the compressor at the injection pressure. Figure 26 shows the P-h diagram of a system with vapor injection.

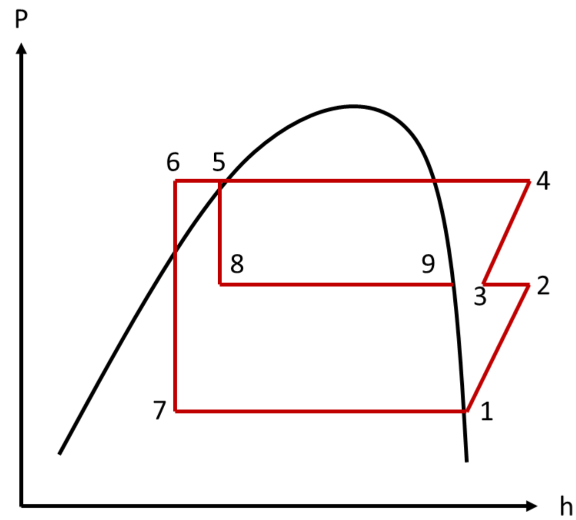


**Figure 26. P-h Diagram of a System with VI**

Equation 85-87 details the vapor injection process. $\dot{m}_{tot}$ represents the mass flow rate in the condenser and $\dot{m}_{inj}$ is the injection mass flow rate. At the outlet of the condenser, refrigerant enthalpy is represented by $h_5$. $h_6$ is the enthalpy of the refrigerant in the mainline being further subcooled in the subcooler and $h_9$ is the vapor enthalpy at the injection site. At the outlet of the condenser, a portion of the working fluid will be pulled and expanded to an intermediate pressure with the enthalpy of $h_8$. Equations 86 and 87 show the enthalpy exchange in the intermediate pressure.

$$h_5\dot{m}_{tot} = h_6(\dot{m}_{tot} - \dot{m}_{inj}) + h_9\dot{m}_{inj} \tag{85}$$

$$h_9 = h_8 + \Delta h_{BPHX} \tag{86}$$

$$\Delta h_{BPHX} = f(\dot{m}_{tot}, \dot{m}_{inj}, P_{cond}, P_{inj}, Subcool) \tag{87}$$

Since expansion through a valve is assumed to be an isenthalpic process, the enthalpy value at $h_8$ is same as $h_5$. The enthalpy increase in the brazed plate subcooler is represented with $\Delta h_{BPHX}$, as a function of $\dot{m}_{tot}$ $\dot{m}_{inj}$, $P_{cond}$, $P_{inj}$, $Subcool$ which are condenser mass flow rate, injection mass flow rate, condenser pressure, injection pressure, and degree of subcool, respectively. Enthalpy at the injection site can be represented as a sum of $h_8$ and $\Delta h_{BPHX}$. Equations 88-90 represent the vapor injection process in the compressor.

$$h_3 \dot{m}_{tot} = h_2 \dot{m}_{evap} + h_9 \dot{m}_{inj} \tag{88}$$

$$h_2 = \frac{(h_{2s} - h_1)}{\eta_a} + h_1 \tag{89}$$

$$h_4 = \frac{(h_{4s} - h_3)}{\eta_a} + h_3 \tag{90}$$

$h_1$ is the enthalpy at the outlet of the evaporator, which gets compressed to an intermediate pressure and enthalpy of $h_2$. The efficiency of the compressor ($\eta_a$) is a given parameter used to calculate the enthalpy increase in the compressor. Refrigerant is then injected as vapor and results in a mixture with the enthalpy of $h_3$. The mixed vapor at state 3 gets compressed further to state 4 and goes into the condenser. Detailed solving procedure for VI is outlined in the Appendix.

CHAPTER V

# SIMULATION TOOL

The simulation software tool was developed based on the component and system models discussed in previous chapters. In this section, features of the simulator will be demonstrated.

## Search Algorithm

The simulator uses MATLAB's built-in gradient-based search algorithm called fmincon. Mine Kaya of Dr. Hajimirza's Lab developed a replacement code in parallel. Details on this home-grown search algorithm are separately documented.

## Initialization

The graphical user interface (GUI) must be initialized first. GUIDE, a built-in MATLAB GUI workspace, can be used to both edit the GUI figures and initialize. First, open MATLAB and set the working directory. In the Command Window, type "guide" as shown in Figure 27 below.


**Figure 27. View of the MATLAB Command Window**

Once GUIDE Quick Start window is open, select EMERSON.fig and click "Open" as shown in Figure 28. Depending on the computer, this procedure might need a few minutes to load.

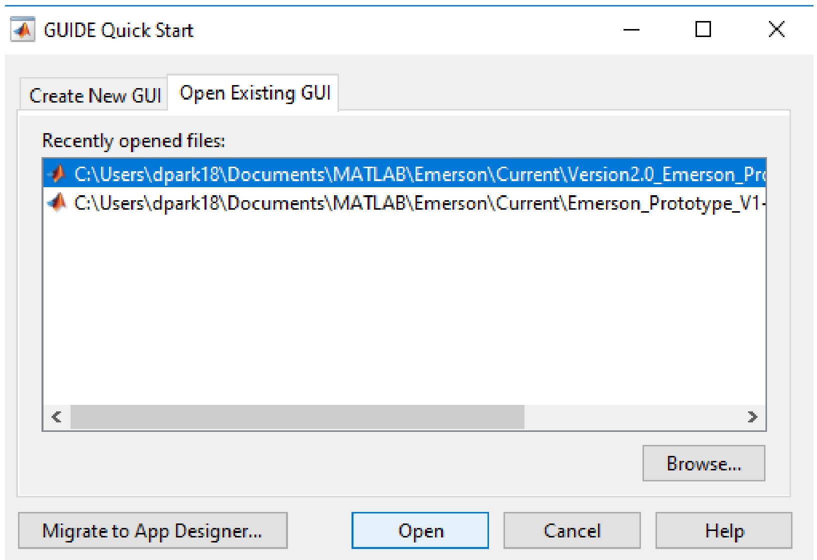


**Figure 28. GUIDE Quick Start Window**

When the window pictured in Figure 29 opens, click "Run Figure" button or hit (Ctrl + T).

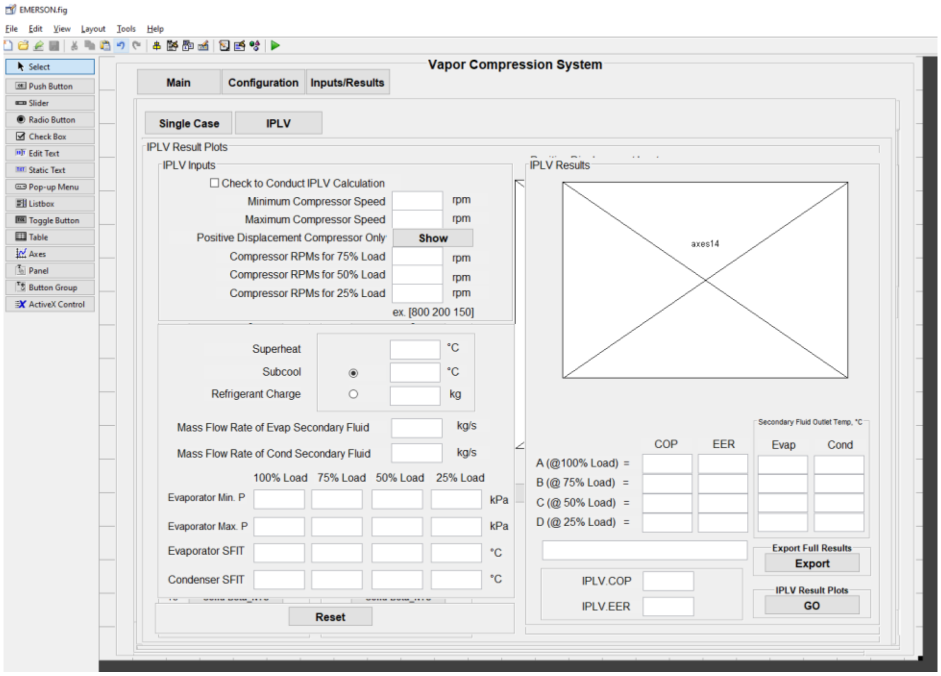


**Figure 29. GUIDE Figure Window**

Once GUI initializes, a pop-up window will open to let the user know of completed initialization. Please click “OK” in Figure 30 and proceed to the main page.

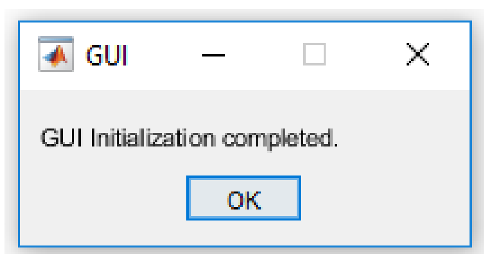


**Figure 30. GUI Initialization Complete Notification Window**

As shown in Figure 31, the main simulator page has options to select units, refrigerants, secondary fluids of both heat exchangers. It also has an option to load a system configuration by entering the file path.

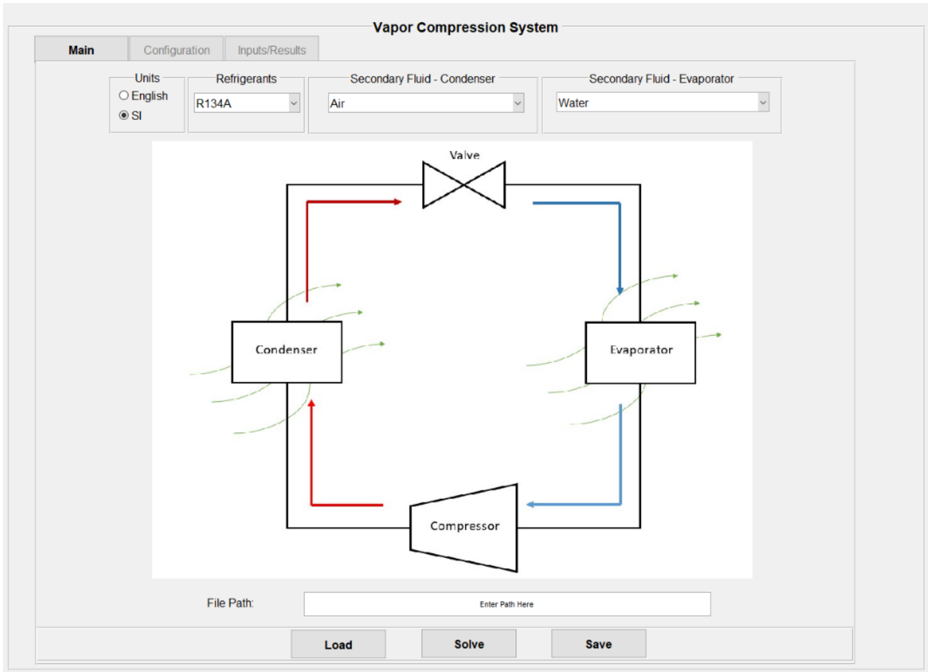


**Figure 31. Main Simulator Page**

## Auto-load Feature using Microsoft Excel

Shown in Figure 32 is a Microsoft Excel sheet used to load the simulator automatically. The formatted sheet follows the layout of the GUI. Therefore, each corresponding element can quickly be identified. In the Main section, there is an option of leaving a comment. Users are encouraged to save the file path and any additional information about the saved configuration here.

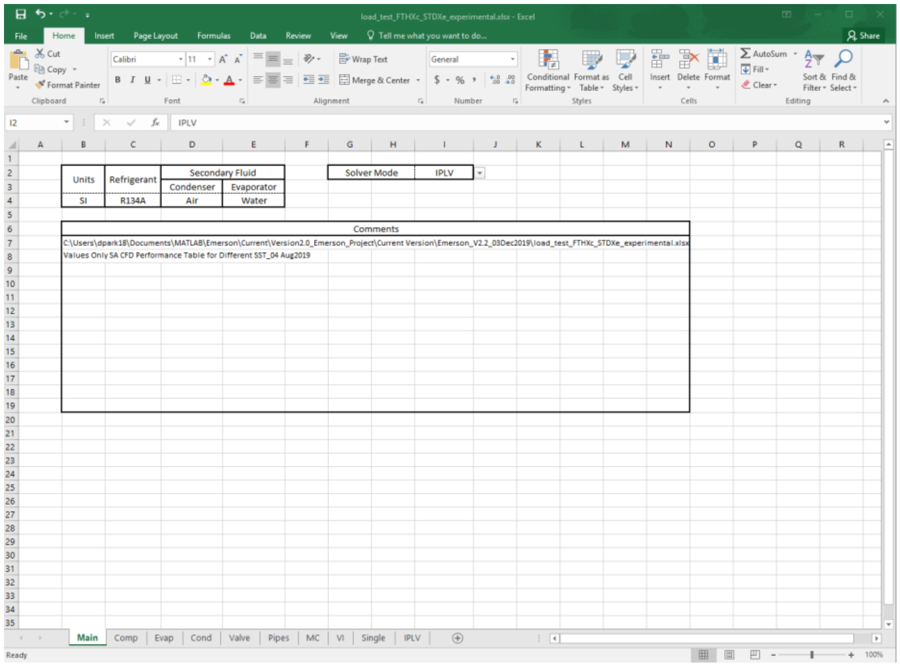


**Figure 32. Main Microsoft Excel Load Page**

“Comp” section in Figure 33 holds the lines to enter in compressor parameters and maps. AHRI coefficients are available for the positive displacement type compressors, and Schiffman coefficients are available for the centrifugal-type compressors.

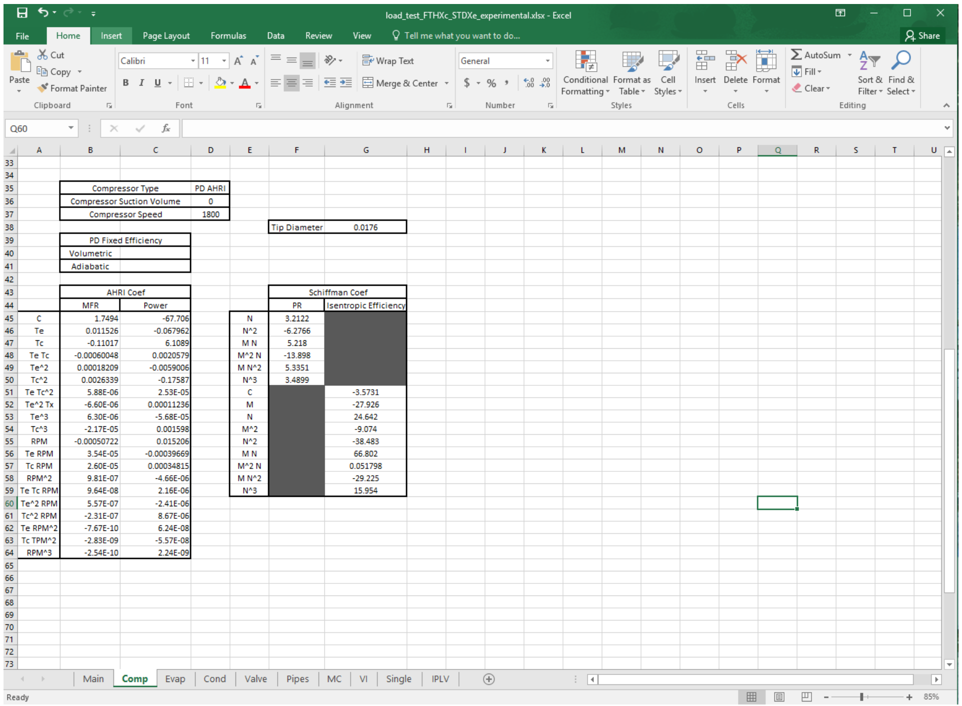

**Figure 33. Microsoft Excel Load Page – Compressor**

Figure 34 and Figure 35 show “Evap” and “Cond” sections. Heat exchanger maps and multipliers can be entered in these sections.

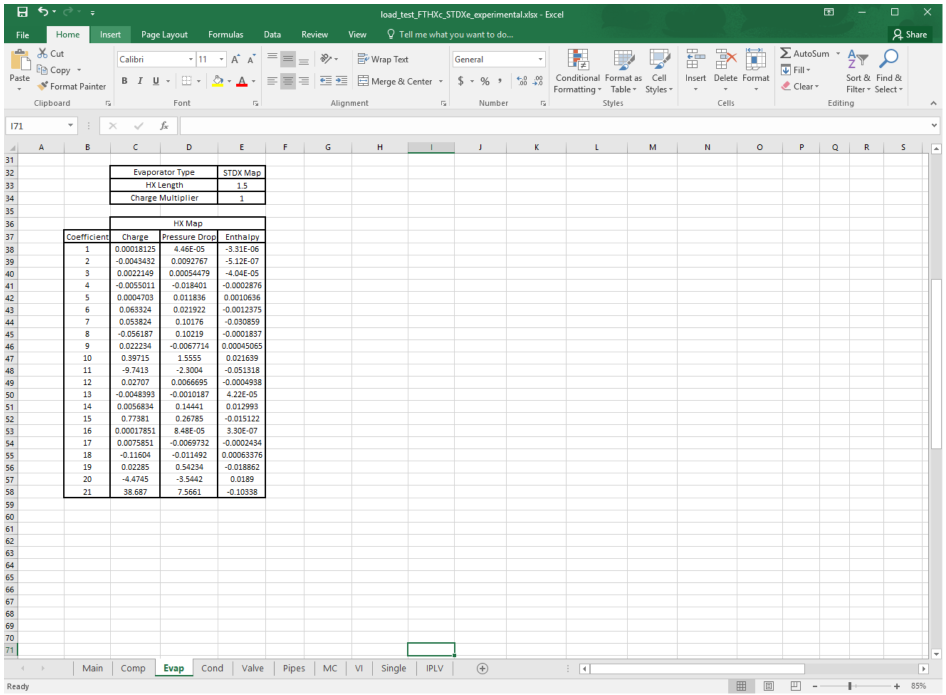


| | |
|---|---|
| Evaporator Type | STDX Map |
| HX Length | 1.5 |
| Charge Multiplier | 1 |

| | HX Map | | |
|---|---|---|---|
| Coefficient | Charge | Pressure Drop | Enthalpy |
| 1 | 0.00018125 | 4.46E-05 | -3.31E-06 |
| 2 | -0.0043432 | 0.0092767 | -5.12E-07 |
| 3 | 0.0022149 | 0.00054479 | -4.04E-05 |
| 4 | -0.0055011 | -0.018401 | -0.0002876 |
| 5 | 0.0004703 | 0.011836 | 0.0010636 |
| 6 | 0.063324 | 0.021922 | -0.0012375 |
| 7 | 0.053824 | 0.10176 | -0.030859 |
| 8 | -0.056187 | 0.10219 | -0.0001837 |
| 9 | 0.022234 | -0.0067714 | 0.00045065 |
| 10 | 0.39715 | 1.5555 | 0.021639 |
| 11 | -9.7413 | -2.3004 | -0.051318 |
| 12 | 0.02707 | 0.0066695 | -0.0004938 |
| 13 | -0.0048393 | -0.0010187 | 4.22E-05 |
| 14 | 0.0056834 | 0.14441 | 0.012993 |
| 15 | 0.77381 | 0.26785 | -0.015122 |
| 16 | 0.00017851 | 8.48E-05 | 3.30E-07 |
| 17 | 0.0075851 | -0.0069732 | -0.0002434 |
| 18 | -0.11604 | -0.011492 | 0.00063376 |
| 19 | 0.02285 | 0.54234 | -0.018862 |
| 20 | -4.4745 | -3.5442 | 0.0189 |
| 21 | 38.687 | 7.5661 | -0.10338 |

**Figure 34. Microsoft Excel Load Page – Evaporator**

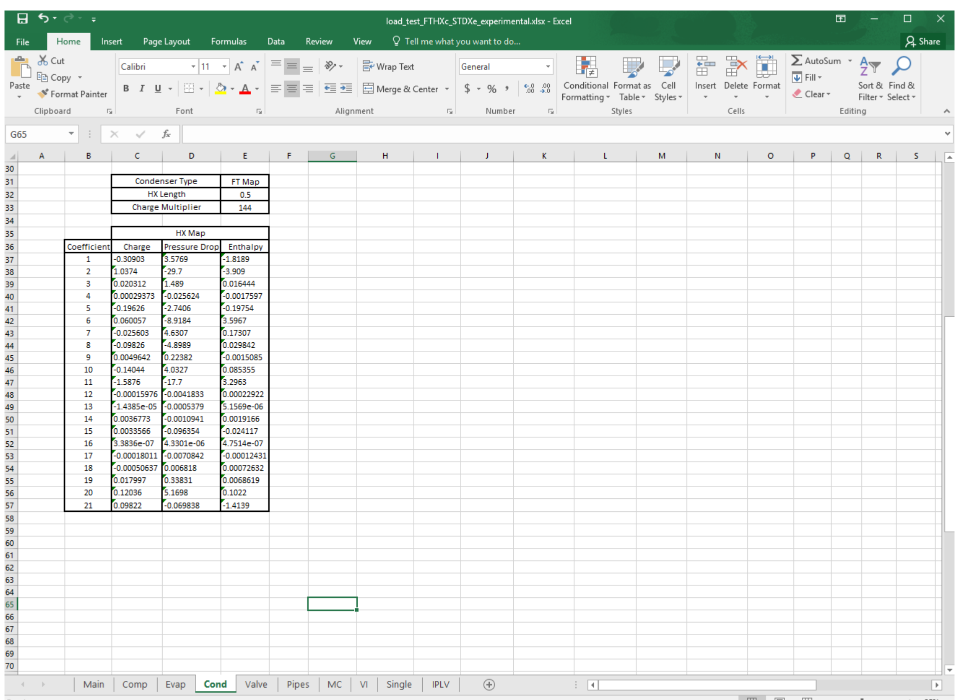


| | |
|---|---|
| Condenser Type | FT Map |
| HX Length | 0.5 |
| Charge Multiplier | 144 |

| | HX Map | | |
|---|---|---|---|
| Coefficient | Charge | Pressure Drop | Enthalpy |
| 1 | -0.30903 | 3.5769 | -1.8189 |
| 2 | 1.0374 | -29.7 | -3.909 |
| 3 | 0.020312 | 1.489 | 0.016444 |
| 4 | 0.00029373 | -0.025624 | -0.0017597 |
| 5 | -0.19626 | -2.7406 | -0.19754 |
| 6 | 0.060057 | -8.9184 | 3.5967 |
| 7 | -0.025603 | 4.6307 | 0.17307 |
| 8 | -0.09826 | -4.8989 | 0.029842 |
| 9 | 0.0049642 | 0.22382 | -0.0015085 |
| 10 | -0.14044 | 4.0327 | 0.085355 |
| 11 | -1.5876 | -17.7 | 3.2963 |
| 12 | -0.00015976 | -0.0041833 | 0.00022922 |
| 13 | -1.4385e-05 | -0.0005379 | 5.1569e-06 |
| 14 | 0.0036773 | -0.0010941 | 0.0019166 |
| 15 | 0.0033566 | -0.096354 | -0.024117 |
| 16 | 3.3836e-07 | 4.3301e-06 | 4.7514e-07 |
| 17 | -0.00018011 | -0.0070842 | -0.00012431 |
| 18 | -0.00050637 | 0.006818 | 0.00072632 |
| 19 | 0.017997 | 0.33831 | 0.0068619 |
| 20 | 0.12036 | 5.1698 | 0.1022 |
| 21 | 0.09822 | -0.069838 | -1.4139 |

**Figure 35. Microsoft Excel Load Page – Condenser**

“Valve” section in Figure 36 presents an option to select either the electronic expansion valve (EXV) and thermostatic expansion valve (TXV).

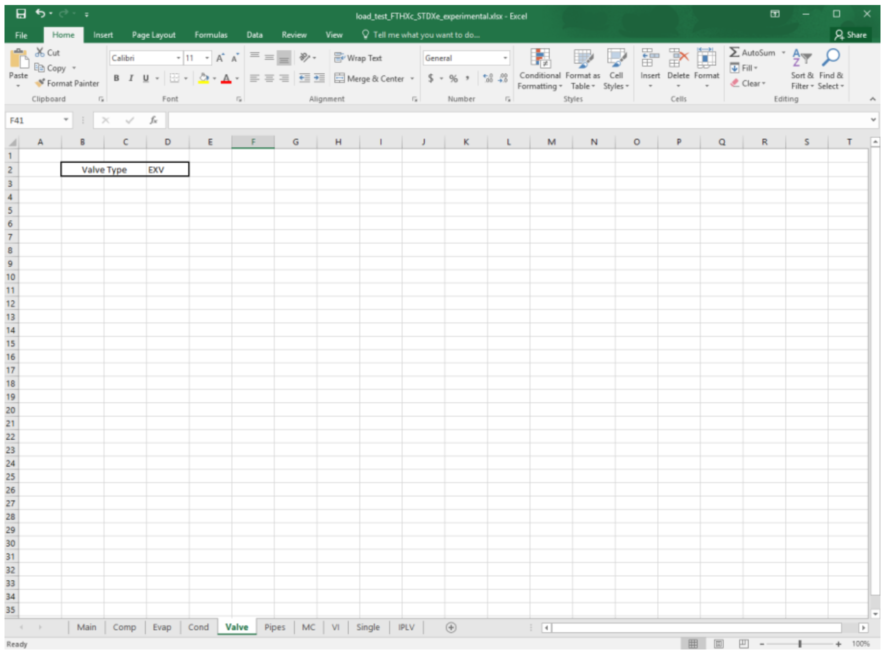


**Figure 36. Microsoft Excel Load Page – Valve**

“Pipes” section in Figure 37 has an option to enter the connecting pipe information.

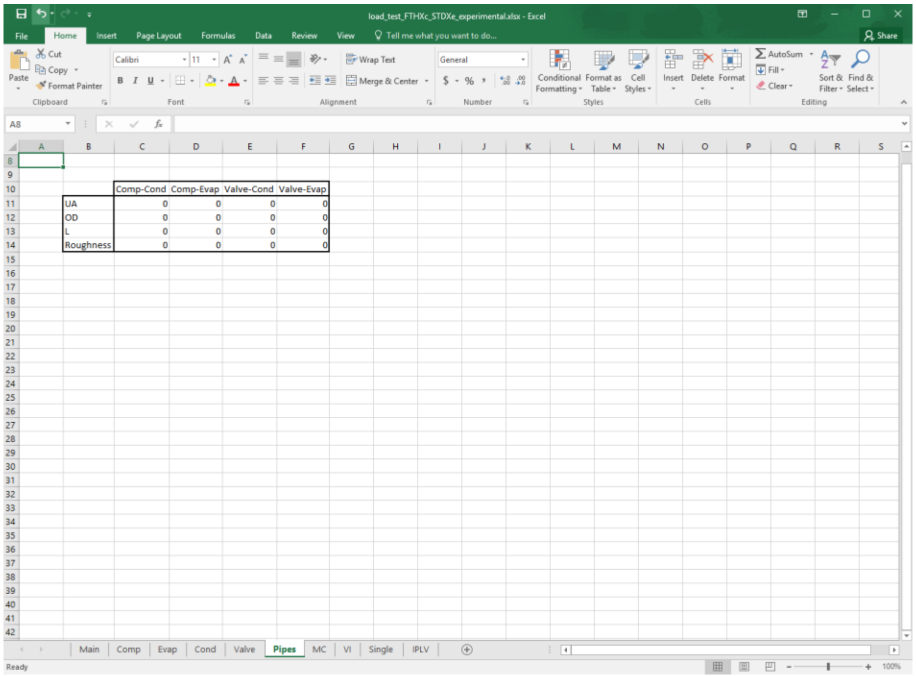


**Figure 37. Microsoft Excel Load Page – Pipes**

"MC" section in Figure 38 allows the users to input motor cooling information.

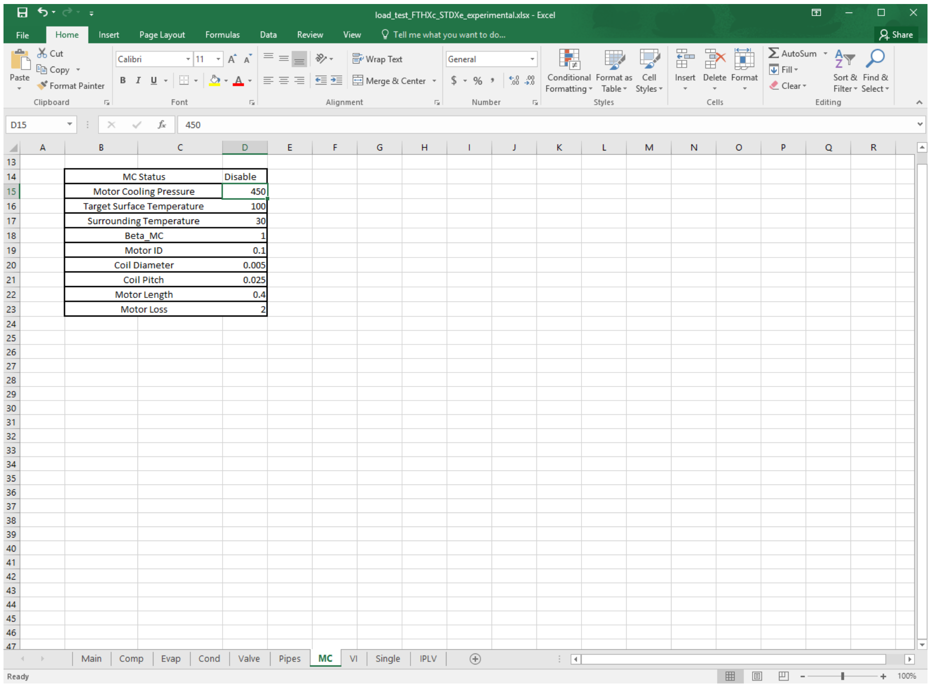


**Figure 38. Microsoft Excel Load Page - Motor Cooling**

"VI" section in Figure 39 allows the user to enter the vapor injection circuit and heat exchanger information.

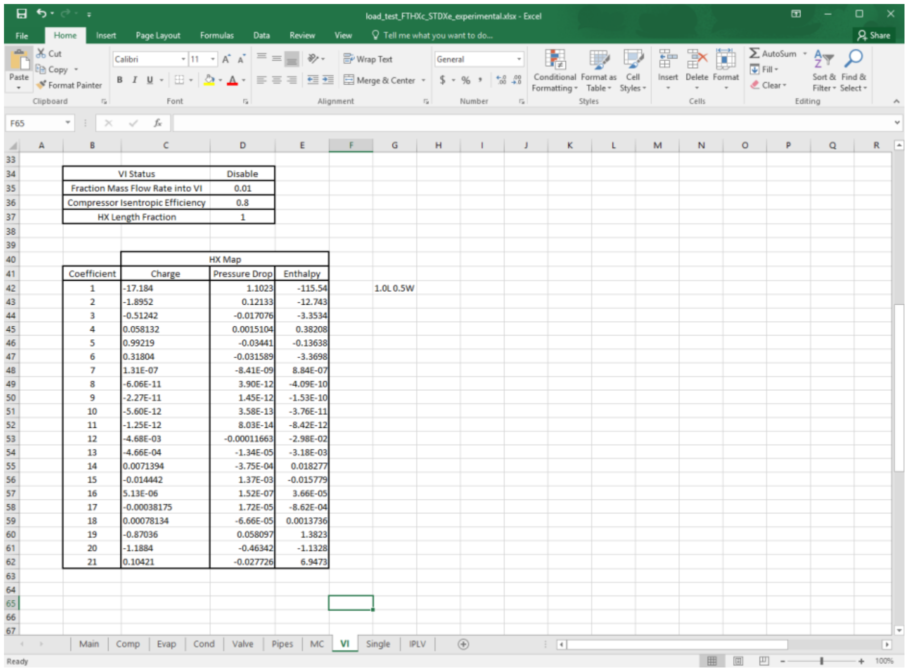

| | |
|---|---|
| VI Status | Disable |
| Fraction Mass Flow Rate into VI | 0.01 |
| Compressor Isentropic Efficiency | 0.8 |
| HX Length Fraction | 1 |

| | HX Map | | |
|---|---|---|---|
| Coefficient | Charge | Pressure Drop | Enthalpy |
| 1 | -17.184 | 1.1023 | -115.54 |
| 2 | -1.8952 | 0.12133 | -12.743 |
| 3 | -0.51242 | -0.017076 | -3.3534 |
| 4 | 0.058132 | 0.0015104 | 0.38208 |
| 5 | 0.99219 | -0.03441 | -0.13638 |
| 6 | 0.31804 | -0.031589 | -3.3698 |
| 7 | 1.31E-07 | -8.41E-09 | 8.84E-07 |
| 8 | -6.06E-11 | 3.90E-12 | -4.09E-10 |
| 9 | -2.27E-11 | 1.45E-12 | -1.53E-10 |
| 10 | -5.60E-12 | 3.58E-13 | -3.76E-11 |
| 11 | -1.25E-12 | 8.03E-14 | -8.42E-12 |
| 12 | -4.68E-03 | -0.00011663 | -2.98E-02 |
| 13 | -4.66E-04 | -1.34E-05 | -3.18E-03 |
| 14 | 0.0071394 | -3.75E-04 | 0.018277 |
| 15 | -0.014442 | 1.37E-03 | -0.015779 |
| 16 | 5.13E-06 | 1.52E-07 | 3.66E-05 |
| 17 | -0.00038175 | 1.72E-05 | -8.62E-04 |
| 18 | 0.00078134 | -6.66E-05 | 0.0013736 |
| 19 | -0.87036 | 0.058097 | 1.3823 |
| 20 | -1.1884 | -0.46342 | -1.1328 |
| 21 | 0.10421 | -0.027726 | 6.9473 |



**Figure 39. Microsoft Excel Load Page - Vapor Injection**

“Single” corresponds to the Single Case solver mode on the GUI. Users can specify the parameters for the Single Case solving mode, shown in Figure 40.

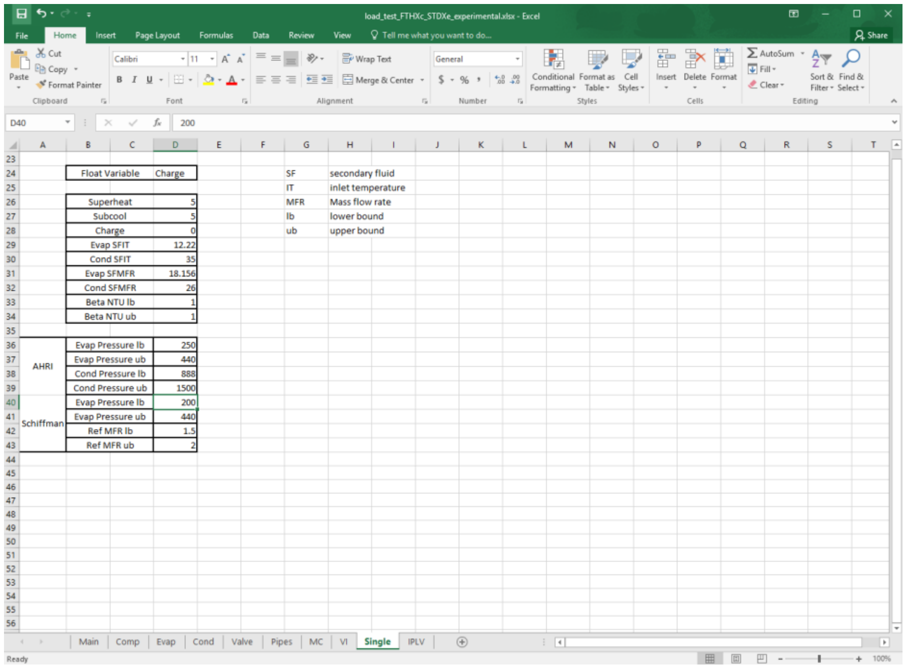


**Figure 40. Microsoft Excel Load Page - Single Case Solver**

“IPLV” section in Figure 41 allows the users to specify the IPLV calculation parameters.

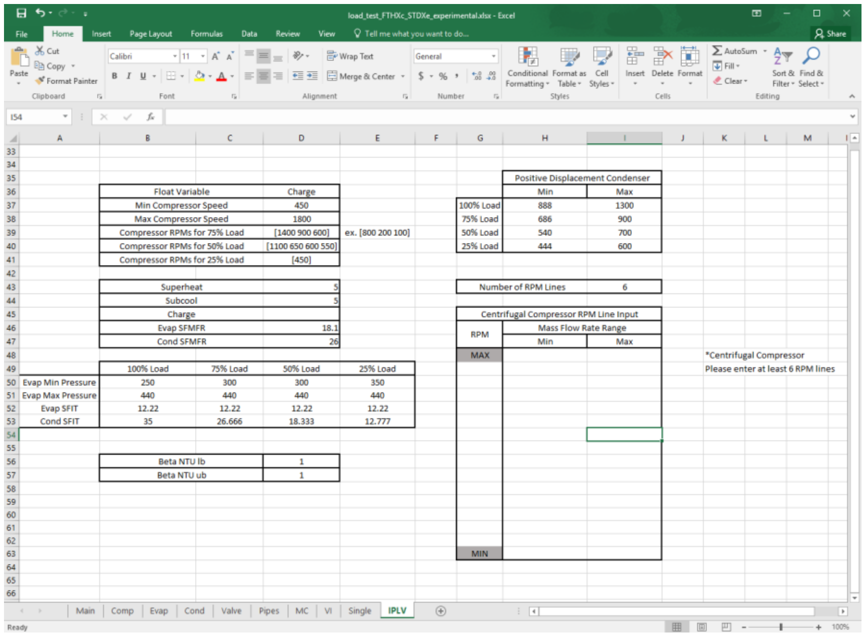

**Figure 41. Microsoft Excel Load Page - IPLV Solver**

The Excel sheet in Figure 42 can now be loaded onto the simulator. First, identify the file location and enter the file path in the simulator. Click on “Load” to load the system configuration from the Excel file. Loading takes around a minute to complete.

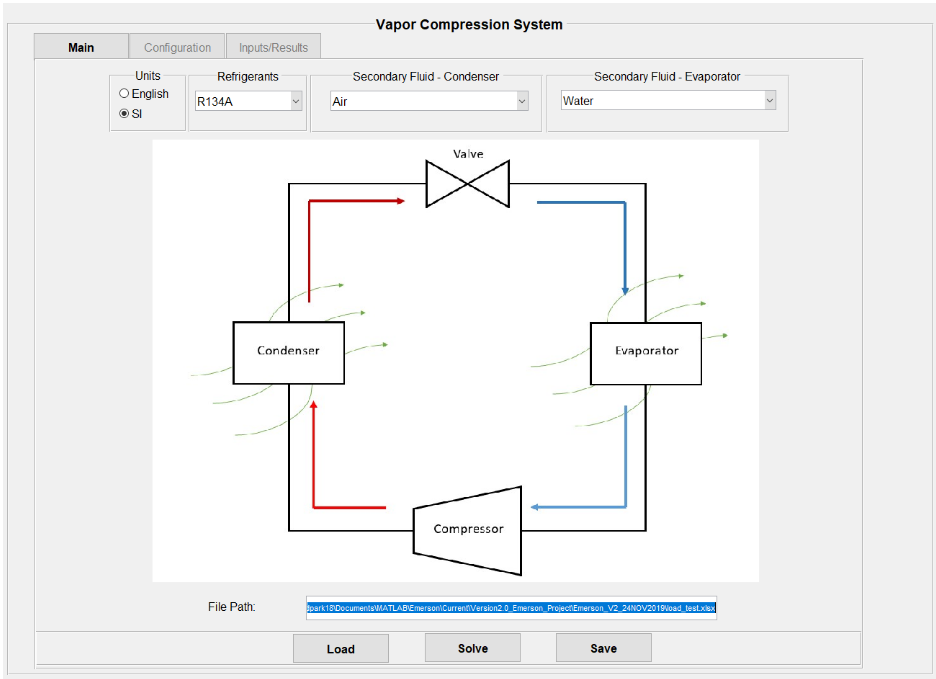


**Figure 42. Main Simulator Window with File Path Specified**

## Simulator – Compressor Specifications

In the “Configuration” tab shown in Figure 43, there are options to specify each system component. First, the compressor is defined by selecting the type of compressor used.

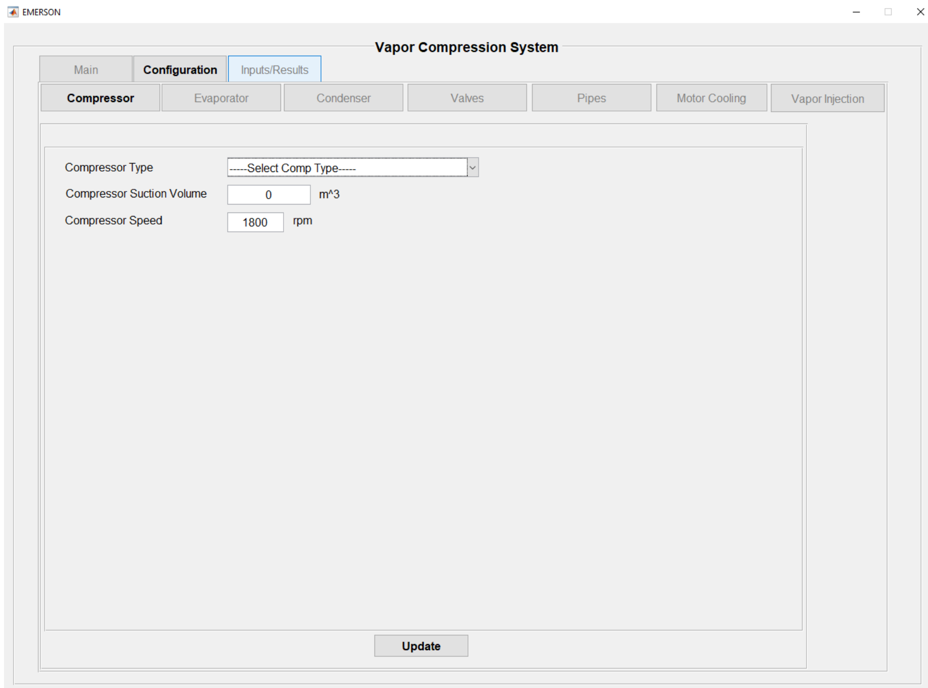


**Figure 43. Simulator Window – Compressor**

The fixed efficiency compressor model will require volumetric efficiency and adiabatic efficiency, as shown in Figure 44.

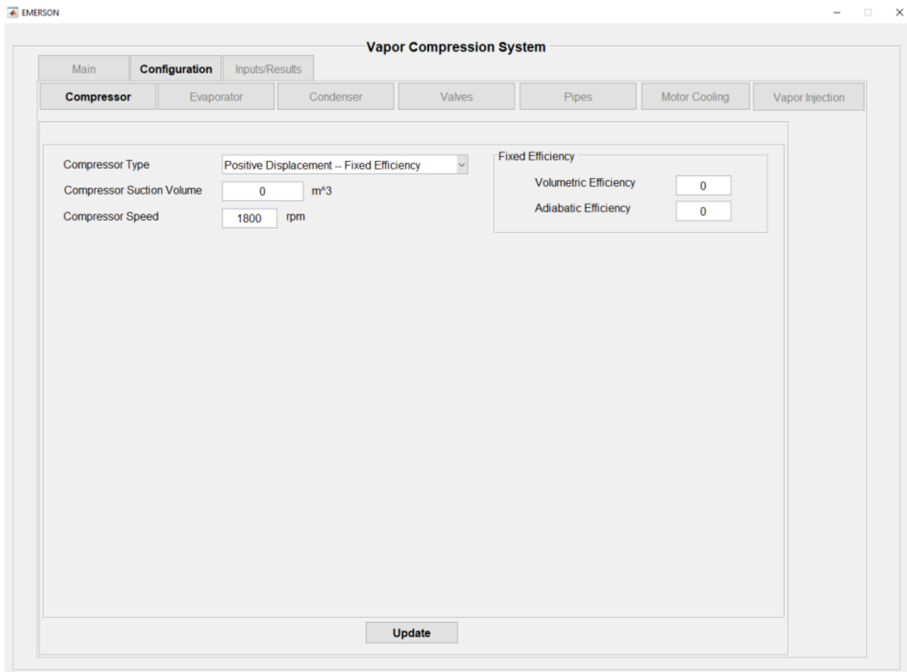


**Figure 44. Simulator Window - Fixed Efficiency Compressor**

Positive displacement compressor with AHRI coefficient map requires 20 variable coefficients for mass flow rates and power input, as shown in Figure 45.

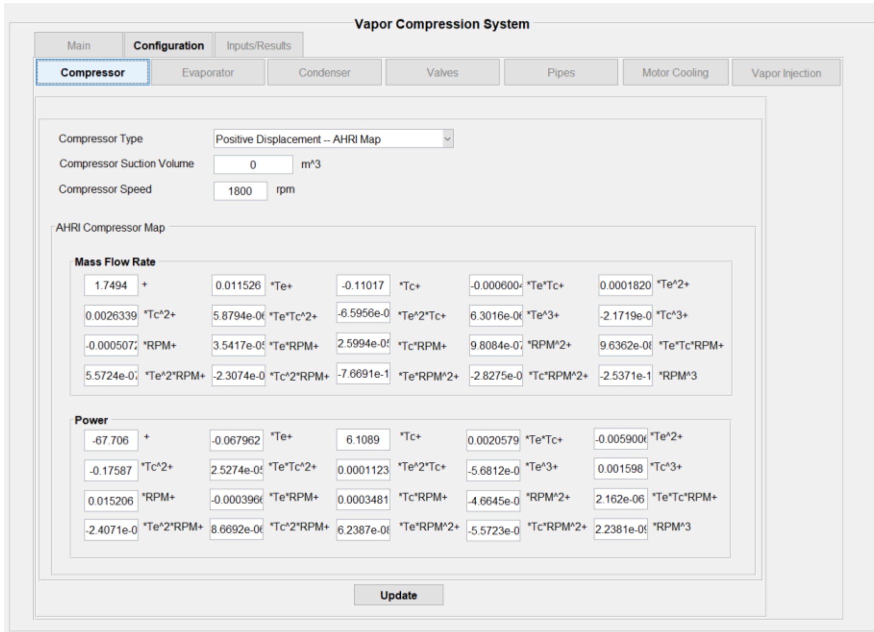


**Figure 45. Simulator Window - AHRI Map Compressor**

Centrifugal compressor with map requires six coefficient pressure ratio and nine coefficient isentropic efficiency maps, as shown in Figure 46.

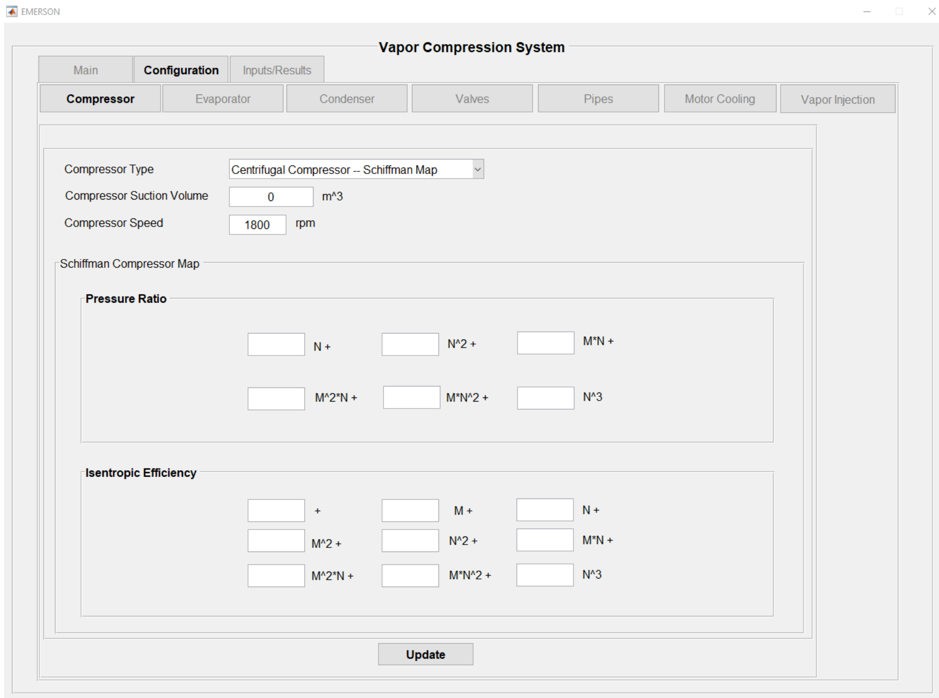


**Figure 46. Simulator Window – Centrifugal Compressor Map**

## Simulator – Heat Exchanger Specifications

Moving onto the heat exchangers, both the evaporator and the condenser can select mapped heat exchangers. In Figure 47, select mapped heat exchangers in the "Type" pull-down menu.

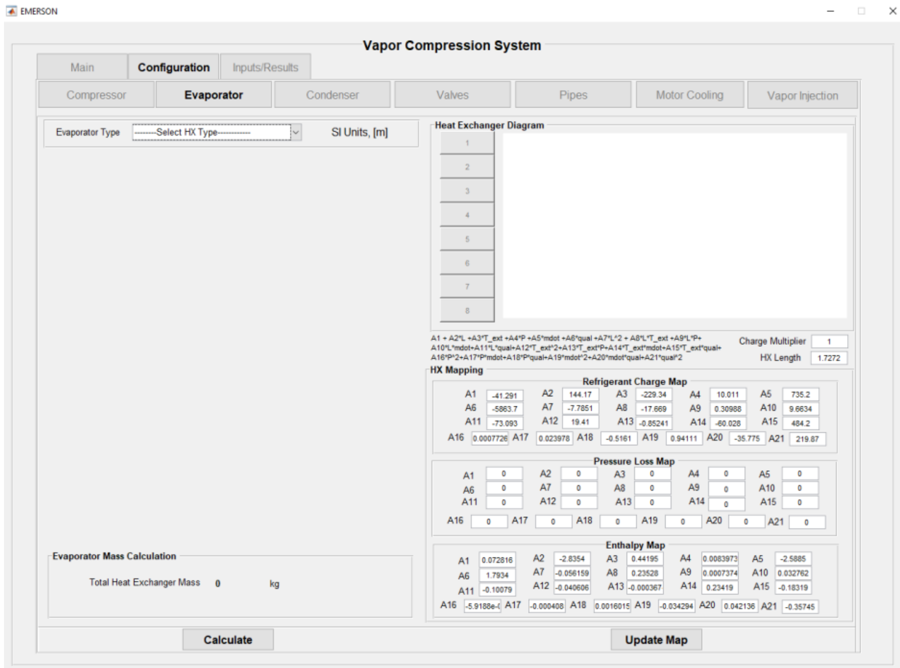


**Figure 47. Simulator Window – Evaporator**

Heat exchanger mapping coefficients can be entered in the “HX Mapping” section and hit “Update Map” when finished. Mass of the heat exchanger materials can be calculated using the “Input” section and hitting “Calculate” in Figure 48. A charge multiplier is used to represent the refrigerant charge in the heat exchangers accurately. For example, a system with ten parallel fin and tube condensers can be modeled with a single condenser map with a charge multiplier of 10. “HX Length” is a geometric multiplier for the heat exchanger length. HX Length value of 1 represents 100% of the heat exchanger design length.

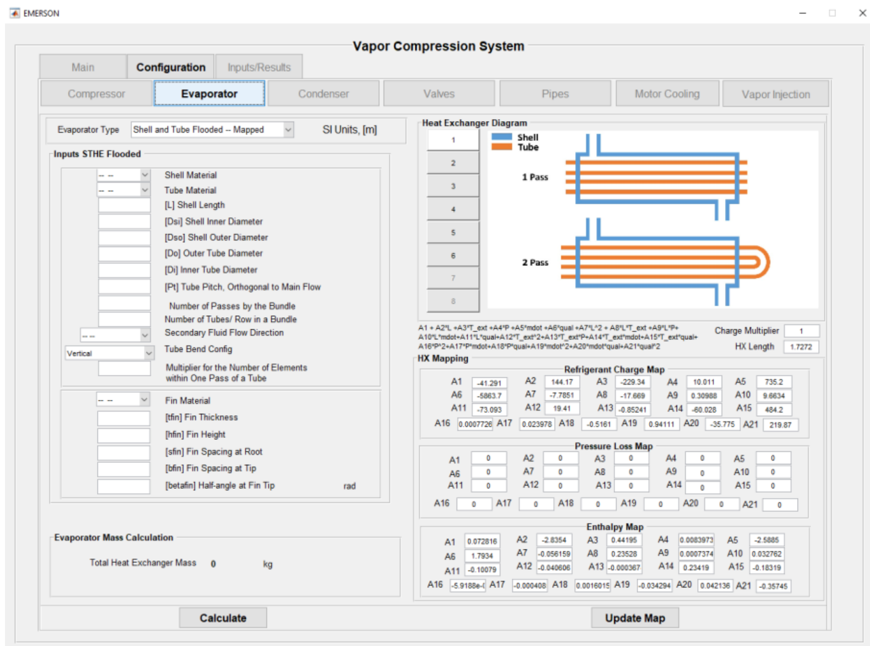

**Figure 48. Simulator Window - Mapped Shell and Tube Flooded Evaporator**

## Simulator – Valve Specifications

The valve section shown in Figure 49 provides an option to select either an electronic expansion valve(EXV) or a thermostatic expansion valve (TXV). Both valves are modeled passively. This means the high pressure and low pressure are solved first, and the valve opening necessary to induce such pressure drop is calculated afterward.

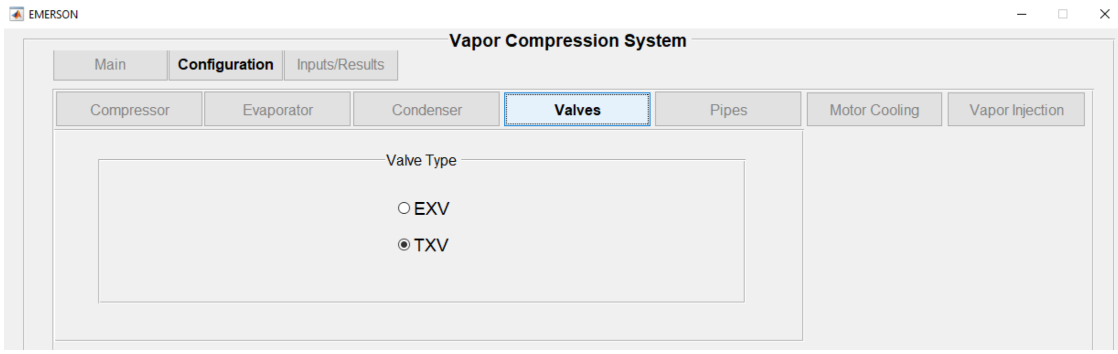


**Figure 49. Simulator Window – Valves**

## Simulator – Pipe Specifications

The pipes section shown in Figure 50 provides an option to include the dimensions for the pipes.

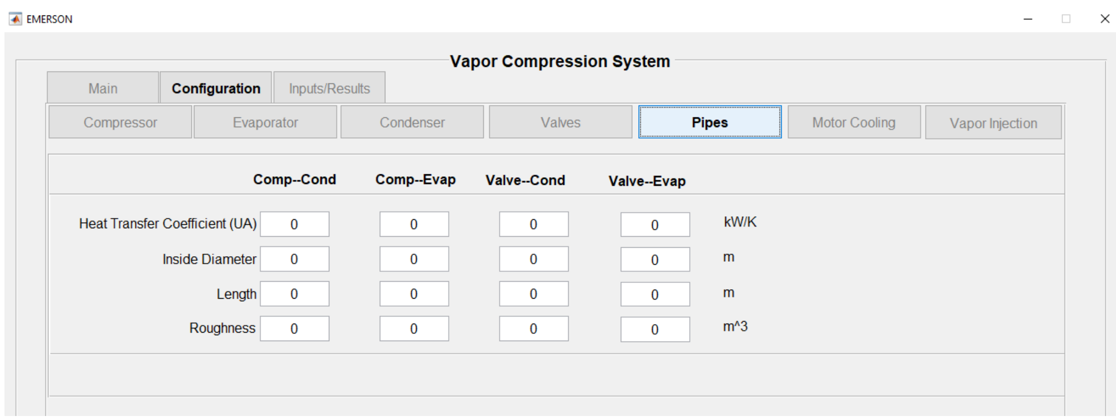


**Figure 50. Simulator Window – Pipes**

## Simulator – Motor Cooling Circuit Specifications

The Motor Cooling section shown in Figure 51 provides an option for the user to include a motor cooling circuit in the system configuration. Users can define the motor loss along with operating conditions to achieve the target temperature.

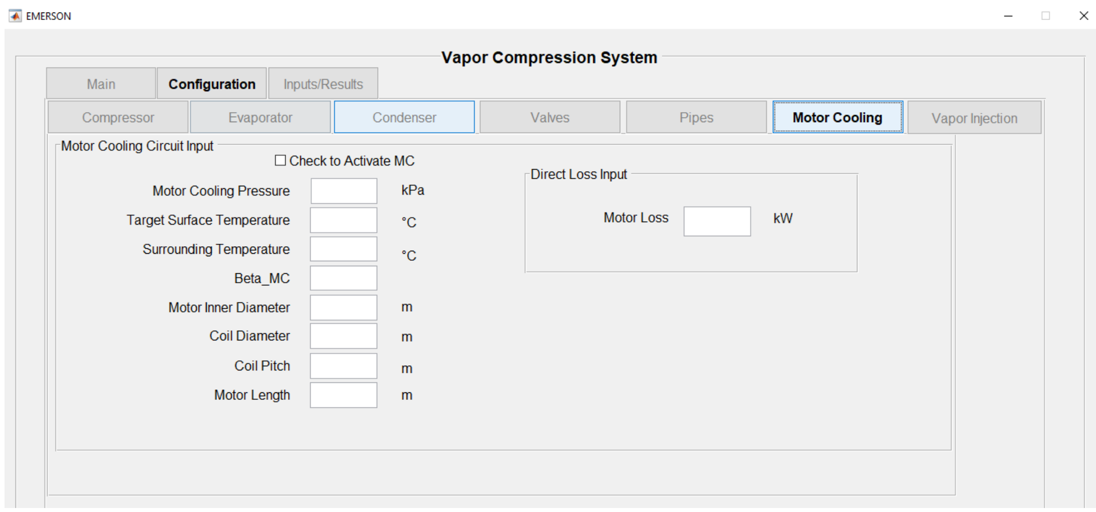


**Figure 51. Simulator Window - Motor Cooling**

## Simulator – Vapor Injection Specifications

The Vapor Injection tab is shown in Figure 52 and Figure 53. The user can enter the map for the subcooling heat exchanger, the fraction of the mass flow rate, compressor isentropic efficiency, and heat exchanger fraction that need to be entered to conduct the vapor injection system solver.

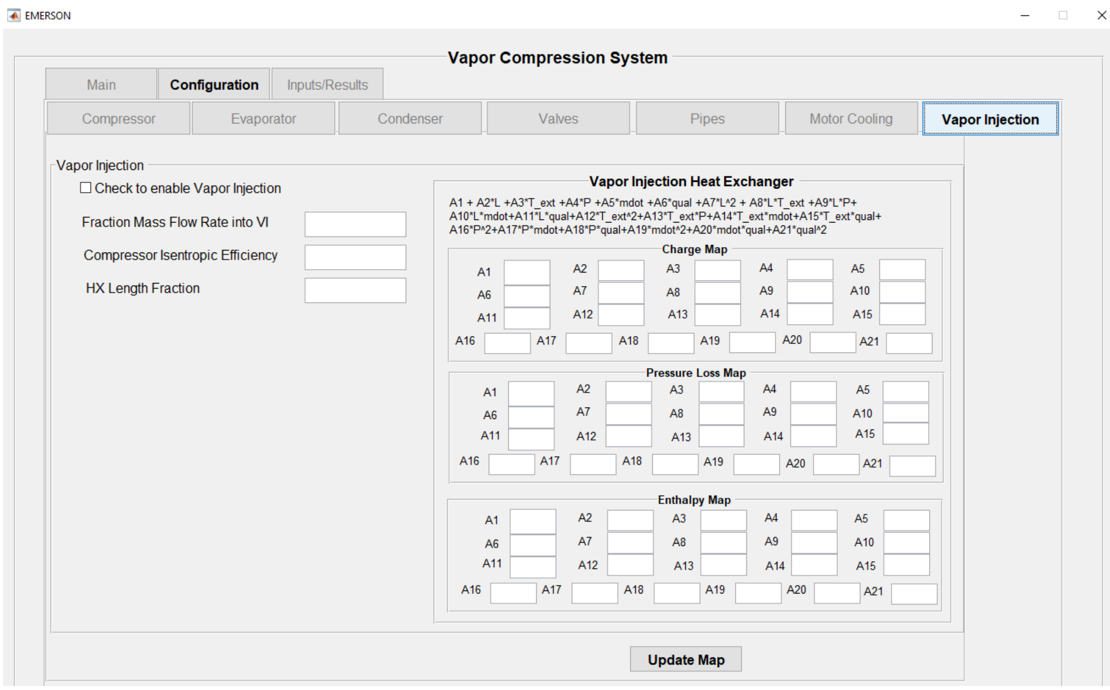


**Figure 52. Simulator Window - Vapor Injection**

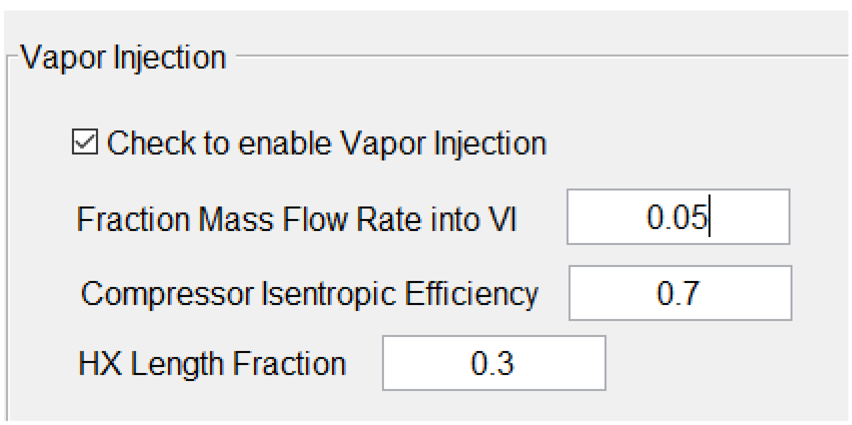


**Figure 53. Vapor Injection Specifications**

## Simulator – Single Case Solver Specifications

There are two solver modes built into the GUI. First is the Single Case solver. This solver takes in the inputs for a specific case and iterates on the system level to converge to a solution. Results are displayed on the right as shown in Figure 54 and can be exported to Excel using the “Export” button.

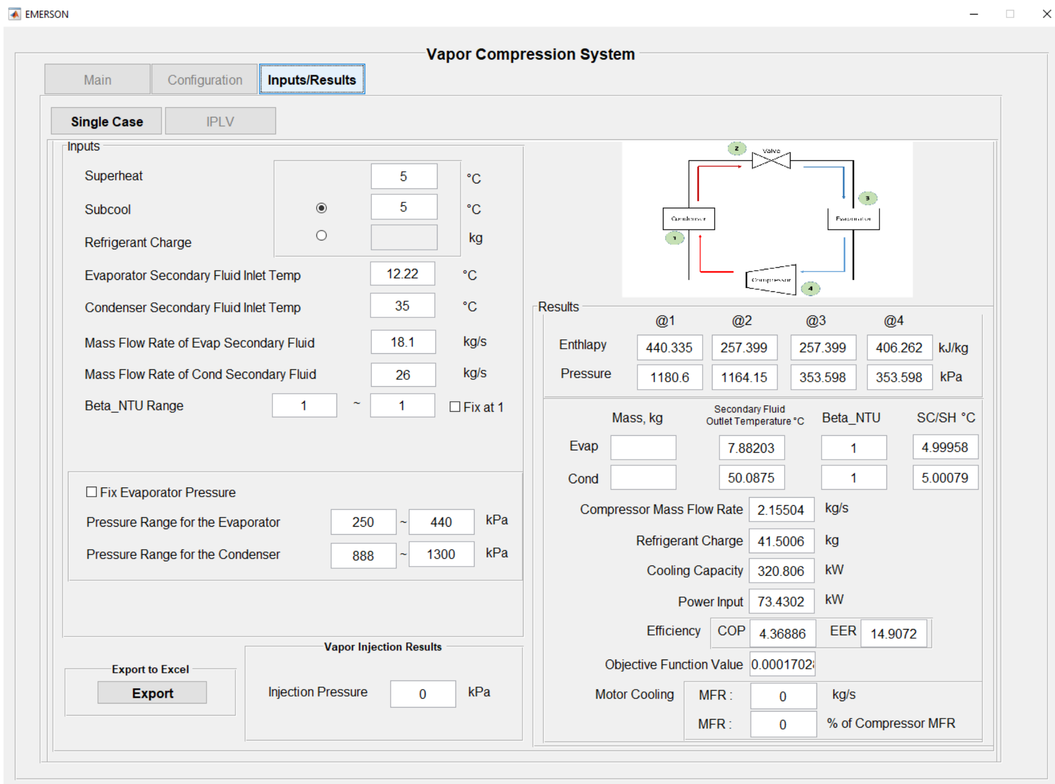


**Figure 54. Simulator Window - Single Case Inputs and Outputs**

### Simulator – Quick IPLV Solver Specifications

Quick IPLV Calculation feature generates an IPLV rating for the given configuration. The user must note that further iteration may be needed if any convergence issues arise. First, to generate an IPLV rating for the system, check off the “Check to Conduct IPLV Calculation” box, enter the minimum and maximum rated speeds. Click on “Show” to enter the condenser pressure ranges for each of the load points. Click “Return” and enter in an array of desired rpm points for the part-load conditions. Similarly to the Single Case solver, enter the operating conditions and click "Solve" in the Main.

**Simulator – Quick IPLV Solver Pseudo Code**

1. Intakes IPLV rating conditions including min and max rated compressor speed, IPLV rating conditions, similarly to the single case but specific for each load point as shown in Figure 55.
2. Runs at maximum rated compressor speed with given superheat and subcool and save results as 100% load point.
3. Refrigerant charge level from 100% load is now held constant, and subcool floats for part load iterations.
4. Move on to the next load point by running with the 75% load IPLV conditions.
5. Move on to the next load point by running with the 50% load IPLV conditions.
6. Move on to the next load point by running with the 25% load IPLV conditions.
7. Remove any iterations with a resulting objective function value of 1 or higher, so iterations with poor system-level convergence are removed.
8. For each 75%, 50%, and 25% load points, check if the cooling capacity is within ±2% of the targeted cooling capacity.
9. If capacity is within ±2%, save result directly.
10. If capacity is more than ±2% off for 75% and 50% load points, try to interpolate between two points.

11. If capacity is more than ±2% off for 25% load point, calculate the new coefficient of performance by accounting for the cyclic degradation factor. Display the cycling rpm in the GUI.
12. Display IPLV plot in the GUI along with the result table.

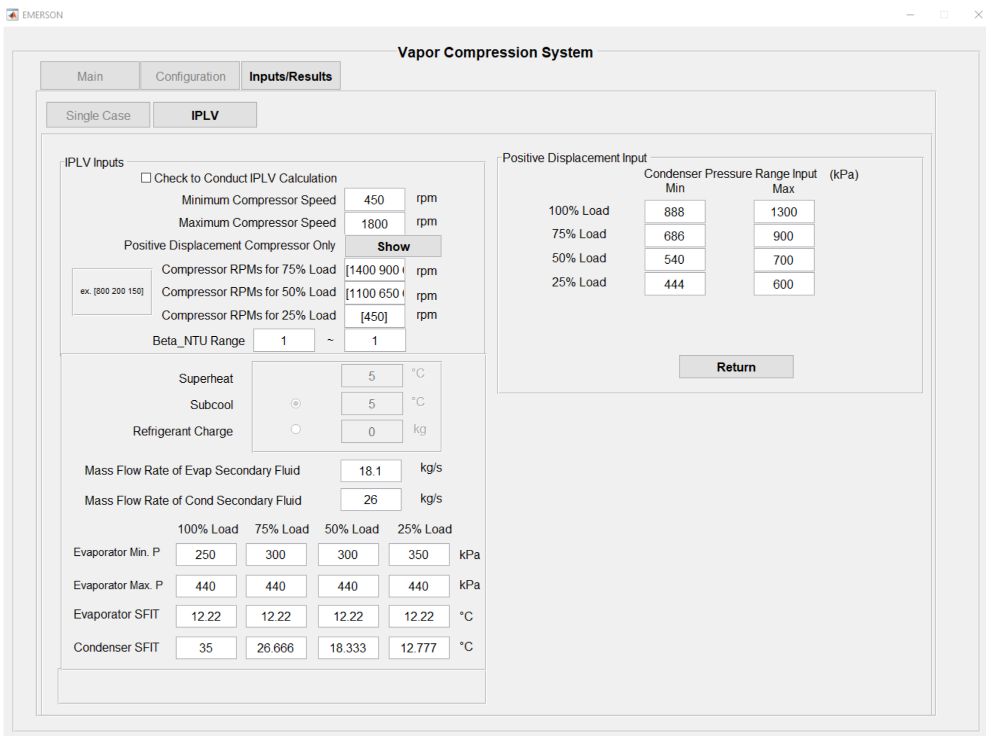


**Figure 55. Simulator Window – IPLV Positive Displacement Input**

Additional information on mass flow ranges to each rpm line is needed for the systems with centrifugal compressors as shown in Figure 56.

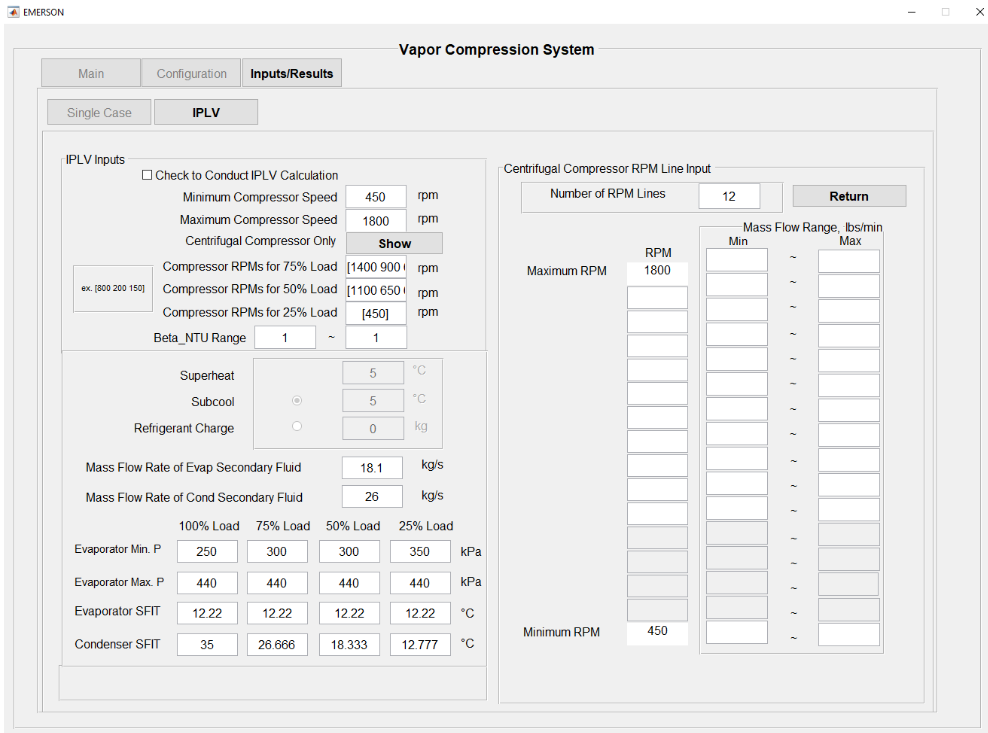


**Figure 56. Simulator Window – IPLV Centrifugal Compressor RPM Line Input**

As shown in Figure 57, the result of the IPLV result shows up on the right side and a graph of % Load vs. COP. The full set of results can be exported with the “Export” button or click “GO” to plot using the IPLV results.

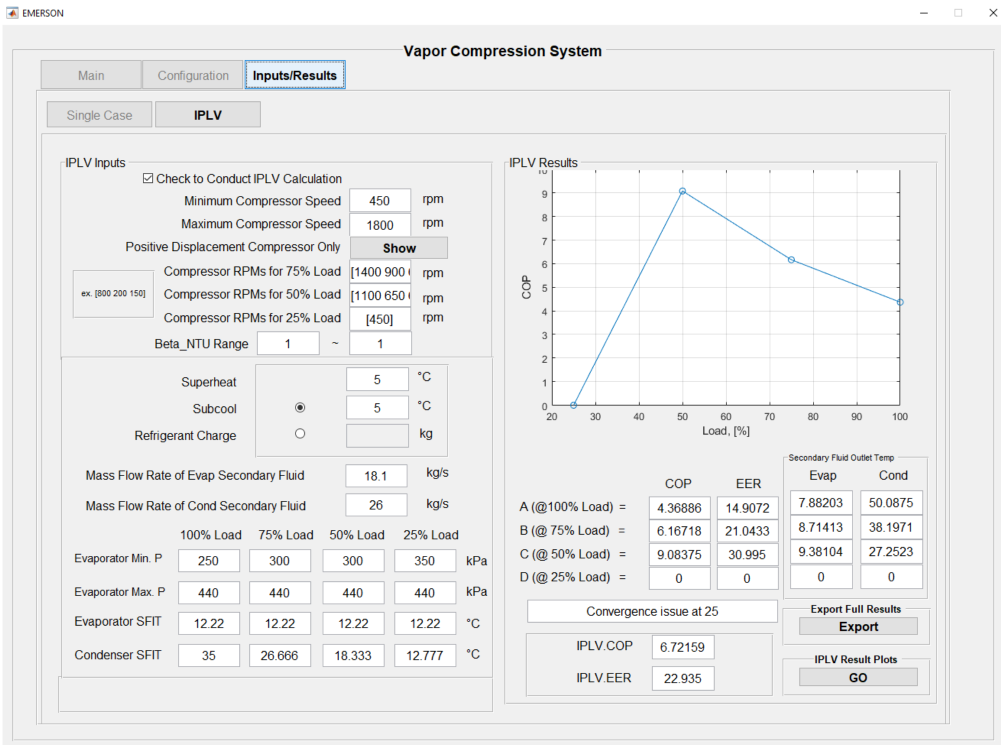


**Figure 57. Simulator Window – IPLV Results**

In the IPLV Result Plots section shown in Figure 58, the user can select the values to be plotted in the x and the y-axis by clicking on the left side. The plot will show up on the right side once the user clicks “Plot”.

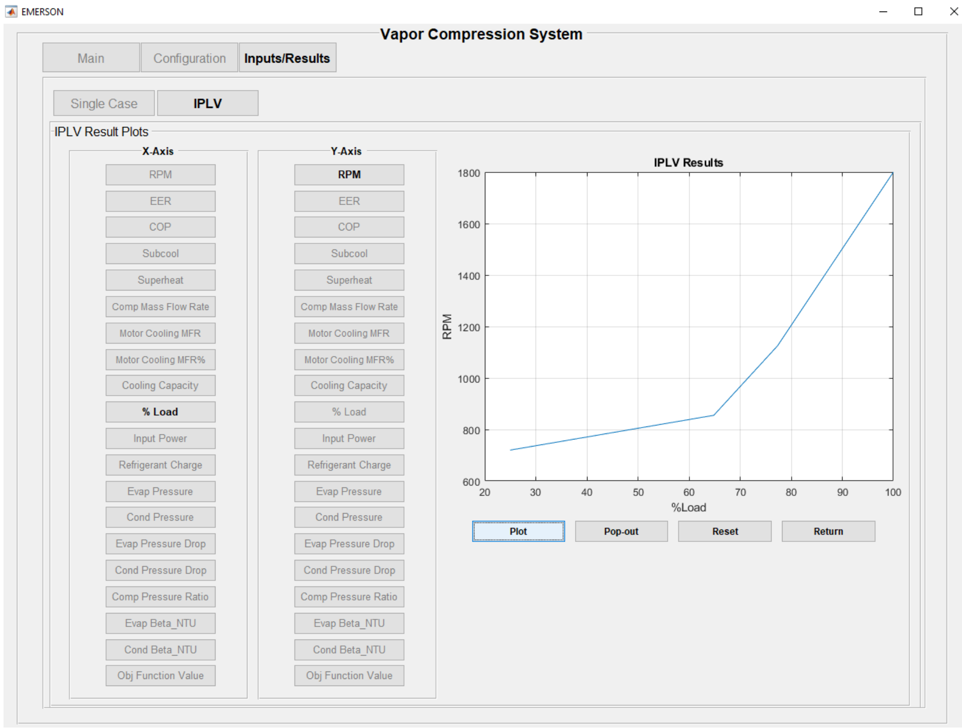


**Figure 58. Simulator Window - IPLV Result Plots**

As shown in Figure 59, the plot can be pop-out with the "Pop-out" button and can be edited and be saved.

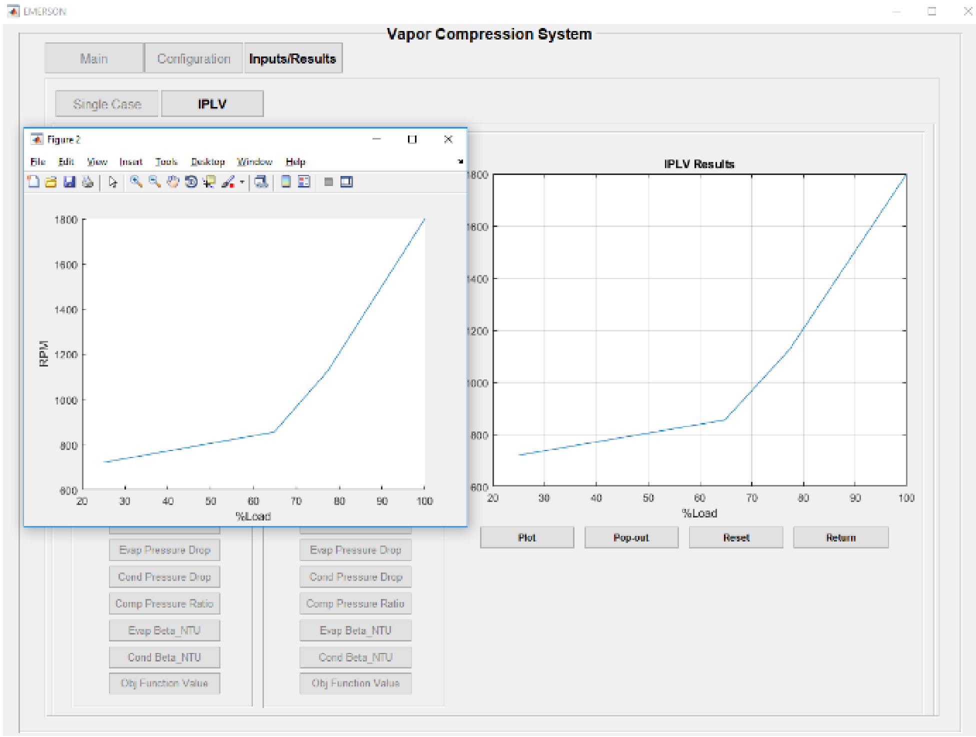


**Figure 59. Simulator Window - IPLV Plot Pop-up**

The plot can be reset using the “Reset” button as demonstrated in Figure 60.

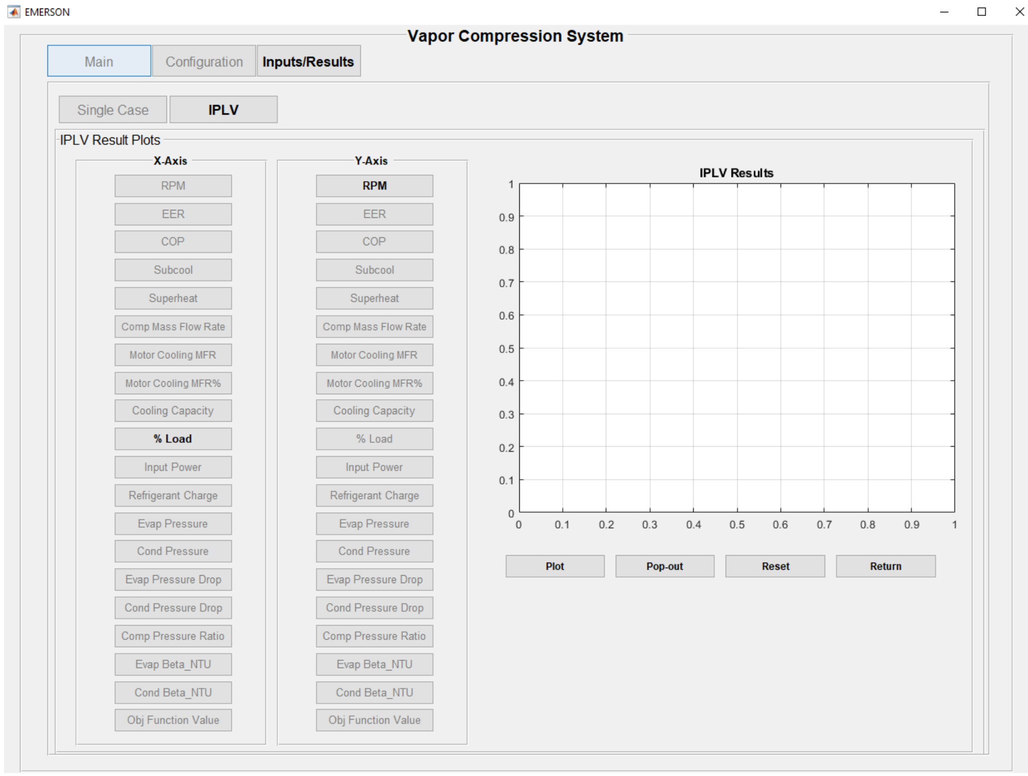


**Figure 60. Simulator Window - IPLV Plot Reset**

# CHAPTER VI

# OPTIMIZATION

With the modeling of the chiller and the software GUI completed, optimization frameworks need to be constructed. In three separate optimization cases, objective functions will be formulated to reflect the optimization goals for each of the cases. First, the assumptions will be made in the next subsection to reflect systems used in the field.

## Assumptions

Following assumptions were made to simplify the model and to roughly reflect industrial systems used in the field. However, the assumptions and model complexity can easily be modified to fit one's optimization goals and needs. Within the first cost of a heat exchanger, there are raw material cost and manufacturing cost. A proportional relationship is assumed between the raw material cost and manufacturing cost to simplify the cost calculations. Thus, capturing only the raw material cost would encompass both the material and manufacturing costs. 5 years of the product life cycle with 876 hours of yearly operation and 10% salvage cost is assumed. Table 3 shows the operational and first costs assumed for the case studies. The system's total refrigerant was constrained to 50% - 200% to ensure the optimization solution is that of a feasible one.

**Table 3. List of Assumptions**

| Amount | Unit |
|---|---|
| 876 | Operating hour/year |
| 0.1 | $/kWh |
| 10 | $/kg of refrigerant |
| 10 | $/kg of metal |

AHRI Standard 550/590 outlines the cycling degradation factor ($C_d$) for the cases where the minimum compressor speed cannot reach an IPLV load point capacity. Cycling degradation and load factor are defined in Equation 91and 92. $LF$ is load factor and $\%Load$ is the percent load point in the IPLV rating equation. $Q_{100e}$ is the full load capacity and $Q_{50e}$ is the cycling point capacity, which was chosen to be at 50% load as an example. Since not all systems can achieve 25% capacity, it is assumed that all of the cases will achieve the 25% load point via cycling of the compressor at a 50% load point.

$$C_d = (-0.13 * LF) + 1.13 \tag{91}$$

$$LF = \frac{\%Load * Q_{100e}}{Q_{50e}} \tag{92}$$

Flooded-type shell and tube heat exchangers and the connecting pipes are assumed to have negligible pressure losses and sufficient insulation from the environment. Lastly, 3°C superheat and subcool were assumed for the 100% load point. Based on the refrigerant charge found at 100% load point, subcool was solved as the refrigerant charge was held constant for the 75%, 50%, and 25% part load points. With assumptions made, a baseline case with a nominal heat exchanger needs to be established to compare the results of heat exchanger optimization.

## Problem Formulation – Baseline

First, baselines for both the centrifugal and the screw compressor with nominal heat exchanger geometry were established. The system capacity, IPLV, and refrigerant charge were solved as the system converges to a solution. The objective function for the baseline cases is defined in Equation 93.

$$J = \beta_1 J_{100Conv} + J_{75Conv} + J_{75Cap} + J_{75Chg} + J_{50Conv} + + J_{50Cap} + J_{50Chg} \qquad (93)$$

The optimization was set up so that the objective function, $J$ is minimized with no other system constraints. Table 4 and Table 5 list the definitions of the variables and subscripts used in this chapter. $\beta_1$ is a constant of 10. Such multiplier ensures the prioritization of the 100% load point so that the refrigerant charge found in the 100% load point can be used to achieve convergence in other subsequent load points.

**Table 4. List of Variables for Objective Function**

| Variable | Definition |
|---|---|
| $\beta$ | Weighting constant |
| $h$ | Enthalpy |
| $J$ | Objective function |
| $m$ | Mass |
| $P$ | Pressure |
| $Q$ | Capacity |

**Table 5. List of Subscripts for Objective Function**

| Subscripts | Definition |
|---|---|
| $100$ | 100% load point |
| $75$ | 75% load point |
| $50$ | 50% load point |
| $25$ | 25% load point |
| $c$ | Condenser |
| $Cap$ | Capacity |
| $Chg$ | Charge |
| $Conv$ | Convergence |
| $e$ | Evaporator |
| $HX$ | Heat exchanger |
| $i$ | Inlet |
| $IPLV$ | Integrated part-load value |
| $k$ | Compressor |
| $o$ | Outlet |
| $r, ref$ | Refrigerant |

As shown in Equation 94, the first term in the objective function can be broken down into three parts: superheat, subcool and pressure convergence. Variables with $'$ markers are the resulting variables, and the ones without the marker denote the estimated value by the optimizer. For example, superheat and subcool at 100% load point are given while the optimizer iteratively solves the condenser and the evaporator pressures. Based on the pressure and degree of superheat or subcool, enthalpy at the evaporator outlet ($h_{100kri}$) and enthalpy at the condenser outlet ($h_{100cro}$) are determined. The optimizer iteratively solves for the pressures in the system using the compressor and heat exchanger maps. The resulting enthalpies at the evaporator outlet ($h'_{100kri}$) and at the condenser outlet ($h'_{100cro}$) are determined and compared to the enthalpies calculated from the given superheat and subcool. The optimizer iterates on this process to minimize the objective function, $J$.

$$J_{100Conv} = \left\|\frac{h'_{100kri} - h_{100kri}}{h_{100kri}}\right\| + \left\|\frac{h'_{100cro} - h_{100cro}}{h_{100cro}}\right\| + \left\|\frac{P'_{100kri} - P_{100kri}}{P_{100kri}}\right\| \quad (94)$$

Equation 95-97 shows the baseline convergence criterion for the 75% load point. Similar to the 100% load point, $J_{75Conv}$ compares the starting enthalpy and pressure matches up with that of the resulting one. In part-load cases, subcool is solved with the given superheat, and the refrigerant charge from the 100% load point. $J_{75Cap}$ ensures that the targeted partial cooling capacity is met by the compressor. $J_{75Chg}$ compares the resulting 75% load refrigerant charge to the refrigerant charge from the 100% load case. Similar to the 75% load case, $J_{50Conv}$, $J_{50Cap}$ and $J_{50Chg}$ defined in Equation 98-100 ensure the convergence, cooling capacity, and refrigerant charge of the 50% load case.

$$J_{75Conv} = \left\|\frac{h'_{75kri} - h_{75kri}}{h_{75kri}}\right\| + \left\|\frac{P'_{75kri} - P_{75kri}}{P_{75kri}}\right\| \quad (95)$$

$$J_{75Cap} = \left\|\frac{Q'_{75e} - Q_{75e}}{Q_{75e}}\right\| \quad (96)$$

$$J_{75Chg} = \left\|\frac{m'_{75ref} - m_{100ref}}{m'_{100ref}}\right\| \quad (97)$$

$$J_{50Conv} = \left\|\frac{h'_{50kri} - h_{50kri}}{h_{50kri}}\right\| + \left\|\frac{P'_{50kri} - P_{50kri}}{P_{50kri}}\right\| \quad (98)$$

$$J_{50Cap} = \left\|\frac{Q'_{50e} - Q_{50e}}{Q_{50e}}\right\| \quad (99)$$

$$J_{50Chg} = \left\|\frac{m'_{50ref} - m_{100ref}}{m'_{50ref}}\right\| \quad (100)$$

## Problem Formulation – Optimized for Refrigerant and First Cost

After the baseline was established, the optimization problem for minimizing the refrigerant charge and the first cost was formulated. With the cooling capacity and IPLV rating targets, the objective function is defined in Equation 101. In addition to the baseline objective function, $J_{100Cap}$ and $J_{IPLV}$ are added to meet the 100% load capacity of 350 kW and IPLV of 8.00. Equations 102 and 103 define $J_{100Cap}$ and $J_{IPLV}$. Heat exchanger mass ($m_{HX}$) and refrigerant charge mass ($m_{ref}$) are defined in Equation 104 and 105, where $m_{evap}$ is the evaporator mass and $m_{cond}$ is the condenser mass. $m_{refe}$ and $m_{refc}$ are the refrigerant charge mass in the evaporator and in the condenser, respectively. $\beta_2$ of 10,000 is multiplied to make the normalized terms comparable to heat exchanger and refrigerant charge cost terms. Mass of the heat exchangers and the refrigerant charge are multiplied by conversion factors, $c_{HX}$ and $c_{ref}$, that translate the mass of material into cost.

$$J = \beta_2\big(\beta_1(J_{100Conv} + J_{100Cap}) + J_{75Conv} + J_{75Cap} + J_{75Chg} + J_{50Conv} + J_{50Cap} + J_{50Chg} + J_{IPLV}\big) + m_{HX}c_{HX} + m_{ref}c_{ref} \tag{101}$$

$$J_{100Cap} = \left\|\frac{Q'_{100e} - Q_{100e}}{Q_{100e}}\right\| \tag{102}$$

$$J_{IPLV} = \left\|\frac{IPLV' - IPLV}{IPLV}\right\| \tag{103}$$

$$m_{HX} = m_e + m_c \tag{104}$$

$$m_{ref} = m_{ref,e} + m_{ref,c} \tag{105}$$

## Problem Formulation – Optimized Life Cycle Cost

The last type of optimization will consider the heat exchanger's entire life cycle cost (LCC). The objective function, $J$, will be minimized while the system cooling capacity is held at 350 kW. Unlike the previous case of optimization, the IPLV value is not included in the objective function. Equation 106 shows the components of the objective function. $C_I$ is the first cost of the heat exchangers and the refrigerant charge in the heat exchangers. Equation 107 defines the first cost. Defined in Equation 108, $C_s$ is present value of the salvage cost, which is assumed to be 10% of the first cost of the metal used in the heat exchangers at the end of its life cycle. $i$ is the interest rate and $n$ is the product life cycle in years. $C_o$, in Equation 109, stands for the present value of the yearly operational cost of the system. Annual operational cost ($C_{yr}$) is defined in Equation 110. $Q_e$ is system cooling capacity and $t_{op}$ is the yearly operational hours. $c_{kwh}$ is a conversion factor that translates the kWh of energy usage into USD.

$$J = C_I - C_s + C_o \tag{106}$$

$$\begin{aligned} C_I = \beta_2\big(\beta_1\big(J_{100Conv} + J_{100Cap}\big) + J_{75Conv} + J_{75Cap} + J_{75Chg} + J_{50Conv} \\ + J_{50Cap} + J_{50Chg}\big) + m_{HX}c_{HX} + m_{ref}c_{ref} \end{aligned} \tag{107}$$

$$C_s = 0.1 * \frac{m_{HX}c_{HX}}{(1+i)^n} \tag{108}$$

$$C_o = C_{yr} * \left[\frac{(1+i)^n - 1}{i * (1+i)^n}\right] \tag{109}$$

$$C_{yr} = \frac{Q_e * t_{op} * c_{kwh}}{IPLV} \tag{110}$$

# CHAPTER VII

# CASE STUDIES AND CONCLUSIONS

A set of case studies will be presented and compared to each other in this section. Baseline cases using the screw and the CFD-based centrifugal compressor are first established in Case 0 and Case 3, respectively. These cases have nominal heat exchanger geometries. Case 0 will be used as a line of comparison for all other cases.

As shown in Figure 61 and Table 6 through Table 8, Case 1 and 4 are optimized for refrigerant charge and first costs while meeting the system cooling capacity of 350 kW and IPLV rating of 8.00.

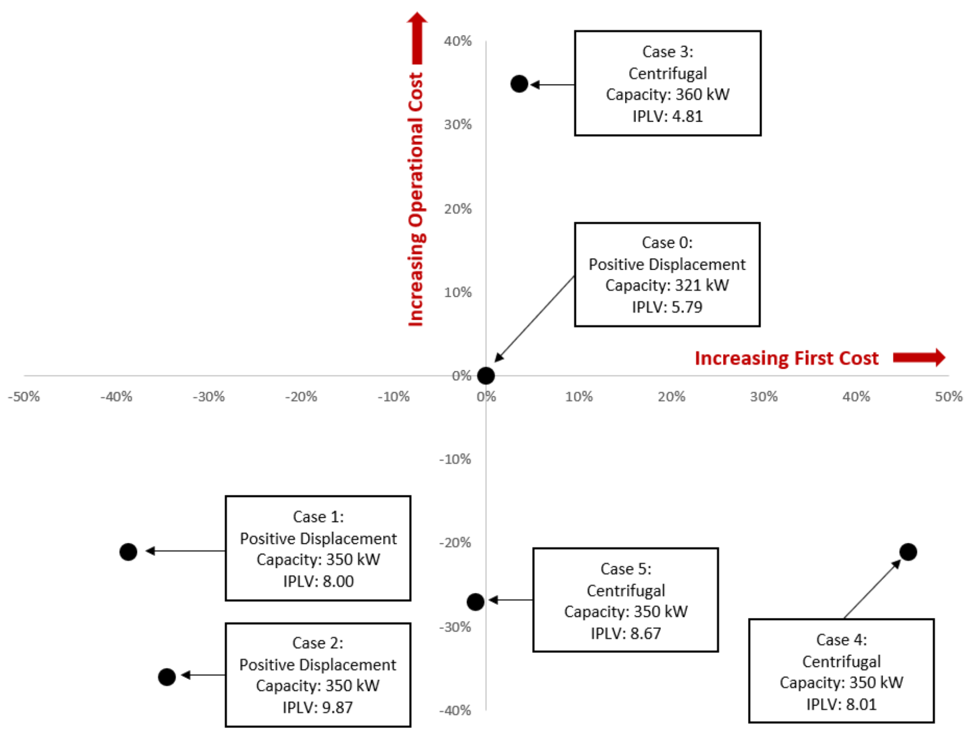


**Figure 61. Case Study Results**

Compared to the baseline Case 0, Case 1 was reduced in both the operational and first costs. The total cost of Case 1 was 21% lower than that of Case 0 while meeting the cooling capacity and the IPLV rating. Compared to Case 3, Case 4 has increased first cost and reduced operational cost to meet the IPLV and the cooling capacity requirements. While Case 3 had a 34% higher first cost than Case 0, the total cost of Case 4 was 20% lower than that of Case 0. Also, the IPLV of Case 4 was 8.01, while the IPLV of Case 3 was at 4.81.

Case 2 and 5 were optimized for the life cycle cost of the system. System capacity is set at 350 kW, while the IPLV was optimized to minimize the system's life cycle cost. Case 2 shows a tradeoff between the increased first cost for reducing the operational cost, which is the dominant factor in this case study. Optimized for the life cycle cost, Case 2 had a total cost of 36% lower than that of baseline, Case 0. Compared to Case 4, Case 5 showed a reduction in both the first and operational costs with increased IPLV value. The total cost of Case 5 was 25% lower than Case 0, while the total cost of Case 4 was 20% lower than Case 0.

Comparison of Case 2 and Case 5 demonstrates the configuration comparison where Case 2 uses a positive displacement compressor, and Case 5 uses a centrifugal compressor. The optimization results show the configuration with the positive displacement compressor having the lowest total cost when optimized for the life cycle cost.

**Table 6. Case Study with Heat Transfer Area and Volume Comparison to Case 0.**

| | | Case 1: Optimized for Refrigerant and Capital Cost | Case 2: Optimized for LCC | Case 3: Baseline with Centrifugal Compressor | Case 4: Optimized for Refrigerant and Capital Cost | Case 5: Optimized for LCC |
|---|---|---|---|---|---|---|
| **Compressor** | | Positive Displacement | | Centrifugal | | |
| Condenser | **Refrigerant Volume** | 2% | 4% | 0% | 7% | 6% |
| | **Secondary Fluid Volume** | -17% | -34% | 0% | -65% | -54% |
| | **Heat Transfer Area** | -17% | -26% | 0% | -46% | -38% |
| Evaporator | **Refrigerant Volume** | 2% | 2% | 0% | 7% | 7% |
| | **Secondary Fluid Volume** | -17% | -17% | 0% | -69% | -64% |
| | **Heat Transfer Area** | -17% | -17% | 0% | -50% | -46% |
| Condenser | Heat Exchanger Length ($L$) | -17% | -17% | 0% | -17% | -17% |
| | Horizontal Tube Pitch ($P_{th}$) | -17% | -29% | 0% | -39% | -26% |
| | Vertical Tube Pitch ($P_{tv}$) | -9% | 1% | 0% | -19% | -20% |
| | Tube Inner Diameter ($D_i$) | 0% | -11% | 0% | -35% | -26% |
| Evaporator | Heat Exchanger Length ($L$) | -17% | -17% | 0% | -17% | -17% |
| | Horizontal Tube Pitch ($P_{th}$) | -17% | -6% | 0% | -16% | -17% |
| | Vertical Tube Pitch ($P_{tv}$) | -6% | -20% | 0% | -18% | -75% |
| | Tube Inner Diameter ($D_i$) | 0% | 0% | 0% | -39% | -35% |

**Table 7. Case Study with Capacity and IPLV Rating Comparison**

| | Case 0: Baseline with Positive Displacement Compressor | Case 1: Optimized for Refrigerant and Capital Cost | Case 2: Optimized for LCC | Case 3: Baseline with Centrifugal Compressor | Case 4: Optimized for Refrigerant and Capital Cost | Case 5: Optimized for LCC |
|---|---|---|---|---|---|---|
| **Compressor** | Positive Displacement | | | Centrifugal | | |
| **Capacity [kW]** | 321 | 350 | 350 | 360 | 350 | 350 |
| **IPLV Rating** | 5.79 | 8.00 | 9.87 | 4.81 | 8.01 | 8.67 |
| *100% Load COP* | 4.55 | 5.95 | 6.09 | 3.65 | 4.02 | 3.93 |
| *75% Load COP* | 5.58 | 7.03 | 7.72 | 4.42 | 5.34 | 8.88 |
| *50% Load COP* | 6.04 | 8.86 | 11.68 | 5.19 | 10.17 | 8.70 |
| *25% Load COP* | 5.67 | 8.32 | 10.97 | 4.88 | 9.55 | 8.17 |

**Table 8. Case Study with Cost Breakdown Comparison**

| | Case 0: Baseline with Positive Displacement Compressor | Case 1: Optimized for Refrigerant and Capital Cost | Case 2: Optimized for LCC | Case 3: Baseline with Centrifugal Compressor | Case 4: Optimized for Refrigerant and Capital Cost | Case 5: Optimized for LCC |
|---|---|---|---|---|---|---|
| Compressor | Positive Displacement | | | Centrifugal | | |
| Capital Cost Condenser | - | -12% | -22% | 0% | -42% | -35% |
| Capital Cost Evaporator | - | -17% | -17% | 0% | -48% | -45% |
| Refrigerant Charge Cost | - | -63% | -50% | 7% | 138% | 38% |
| Operational Cost | - | -21% | -36% | 35% | -21% | -27% |
| Salvage Cost | - | -14% | -19% | 0% | -45% | -40% |
| **Total Cost** | - | -21% | -36% | 34% | -20% | -25% |

# REFERENCES


Achaichia, A., & Cowell, T. A. (1988). Heat transfer and pressure drop characteristics of flat tube and louvered plate fin surfaces. *Experimental Thermal and Fluid Science*, *1*(2), 147–157. https://doi.org/10.1016/0894-1777(88)90032-5

Ahilan, C., Kumanan, S., & Sivakumaran, N. (2011a). Online performance assessment of heat exchanger using artificial neural networks. *International Journal of Energy and Environment (IJEE)*, *2*, 829–844.

Ahilan, C., Kumanan, S., & Sivakumaran, N. (2011b). Prediction of Shell and Tube Heat Exchanger Performance using Artificial Neural Networks. *Proc. of the International Conference on Advanced Computing and Communication Technologies (ACCT 2011)*, 307–312.

AHRI. (2016). *2015 Standard for Performance Rating of Water-chilling and Heat Pump Water-heating Packages Using the Vapor Compression Cycle*. http://www.ahrinet.org/App_Content/ahri/files/STANDARDS/AHRI/AHRI_Standard_550-590_I-P_2015_with_Errata.pdf

AHRI. (2020). *2020 Standard for Performance Rating of Positive Displacement Refrigerant Compressors*. https://ahrinet.org/App_Content/ahri/files/STANDARDS/AHRI/AHRI_Standard_540_(I-P_and_SI)_2020_Standard_for_Performance_Rating_of_Positive_Displacement_Refrigerant_Compressors_and_Compressor_Units.pdf

Arpagaus, C., Bless, F., Bertsch, S. S., & Javed, A. (2017). *Heat Pump driven by a Small-Scale Oil-Free Turbocompressor – System Design and Simulation*. 11.

ASHRAE. (2019). *ANSI/ASHRAE/IES Standard 90.1-2019—Energy Standard for Buildings Except Low-Rise Residential Buildings*. https://www.ashrae.org/technical-resources/bookstore/standard-90-1

Azad, A. V., & Amidpour, M. (2011). Economic optimization of shell and tube heat exchanger based on constructal theory. *Energy*, *36*(2), 1087–1096. https://doi.org/10.1016/j.energy.2010.11.041

*BITZER Software v6.16.0 rev2522*. (n.d.). Retrieved January 14, 2021, from https://www.bitzer.de/websoftware/Calculate.aspx?cid=1610609838952&mod=CS

Bogaert, R., & Böles, A. (1995). Global Performance of a Prototype Brazed Plate Heat Exchanger in a Large Reynolds Number Range. *Experimental Heat Transfer*, *8*(4), 293–311. https://doi.org/10.1080/08916159508946508

Briggs, A., & Rose, J. W. (1994). Effect of fin efficiency on a model for condensation heat transfer on a horizontal, integral-fin tube. *International Journal of Heat and Mass Transfer*, *37*, 457–463. https://doi.org/10.1016/0017-9310(94)90045-0

Chang, Y.-C. (2004). A novel energy conservation method—Optimal chiller loading. *Electric Power Systems Research*, *69*(2), 221–226. https://doi.org/10.1016/j.epsr.2003.10.012

Chen, J. C. (1966). Correlation for Boiling Heat Transfer to Saturated Fluids in Convective Flow. *Industrial & Engineering Chemistry Process Design and Development*, *5*(3), 322–329. https://doi.org/10.1021/i260019a023

Churchill, S. W., & Bernstein, M. (1977). A Correlating Equation for Forced Convection From Gases and Liquids to a Circular Cylinder in Crossflow. *Journal of Heat Transfer*, *99*(2), 300–306. https://doi.org/10.1115/1.3450685

Dobson, M. K., & Chato, J. C. (1998). Condensation in Smooth Horizontal Tubes. *Journal of Heat Transfer*, *120*(1), 193–213. https://doi.org/10.1115/1.2830043

El-Said, E. M. S., Abd Elaziz, M., & Elsheikh, A. H. (2021). Machine learning algorithms for improving the prediction of air injection effect on the thermohydraulic performance of shell and tube heat exchanger. *Applied Thermal Engineering*, *185*, 116471. https://doi.org/10.1016/j.applthermaleng.2020.116471

ETU Software GmbH. (n.d.). *Hottgenroth Software GmbH & Co. KG- Startseite*. Retrieved July 31, 2020, from https://www.etu-software.com/index.html

Fang, X., Chen, W., Zhou, Z., & Xu, Y. (2014). Empirical models for efficiency and mass flow rate of centrifugal compressors. *International Journal of Refrigeration*, *41*, 190–199. https://doi.org/10.1016/j.ijrefrig.2014.03.005

Gang, W., & Wang, J. (2013). Predictive ANN models of ground heat exchanger for the control of hybrid ground source heat pump systems. *Applied Energy*, *112*, 1146–1153. https://doi.org/10.1016/j.apenergy.2012.12.031

Gnielinski, V. (1975). New equations for heat and mass transfer in the turbulent flow in pipes and channels. *NASA STI/Recon Technical Report A*, *75*, 8–16.

Guo, J., Xu, M., & Cheng, L. (2009). The application of field synergy number in shell-and-tube heat exchanger optimization design. *Applied Energy*, *86*(10), 2079–2087. https://doi.org/10.1016/j.apenergy.2009.01.013

Han, D.H., Lee, K.J., & Kim, Y.H. (2003). Experiments on the characteristics of evaporation of R410A in brazed plate heat exchangers with different geometric configurations. *Applied Thermal Engineering*, *23*(10), 1209–1225. https://doi.org/10.1016/S1359-4311(03)00061-9

Hellborg, J. (2017). *Modelling of shell and tube heat exchangers* [Lund University]. http://lup.lub.lu.se/luur/download?func=downloadFile&recordOId=8900243&fileOId=8900249

Hojjat, M. (2020). Nanofluids as coolant in a shell and tube heat exchanger: ANN modeling and multi-objective optimization. *Applied Mathematics and Computation*, *365*, 124710. https://doi.org/10.1016/j.amc.2019.124710

Hsieh, Y. Y., & Lin, T. F. (2002). Saturated flow boiling heat transfer and pressure drop of refrigerant R-410A in a vertical plate heat exchanger. *International Journal of Heat and Mass Transfer*, *45*(5), 1033–1044. https://doi.org/10.1016/S0017-9310(01)00219-8

Hu, S.-C., & Chuah, Y. K. (2003). Power consumption of semiconductor fabs in Taiwan. *Energy*, *28*(8), 895–907. https://doi.org/10.1016/S0360-5442(03)00008-2

Hwang, T. H., & Yao, S. C. (1986). Forced convective boiling in horizontal tube bundles. *International Journal of Heat and Mass Transfer*, *29*(5), 785–795. https://doi.org/10.1016/0017-9310(86)90130-4

Islamoglu, Y., Kurt, A., & Parmaksizoglu, C. (2005). Performance prediction for non-adiabatic capillary tube suction line heat exchanger: An artificial neural network approach. *Energy Conversion and Management*, *46*(2), 223–232. https://doi.org/10.1016/j.enconman.2004.02.015

Iyengar, A. S. (2015). Thermal analysis of shell and tube heat exchangers using artificial neural networks. *Ethiopian Journal of Science and Technology*, *8*(2), 107–120. https://doi.org/10.4314/ejst.v8i2.5

Jasim, H. H. (2013). Estimated Outlet Temperatures in Shell-and-Tube Heat Exchanger Using Artificial Neural Network Approach Based on Practical Data. *Al-Khwarizmi Engineering Journal*, *9*(2), 2–20.

Kalogirou, S. A., & Bojic, M. (2000). Artificial neural networks for the prediction of the energy consumption of a passive solar building. *Energy*, *25*(5), 479–491. https://doi.org/10.1016/S0360-5442(99)00086-9

Kumar, V., Faizee, B., Mridha, M., & Nigam, K. D. P. (2008). Numerical studies of a tube-in-tube helically coiled heat exchanger. *Chemical Engineering and Processing: Process Intensification*, *47*(12), 2287–2295. https://doi.org/10.1016/j.cep.2008.01.001

Mandavgane, S. A., & Pandharipande, S. L. (2006). Application of ANN for modeling of heat exchanger with concentration as variable. *IJCT Vol.13(2) [March 2006]*. http://nopr.niscair.res.in/handle/123456789/7004

Mohanraj, M., Jayaraj, S., & Muraleedharan, C. (2015). Applications of artificial neural networks for thermal analysis of heat exchangers – A review. *International Journal of Thermal Sciences*, *90*, 150–172. https://doi.org/10.1016/j.ijthermalsci.2014.11.030

Mori, Y., & Nakayama, W. (1967). Study on forced convective heat transfer in curved pipes: (3rd report, theoretical analysis under the condition of uniform wall temperature and practical formulae). *International Journal of Heat and Mass Transfer*, *10*(5), 681–695. https://doi.org/10.1016/0017-9310(67)90113-5

Navvab Kashani, M., Aminian, J., Shahhosseini, S., & Farrokhi, M. (2012). Dynamic crude oil fouling prediction in industrial preheaters using optimized ANN based moving window technique. *Chemical Engineering Research and Design*, *90*(7), 938–949. https://doi.org/10.1016/j.cherd.2011.10.013

North Carolina Energy Office. (2010). *Chillers Energy Saving Fact Sheet*. https://files.nc.gov/ncdeq/Environmental%20Assistance%20and%20Customer%20Service/IAS%20Energy%20Efficiency/Opportunities/Chillers.pdf

ORNL. (n.d.). *DOE/ORNL Heat Pump Design Model (HPDM)*. Retrieved July 31, 2020, from https://hpdmflex.ornl.gov/hpdm/wizard/welcome.php

Pandharipande, S. L., Siddiqui, M. A., Dubey, A., & Mandavgane, S. A. (2004). Optimising ANN architecture for shell and tube heat exchanger modelling. *IJCT Vol.11(6) [November 2004]*. http://nopr.niscair.res.in/handle/123456789/9550

Park, D., Guo, F., & Rasmussen, B. P. (2021). A Method of Mapping Heat Exchanger as Simple Polynomials. *International Refrigeration and Air Conditioning Conference*. (In Press).

Rafiq, M. Y., Bugmann, G., & Easterbrook, D. J. (2001). Neural network design for engineering applications. *Computers & Structures*, *79*(17), 1541–1552. https://doi.org/10.1016/S0045-7949(01)00039-6

Rao, R. V., & Patel, V. K. (2010). Thermodynamic optimization of cross flow plate-fin heat exchanger using a particle swarm optimization algorithm. *International Journal of Thermal Sciences*, *49*(9), 1712–1721. https://doi.org/10.1016/j.ijthermalsci.2010.04.001

Sanaye, S., & Hajabdollahi, H. (2010). Multi-objective optimization of shell and tube heat exchangers. *Applied Thermal Engineering*, *30*(14–15), 1937–1945. https://doi.org/10.1016/j.applthermaleng.2010.04.018

The U.S. Department of Energy. (2015). *Quadrennial Technology Review an Assessment of Energy Technologies and Research Opportunities Chapter 5: Increasing Efficiency of Building Systems and Technologies*. https://www.energy.gov/sites/prod/files/2017/03/f34/qtr-2015-chapter5.pdf

US EPA, O. (2015, July 27). *Substitutes in Chillers* [Collections and Lists]. US EPA. https://www.epa.gov/snap/substitutes-chillers

US EPA, O. (2016, January 12). *Understanding Global Warming Potentials* [Overviews and Factsheets]. US EPA. https://www.epa.gov/ghgemissions/understanding-global-warming-potentials

US EPA, O. (2017, September 8). *Substitutes in Positive Displacement Chillers* [Collections and Lists]. US EPA. https://www.epa.gov/snap/substitutes-positive-displacement-chillers

Wang, C.-C., Lo, J., Lin, Y.-T., & Wei, C.-S. (2002). Flow visualization of annular and delta winlet vortex generators in fin-and-tube heat exchanger application. *International Journal of Heat and Mass Transfer*, *45*(18), 3803–3815. https://doi.org/10.1016/S0017-9310(02)00085-6

Wang, Q., Xie, G., Zeng, M., & Luo, L. (2006). Prediction of heat transfer rates for shell-and-tube heat exchangers by artificial neural networks approach. *Journal of Thermal Science*, *15*(3), 257–262. https://doi.org/10.1007/s11630-006-0257-6

Wang, S., & Burnett, J. (2001). Online adaptive control for optimizing variable-speed pumps of indirect water-cooled chilling systems. *Applied Thermal Engineering*, *21*(11), 1083–1103. https://doi.org/10.1016/S1359-4311(00)00109-5

Wattelet, J. P., Chato, J. C., Christoffersen, B. R., Gaibel, J. A., Ponchner, M., Kenney, P. J., Shimon, R. L., Villaneuva, T. C., Rhines, N. L., Sweeney, K. A., Allen, D. G., & Hershberger, T. T. (1994). *Heat Transfer Flow Regimes of Refrigerants in a Horizontal-Tube Evaporator* (ACRC TR-55). Air Conditioning and Refrigeration Center at University of Illinois.

Westphalen, D., & Koszalinski, S. (2001). *Energy consumption characteristics of commercial building HVAC systems. Volume I: Chillers refrigerant compressors, and heating systems* (No. 36922–00; Energy Consumption Characteristics of Commercial Building HVAC Systems). https://www1.eere.energy.gov/buildings/publications/pdfs/commercial_initiative/hvac_volume1_final_report.pdf

Wijayasekara, D., Manic, M., Sabharwall, P., & Utgikar, V. (2011). Optimal artificial neural network architecture selection for performance prediction of compact heat exchanger with the EBaLM-OTR technique. *Nuclear Engineering and Design*, *241*(7), 2549–2557. https://doi.org/10.1016/j.nucengdes.2011.04.045

Wongwises, S., & Polsongkram, M. (2006a). Evaporation heat transfer and pressure drop of HFC-134a in a helically coiled concentric tube-in-tube heat exchanger. *International Journal of Heat and Mass Transfer*, *49*(3), 658–670. https://doi.org/10.1016/j.ijheatmasstransfer.2005.08.017

Wongwises, S., & Polsongkram, M. (2006b). Condensation heat transfer and pressure drop of HFC-134a in a helically coiled concentric tube-in-tube heat exchanger. *International Journal of Heat and Mass Transfer*, *49*(23), 4386–4398. https://doi.org/10.1016/j.ijheatmasstransfer.2006.05.010

Xie, G. N., Sunden, B., & Wang, Q. W. (2008). Optimization of compact heat exchangers by a genetic algorithm. *Applied Thermal Engineering*, *28*(8–9), 895–906. https://doi.org/10.1016/j.applthermaleng.2007.07.008

Xie, G. N., Wang, Q. W., Zeng, M., & Luo, L. Q. (2007). Heat transfer analysis for shell-and-tube heat exchangers with experimental data by artificial neural networks approach. *Applied Thermal Engineering*, *27*(5), 1096–1104. https://doi.org/10.1016/j.applthermaleng.2006.07.036

Yin, C., Rosendahl, L., & Luo, Z. (2003). Methods to improve prediction performance of ANN models. *Simulation Modelling Practice and Theory*, *11*(3), 211–222. https://doi.org/10.1016/S1569-190X(03)00044-3

Yu, F. W., Chan, K. T., Sit, R. K. Y., & Yang, J. (2008). Optimizing condenser fan control for air-cooled centrifugal chillers. *International Journal of Thermal Sciences*, *47*(7), 942–953. https://doi.org/10.1016/j.ijthermalsci.2007.07.018

Yu, F. W., Chan, K. T., Sit, R. K. Y., & Yang, J. (2014). Review of Standards for Energy Performance of Chiller Systems Serving Commercial Buildings. *Energy Procedia*, *61*, 2778–2782. https://doi.org/10.1016/j.egypro.2014.12.308

Yung-Chung Chang & Hung-Chiu Tu. (2002). An effective method for reducing power consumption-optimal chiller load distribution. *Proceedings. International Conference on Power System Technology*, *2*, 1169–1172 vol.2. https://doi.org/10.1109/ICPST.2002.1047586

APPENDIX A

CODE INSTRUCTIONS

Heat exchanger mapping

Mapping_Heat_Exchanger.m is the master file for generating a heat exchanger map. Following is the step-by-step procedure on heat exchanger map generation.

1. Go to Mapping/HX Solvers folder and select the type of heat exchanger to be mapped.
2. Open up ****_ss.m file

Ex) Shell and tube flooded heat exchanger map would require an opening of STFL_ss.m in step 2.

3. Uncomment mapping mode function head.
4. Select mapping mode in section 0.1 of ****_ss.m file.
5. Define heat exchanger geometry in the ****_ss.m file.
6. Open Mapping_Heat_Exchanger.m
7. Define mapping inputs in section 0.0 of Mapping_Heat_Exchanger.m
8. Run Mapping_Heat_Exchanger.m

If there is a mapped file, which just requires a map, select Op_type to be 2

Compressor mapping

Compressor_Mapping_AHRI_and_Schiffman.m is the master file for generating a compressor map. In order to generate AHRI and Schiffman maps, open Compressor_Mapping_AHRI_and_Schiffman.m and specify section 0.0 before running the script. The coefficients of the map will be displayed in the MATLAB Command Window.

## Adding a New Refrigerant to the System

Following are the instructions on adding a new refrigerant to the GUI. Firstly, the GUI option for the new refrigerant needs to be added.

1. Open up GUI through GUIDE and double click on the refrigerant box.
2. Under "String", add the name of the refrigerant.
3. Click "OK" and save the GUI figure.
4. Open Emerson.m and go to run_system_Callback function. Add a line to load the refrigerant and add refrigerant properties.  Ensure the fluid property file is in the same file directory and initiate GUI to try the new refrigerant.

## Physics-based System Solver

Although not recommended, the option to run a physics-based solver is available. Please beware that running the physics-based system solver takes a long time, and it is likely to cause poor system-level convergence. Following is the instruction on how to run the physics-based solver. First, open the heat exchanger solver (XXXX_ss.m).

1. Uncomment the physics-based function line on top. Comment out other function lines.
2. In section 0.1, change the mode to the system run mode.

3. Initiate GUI and select an option that is not labeled as “Mapped” in the heat exchanger section.
4. Run the system solver.

APPENDIX B

SAMPLE CODE – FIN AND TUBE HEAT EXCHANGER SOLVER

```
% function  FTHE_ss() %uncomment to start normal running mode

% function [u_final,fval,exitflag,output,finaltime, refcharge_hx,
delta_P, delta_h_HX] = ...
%     FTHE_ss(Op_type, P, H_ri_fixed, mdot, m_air,HX_var,
L_per,T_ai,beta_i_adj,beta_o_adj,SF) %uncomment to have mapping mode

function [refcharge_hx, delta_P,delta_h_HX] = FTHE_ss(HX_var, P,
H_ri_fixed, T_ai, mdot, m_air) %uncomment to run physics-based system
model


%%%%%%%%%%%%%%%%%%%%%%%%%%%%%%%%%%%%%%%%%%%%%%%%%%%%%%%%%%%%%%%%%%%%%%%%
%%%%
%  FILENAME:        FTHE.m
%
%  COMMENTS:        Fin and Tube Steady State Heat Exchanger Model
%
%
%  FUNCTION USAGE:
%
%       [] = FTHE_ss()
%
%           INPUTS
%           TBA                 To be added
%
%           OUTPUTS
%           TBA                 To be added
%
%  MODIFICATION HISTORY:
%  DATE:    AUTHOR:                     COMMENT:
%  5/2019   Deokgeun Park, TAMU         Original write of program
% 11/2019   Deokgeun Park, TAMU         Added features for length
variation
%                                       in the mapping mode.
%  2/2020   Deokgeun Park, TAMU         Formatting and minor revisions

%  Copyright Texas A&M University
%  $Revision: 1.0.1$
%
%  PROBLEMS/MODIFICATIONS FOR FUTURE WORK:
%
%
%%%%%%%%%%%%%%%%%%%%%%%%%%%%%%%%%%%%%%%%%%%%%%%%%%%%%%%%%%%%%%%%%%%%%%%%
%%%%
tic
%%%%%%%%%%%%%%%%%%%%%%%%%%%%%%%%%%%%%%%%%%%%%%%%%%%%%%%%%%%%%%%%%%%%%%%%
%%%%
```

```
%% 0.0 Define Function Inputs
%%%%%%%%%%%%%%%%%%%%%%%%%%%%%%%%%%%%%%%%%%%%%%%%%%%%%%%%%%%%%%%%%%%%%%%%%
%%%%



%%%%%%%%%%%%%%%%%%%%%%%%%%%%%%%%%%%%%%%%%%%%%%%%%%%%%%%%%%%%%%%%%%%%%%%%%
%%%%
    % 0.1 Define Heat Exchanger Inputs

%%%%%%%%%%%%%%%%%%%%%%%%%%%%%%%%%%%%%%%%%%%%%%%%%%%%%%%%%%%%%%%%%%%%%%%%%
%%%%

    mode                = 3;              % 1 = normal running mode, 2=
mapping mode, 3= system run mode
    if mode==1
       mapflag = exist('Op_type');
       if mapflag==1
           disp('Please select mapping mode prior to mapping')
           return

       end
    end
    if mode==1
        HX_var          = 2;              % 1 = evaporator, 2 = condensor
    end
    nele_tube           = 2;              % number of elements per tube

    global RefProp
    reftype             = 'R134a';
    load(['RefProp_',reftype,'.mat']);


%%%%%%%%%%%%%%%%%%%%%%%%%%%%%%%%%%%%%%%%%%%%%%%%%%%%%%%%%%%%%%%%%%%%%%%%%
%%%%
    % 0.2 Define Heat Exchanger Geometry

%%%%%%%%%%%%%%%%%%%%%%%%%%%%%%%%%%%%%%%%%%%%%%%%%%%%%%%%%%%%%%%%%%%%%%%%%
%%%%

    tube_config         = 1;                  % 1 = inline %2 = staggered
    per_2_deci          = 1/100;              % Conversion factor
[dimensionless]

    H                   = 3.98540146*0.3048;  % HX height, [m]
    L                   = 85.625*0.3048/12;   % HX length, [m]
    L_total             = L*12;               % total tube length, [m]
    if mode ==2
       L_total=L_total*L_per;
    end

    Di                  = (1/2-0.032*2)*2.54/100; % inner diameter,[m]
```

```
    Do                  = 0.40*2.54/100;
    D_h                 = Di;                   % Hyd diameter, [m] -> this
can change for other HX, not fin and tube
    RH_in               = 50;                   % relative humidity, [%]
    RH_in               = RH_in*per_2_deci;

    ntubes              = 2;                    % number of tubes per row
    nrow                = 6;                    % number of rows
    circuit             = [6 5 4 3 2 1 7 8 9 10 11 12]; % circuiting
geometry

    num_module    = 9;


    num_circuit         = 8;                    % number of equivalent
circuit
    ntube_total         = ntubes*nrow;          % total number of tubes in
the HX
    if length(circuit)== ntube_total            % make sure there is a
appropriately dimensioned circuiting input
    else
        disp('Please provide an appropiate circuiting input')
        return
    end

    n_el                = ntube_total*nele_tube;            % total number
of dividing elements for the HX

    A_i                 = L_total*Di*pi/n_el;               % internal
surface area per element, [m^2]
    A_o                 = ((0.8*L*20)*0.0635*1.219)/n_el;   % external
surface area per element, [m^2]
    A_cs                = (D_h/2)^2*pi;                     % cross
sectional area of refrigerant passage, [m^2]
    Af_e                = (L*H)/num_circuit;                % total HX
frontal area, [m^2]

    if mode ==2
        Af_e=Af_e*L_per;
    end


%%%%%%%%%%%%%%%%%%%%%%%%%%%%%%%%%%%%%%%%%%%%%%%%%%%%%%%%%%%%%%%%%%%%%%%%%
%%%%
    % 0.3 Define External Fluid Properties

%%%%%%%%%%%%%%%%%%%%%%%%%%%%%%%%%%%%%%%%%%%%%%%%%%%%%%%%%%%%%%%%%%%%%%%%%
%%%%
     CJF_e.Re_data     = [500 600 800 1000 1200 1500 2000 2500 3000 4000
5000 6000 8000 10000];
     CJF_e.jH_data     = [0.014 0.013 0.012 0.0105 0.0099 0.009 0.008
0.0073 0.0068 0.006 0.0055 0.005 0.0046 0.0041];
```

```
%       CJF_e.Re_data     = [550 1000 2000 6000];
%       CJF_e.jH_data     = [0.011 0.011 0.009 0.007];


     CJF_e.sigma       = 0.500;
     CJF_e.Dh          = D_h;
     CJF_e.Afr         = Af_e;

     Diameter=D_h;

     PGW.mu_T         = [273.15; 296.65; 313.05; 333.1; 353.05; 363.3;
373.45; 384.15; 394.55; 411.75; 429.55; 449.55];   % air  temperature
in Kelvin
     PGW.mu_data      = 1e-5*[1.71; 1.838; 1.916; 2.01; 2.1; 2.146;
2.191; 2.238; 2.282; 2.355; 2.429; 2.511];           % air  viscosity
     PGW.k_T          = [273.15; 299.6; 322.1; 347.2; 372.1; 396.4;
420.4; 440.4];                            % air temperature in Kelvin
     PGW.k_data       = 1e-2*[2.4; 2.635; 2.801; 2.981; 3.155; 3.321;
3.482; 3.614];                       % air conductivity
     PGW.Cp_T         = [273.15; 288.6; 299.7; 310.8; 321.9; 333.0;
344.1; 355.2; 366.3; 377.4; 388.5];      % air temperature in Kelvin
     PGW.Cp_data      = [1.005; 1.006; 1.007; 1.007; 1.008; 1.008;
1.009; 1.01; 1.011; 1.012; 1.013];      % air specific heat
     % 1.005*ones(length(PGW.Cp_T),1)%

     % saturated water properties
     Swater_data.T_data  = [-40 -36 -30 -26 -20 -16 -10 -6 0 5 10 15 20
25 30 35 40 45 50 55 60];
     Swater_data.Ps_data = [0.01285 0.02004 0.03802 0.05725 0.10326
0.15068 0.25990   0.36873   0.6115 0.8725 1.2281 1.7057 2.3392 3.1698
4.2469 5.6291 7.3851 9.5953 12.352 15.763 19.947];
     Swater_data.h_data  = [2426.6 2434.0 2445.1 2452.5 2463.6 2471.0
2482.1 2489.5  2500.5 2510.1 2519.2 2528.3 2537.4 2546.5 2555.6 2564.6
2573.5 2582.4 2591.3 2600.1 2608.8];

     %Swater_data=Swater;
     CJF_data        = CJF_e;
     Ext_Fluid       = PGW;
     Cp_ext          = 1.005;  %Specific heat of air,[kJ/kg.K]

   if mode==2
         T_SF_prop=T_ai+273.15;

        mu_diff=SF.mu_T-T_SF_prop;
        k_diff =SF.k_T-T_SF_prop;
        Cp_diff=SF.Cp_T-T_SF_prop;
        den_diff=SF.den_T-T_SF_prop;

        mu_min=min(abs(mu_diff));
        k_min =min(abs(k_diff));
```

```
        Cp_min =min(abs(Cp_diff));
        den_min =min(abs(den_diff));

        mu_index=find(abs(mu_diff)==mu_min);
        k_index=find(abs(k_diff)==k_min);
        Cp_index=find(abs(Cp_diff)==Cp_min);
        den_index=find(abs(den_diff)==den_min);

        mu_ext = SF.mu_data(mu_index);
        k_ext  = SF.k_data(k_index);
        Cp_ext = SF.Cp_data(Cp_index);
        rho_ext = SF.den_data(den_index);
   end

%%%%%%%%%%%%%%%%%%%%%%%%%%%%%%%%%%%%%%%%%%%%%%%%%%%%%%%%%%%%%%%%%%%%%%%
%%%%
    % 0.4 Fluid inlet conditions

%%%%%%%%%%%%%%%%%%%%%%%%%%%%%%%%%%%%%%%%%%%%%%%%%%%%%%%%%%%%%%%%%%%%%%%
%%%%

    oil_cir_per        = 0;          % Oil Circulation Percentage
    ht_deg_oil         = -0.008;      % HT degredation factor with oil
effect
    deg_factor         = oil_cir_per*ht_deg_oil+1;          % 0<DF<1

    if mode==2 || mode==3
        m_air          = m_air/2/(num_circuit);
        mdot           = mdot/num_circuit/2/num_module;
    elseif mode==1
        m_air          = 52/1.5/2/(num_circuit);                %
Secondary fluid mass flow rate per circuit, [kg/s]
        mdot           = 2/num_circuit/2/num_module;            % Total
refrigerant mass flow rate, [kg/s]
        %mdot          = 2.0267/num_circuit/2/num_module
        %mdot          = 2.0267/num_circuit/3/2/15
        P              = 1050;                                  % inlet
refrigerant pressure [kPa]
        T_ai           = 35;                                    %
secondary fluid temperature [deg C]
    end

    Tsat               = qginterp1(RefProp.Psat,RefProp.Tsat,P);
    Hf                 = qginterp1(RefProp.Psat,RefProp.Hf,P);
    Hg                 = qginterp1(RefProp.Psat,RefProp.Hg,P);

    if mode==2
    elseif mode==1
        H_ri_fixed     =
qminterp2(RefProp.Tv,RefProp.P,RefProp.Hv_pt,Tsat+5,P); %435.8;
% inlet refrigerant enthalpy [kJ/kg]
    end
```

```
    H_ro_fixed        = Hf*0.95;
%qminterp2(RefProp.Tl,RefProp.P,RefProp.Hl_pt,Tsat,P) %253;         %
inlet refrigerant enthalpy [kJ/kg]
    Q_estimate        = -mdot*(H_ro_fixed-H_ri_fixed)/n_el; %Estimate
of Qdot (used for refrg side two-phase heat transfer coef correlation
only),[kJ/kg]


%%%%%%%%%%%%%%%%%%%%%%%%%%%%%%%%%%%%%%%%%%%%%%%%%%%%%%%%%%%%%%%%%%%%%%%%
%%%%
    % 0.6 User selected tuning factors

%%%%%%%%%%%%%%%%%%%%%%%%%%%%%%%%%%%%%%%%%%%%%%%%%%%%%%%%%%%%%%%%%%%%%%%%
%%%%

    beta_flag         = 2;       % 1 = adjust beta_o to match desired
outlet enthalpy, 2 = user defined beta_o
    beta_i            = 1;       % Refrigerant Heat Transfer
multiplicative adjustment factor
    lamda             = 1;       % Objective Function Weight for
matching desired outlet enthalpy

    if beta_flag==1
        beta_o        = 1;       % Not actually used for beta_flag==1
    else
        beta_o        = 1;       % Secondary Fluid Heat Transfer
multiplicative adjustment factor
    end

%%%%%%%%%%%%%%%%%%%%%%%%%%%%%%%%%%%%%%%%%%%%%%%%%%%%%%%%%%%%%%%%%%%%%%%%
%%%%
% 1.0 Define Interconnection Matrices for each element
%%%%%%%%%%%%%%%%%%%%%%%%%%%%%%%%%%%%%%%%%%%%%%%%%%%%%%%%%%%%%%%%%%%%%%%%
%%%%

%% Define M1 Circuiting Geometry for SF Temperatures (Tair_out_vec to
Tair_in_vec)

    M1=zeros(n_el,n_el);
    for i=1:ntube_total
         if circuit(i)>nrow
            if (mod(i,2)== mod(find(circuit==(circuit(i)-nrow)),2))
%same flow direction between tubes
                for k=1:nele_tube
                    M1(nele_tube*(i-1)+k, nele_tube*(
find(circuit==(circuit(i)-(nrow)))-1 )+k )=1;
                end
            else % opposite direction
                for k=1:nele_tube
                    M1(nele_tube*i+1-k, nele_tube*(
find(circuit==(circuit(i)-(nrow)))-1 )+k )=1;
```

```
                end
            end
        end
    end
    [m,n]=size(M1);
    if m==n
    else
        disp('M1 formula incorrect')
        return
    end

%% Define M2 External Inlet Temperature to Tair_in_vec

    M2=zeros(n_el,1);
    for i=1:ntube_total
        if circuit(i)<=nrow
            for k=1:nele_tube
                M2(nele_tube*(i-1)+k,1)=1;
            end
        end
    end

%% Define N1 External Inlet Temperature to Tair_in_vec

    N1=zeros(n_el,n_el);
    for i=1:n_el-1
       N1(i+1,i)=1;
    end

%% Define N2 (hr_in_1 to hr_in_vec)

    N2=zeros(n_el,1);
    N2(1,1)=1;

%% Define NM1

    NM1=[N1 zeros(length(N1)); zeros(length(N1)) M1];

%% Define NM2

    NM2=[N2 zeros(length(N2),1); zeros(length(N2),1) M2];

%% Define K

    K=inv(eye(length(NM1))-NM1);

%% Define uext

    uext=[H_ri_fixed; T_ai];
```

```
%%%%%%%%%%%%%%%%%%%%%%%%%%%%%%%%%%%%%%%%%%%%%%%%%%%%%%%%%%%%%%%%%%%%%%%%%
%%%%
%% 2.0 fmincon Initialization
%%%%%%%%%%%%%%%%%%%%%%%%%%%%%%%%%%%%%%%%%%%%%%%%%%%%%%%%%%%%%%%%%%%%%%%%%
%%%%

hstep=-(H_ri_fixed-Hf)*10/n_el;

%initial guess of enthalpy change in each element
u0=ones(n_el,1);
for i=1:n_el
    u0(i)=hstep;
end
u0=zeros(n_el,1);

%specified lower bound of enthalpy change in each element
lb=-50*ones(n_el,1);
for i=1:n_el
    lb(i)=-(H_ri_fixed-Hf)*15/n_el;
end
%specified upper bound of enthalpy change in each element
% lb
ub=ones(n_el,1);

%if beta_flag==1, beta_o will be optimized, so specify initial guess,
lower bound and upper bound of beta_o

if beta_flag==1
    u0=[1;u0];
    lb=[0.01;lb];
    ub=[100;ub];
end

% R=[eye(n_el);(-mdot/((m_air/n_el)*Cp_ext))*eye(n_el)]
r1=mdot*ones(n_el);
r2=r1.*eye(n_el)/(-1*(m_air/n_el)*Cp_ext);
R=[eye(n_el);r2];

%%%%%%%%%%%%%%%%%%%%%%%%%%%%%%%%%%%%%%%%%%%%%%%%%%%%%%%%%%%%%%%%%%%%%%%%%
%%%%
%% 3.0 fmincon Optimization
%%%%%%%%%%%%%%%%%%%%%%%%%%%%%%%%%%%%%%%%%%%%%%%%%%%%%%%%%%%%%%%%%%%%%%%%%
%%%%


fun= @(u) (ObjFuction_FTHE(Tsat, R,lamda,K, NM1, NM2, uext,
beta_flag,beta_o, H_ro_fixed, beta_i,Tsat,...
Hf, Hg,u, n_el, H_ri_fixed, P,
A_i,A_o,Diameter,m_air,Cp_ext,mdot,A_cs,CJF_data,...
Swater_data,Ext_Fluid,HX_var,Q_estimate,RH_in,deg_factor))
```

```
A=[];
b=[];
Aeq = [];
beq = [];
options = optimoptions('fmincon','Display','iter','Algorithm','sqp');
options.MaxFunctionEvaluations = 10000;
options.StepTolerance = 1.0000e-6;
options.MaxIterations = 1000;

nonlcon=[];

[u_final,fval,exitflag,output]=
fmincon(fun,u0,A,b,Aeq,beq,lb,ub,nonlcon,options);
%%%%%%%%%%%%%%%%%%%%%%%%%%%%%%%%%%%%%%%%%%%%%%%%%%%%%%%%%%%%%%%%%%%%%%
%%%%
%% 4.0 Pressure Loss, Refrigerant Charge and Enthalpy Change
Calculations
%%%%%%%%%%%%%%%%%%%%%%%%%%%%%%%%%%%%%%%%%%%%%%%%%%%%%%%%%%%%%%%%%%%%%%
%%%%

%%%%%%%%%%%%%%%%%%%%%%%%%%%%%%%%%%%%%%%%%%%%%%%%%%%%%%%%%%%%%%%%%%%%%%
%%%%
%% 4.1 Pressure Loss Calculation
%%%%%%%%%%%%%%%%%%%%%%%%%%%%%%%%%%%%%%%%%%%%%%%%%%%%%%%%%%%%%%%%%%%%%%
%%%%

muf        = qginterp1(RefProp.Psat,RefProp.muf,P);             %
Saturated liquid viscosity
mug        = qginterp1(RefProp.Psat,RefProp.mug,P);             %
Saturated vapor viscosity
Rhof       = qginterp1(RefProp.Psat,RefProp.Rhof,P);            %
Saturated liquid density
Rhog       = qginterp1(RefProp.Psat,RefProp.Rhog,P);            %
Saturated vapor density
vg         = 1/Rhog;                                           %
Saturated vapor specific volume
vf         = 1/Rhof;                                           %
Saturated liquid specific volume
Roughness  = 1e-6;
Slip       = 2;

if beta_flag==1
    beta_o=u_final(1);
    u_final(1)=[];
else
end

% V          = inv(eye(length(N1))-N1);                         %
Mapping of elemental enthalpy change to actual enthalpy values
% h          = V*(N1*(u_final)+N2*H_ri_fixed);                  % vector
of actual enthalpy values at each element inlet
    h  = K*(NM1*(R*u_final)+NM2*uext);
```

```
for k=1:n_el
    if k == 1
        h1 = H_ri_fixed;
    else
        h1 = h(k-1);
    end
        h2 = h(k);

    G      = mdot/A_cs;

    try
        delta_P_individual(k)=
pressuredrop(Diameter,h1,h2,L_total/n_el,P,...
                           Roughness,Slip,Hf,Hg,Rhof ,Rhog ,muf ,mug
,vg ,vf,G);

    catch
        %     delta_P_individual(k)=
pressuredrop(A_cs,Diameter,h1,h2,mdot, L_total/n_el,P,...
        %                             Roughness,Slip,Hf,Hg,Rhof ,Rhog
,muf ,mug ,vg ,vf,G);
        delta_P_individual(k)=NaN;
    end
end

delta_P    = sum(delta_P_individual);

if  isnan(delta_P)
% Catch NaN
    delta_P = 0;
end
% delta_P=0;
%%%%%%%%%%%%%%%%%%%%%%%%%%%%%%%%%%%%%%%%%%%%%%%%%%%%%%%%%%%%%%%%%%%%%%
%%%%
%% 4.2 Refrigerant Charge Calculation
%%%%%%%%%%%%%%%%%%%%%%%%%%%%%%%%%%%%%%%%%%%%%%%%%%%%%%%%%%%%%%%%%%%%%%
%%%%

for k = 1:n_el

    if h(k) > Hg
        Rho(k)            =
qminterp2(RefProp.Hv,RefProp.P,RefProp.Rhov_ph,h(k),P);
    elseif h(k) <= Hg && h(k) >= Hf
        xQ(k)             = (h(k) - Hf)/(Hg - Hf);
        Gamma(k)          = Rhof*xQ(k)/(Rhof*xQ(k) + Rhog*(1-
xQ(k))*Slip);
        Rho(k)            = Rhof*(1-Gamma(k)) + Rhog*Gamma(k);
    elseif h(k) < Hf
        Rho(k)            =
qminterp2(RefProp.Hl,RefProp.P,RefProp.Rhol_ph,h(k),P);
```

```
    end
        m_fcv_hx(k)      = Rho(k)*((pi*Di^2*0.25)*L_total/n_el);     %
refrigerant mass in an element
end


        refcharge_hx     = sum(m_fcv_hx);                % total
refrigerant mass, [kg]

%%%%%%%%%%%%%%%%%%%%%%%%%%%%%%%%%%%%%%%%%%%%%%%%%%%%%%%%%%%%%%%%%%%%%%%
%%%%
%% 4.3 Enthalpy Charge Calculation
%%%%%%%%%%%%%%%%%%%%%%%%%%%%%%%%%%%%%%%%%%%%%%%%%%%%%%%%%%%%%%%%%%%%%%%
%%%%

    delta_h_HX=0;
    if beta_flag==1
        for i=1:n_el
        delta_h_HX=u_final(i)+delta_h_HX;
        end
    else
        for i=1:n_el
        delta_h_HX=u_final(i)+delta_h_HX;
        end
    end

%%%%%%%%%%%%%%%%%%%%%%%%%%%%%%%%%%%%%%%%%%%%%%%%%%%%%%%%%%%%%%%%%%%%%%%
%%%%
%% 5.0 Output
%%%%%%%%%%%%%%%%%%%%%%%%%%%%%%%%%%%%%%%%%%%%%%%%%%%%%%%%%%%%%%%%%%%%%%%
%%%%

disp('H_ro_fixed-H_ri_fixed [kJ/kg]')
disp(H_ro_fixed-H_ri_fixed)

disp('Refrigerant side heat transfer multiplicative adjustment factor')
disp(beta_i)

disp('Secondary fluid heat transfer multiplicative adjustment factor')
disp(beta_o)

disp('Total Enthalpy Change Output')
disp(delta_h_HX)

finaltime=toc;
disp('Total time consumed [sec]')
disp(finaltime)
end
```

# APPENDIX C

## CENTRIFUGAL COMPRESSOR MODELING

In this section, physical modeling of centrifugal type compressor, conducted by Dr. S. Mostafa Ghoreyshi, will be presented. Modeled loss mechanisms of the centrifugal compressor are tabularized in Table 9.

**Table 9. Centrifugal Compressor Loss Mechanisms**

| **Category** | **Loss Mechanism** | **Definition** |
|---|---|---|
| Mechanical (parasitic) losses | Disk friction and windage loss | Loss due to the friction work in the clearance gaps between the impeller and the housing |
| | Leakage loss | Energy loss due to leakage through the seals and clearances |
| | Recirculation loss | Loss due to recirculation of flow back into the impeller tip |
| Impeller losses | Shock loss | Loss due to shock waves if any velocities exceed sonic flow conditions |
| | Clearance loss | Loss due to tip clearance flow between impeller and casing |
| | Incidence loss | Loss due to incidence angle between inlet flow and blade metal angle in off-design conditions |
| | Diffusion loss | Diffusion loss between impeller inlet and throat |
| | Skin friction loss | Loss from the shear forces on the impeller surface due to turbulent friction |
| | Blade loading loss | Mixing losses due to blade loading |
| | Hub-to-shroud loss | Mixing losses due to hub-to-shroud loading on the blade |
| Diffuser and discharge losses | Vaneless diffuser loss | Loss in the vanless diffuser section |
| | Vaned diffuser loss | Loss in the vaned diffuser channel |
| | Exit volute loss | Volute and exit losses |

Fluid first hits the guide vanes and changes its direction of flow to align with the angle of attack of the inducer. As the impeller rotates and pulls the fluid forward, the working fluid passes the eye and enters the inducer of the impellor. The inducer accelerates the fluid, and the impeller pushes the fluid into the diffuser. The diffuser slows down the velocity of the fluid and increases the static pressure. Scroll collects the fluid and channels it to the next stage.

# APPENDIX D

# VAPOR INJECTION SOLVING PROCESS

The solver procedure in solving the injection pressure is detailed below:

1. fmincon guesses an injection pressure.
2. With given SC input and condensing pressure, find $h_5$.
3. Find $h_6$ and $h_9$ with mapped BPHX.
4. Calculate $h_3$ and $h_4$ using given SH, evaporating pressure, compressor isentropic efficiency, and previously calculated $h_9$.
5. $h_4$ goes to the inlet of the condenser and $h_7$ (which is equal to $h_6$) goes to the inlet of the evaporator.
6. Degree of superheat at $h_9$ is compared to the given superheat requirement.
7. fmincon iterates until the superheat is matched.